

**ANALYSIS OF LONG COMPRESSIONAL ELASTIC WAVES
IN RODS OF ARBITRARY CROSS SECTION AND ELASTIC
WAVE FRONTS IN PLATES AND CIRCULAR RODS**

Thesis by

Robert Leopold Rosenfeld

In Partial Fulfillment of the Requirements

For the Degree of

Doctor of Philosophy

California Institute of Technology

Pasadena, California

1962

ACKNOWLEDGMENTS

The author is deeply indebted to his advisor, Prof. Julius Miklowitz, for his continual assistance. Prof. Miklowitz's thorough background in elastic wave propagation enabled him to provide uncommonly effective guidance.

The author wishes to thank the Garrett Corporation and the National Science Foundation for fellowships and the California Institute of Technology both for a teaching assistantship and for its fine facilities and stimulating atmosphere.

The Western Data Processing Center deserves thanks for providing time on a scientific computer and assisting in its use. Thanks are due to Mr. Ken Hebert for extensive assistance in the wave front calculations.

The author's parents, wife, and her parents should all be thanked for their continual encouragement.

ABSTRACT

Long waves in elastic rods of arbitrary cross section are studied by writing a general expansion of the exact solution for three dimensional linear elasticity. The solution holds for transient excitation of the end of a semi-infinite cylinder and is in terms of the harmonic modes of wave propagation for the infinite elastic cylinder. The major contribution to the solution for large distances from the end of the rod is found by making approximations to the infinitely long wave length part of the solution. This is aided by using a perturbation method for long wave length to study the modes of propagation. An approximate theory for rods of arbitrary cross section is developed and compared to the exact theory for harmonic waves of infinitely long wave lengths.

The amplitudes and locations of all wave fronts caused by certain suddenly applied loads on elastic plates and circular rods are presented. Both end loads on the rod and plate as well as normal line and point forces on the plate are considered. The problems are solved by expanding double transforms into a series of terms, each term representing the disturbance following a single wave front. Evaluation of the terms for the wave front behavior is accomplished by Cagniard's method and the saddle point method. Ray theory aids in the interpretation of the results and also serves to verify most of the formulas. The solution by Cagniard's method is exact for the plane strain problems studied and is plotted and compared to experiments.

TABLE OF CONTENTS

I. INTRODUCTION	1
II. MODES OF PROPAGATION	6
A. THEORY OF ELASTICITY, MODES OF VIBRATION	7
B. DOUBLE TRANSFORMS	10
C. SOLUTION USING MODES OF PROPAGATION	16
Orthogonality Properties	16
Expansion in Terms of Modes	19
Inversion of the Transforms	23
III. LONG WAVES IN A NONCIRCULAR ROD	28
A. THE PERTURBATION SCHEME	29
B. THE FIRST MODE	35
C. HIGHER MODES	39
Longitudinal Shear Modes	39
Radial Modes	42
D. THE LONG TIME RESPONSE	44
E. APPROXIMATE THEORY	53
IV. THEORY OF WAVE FRONT AMPLITUDES AND LOCATIONS	68
A. DERIVATION OF THE DOUBLE TRANSFORMS	73
B. EXPANSION OF THE TRANSFORMS FOR PLANE STRAIN	88

C. EVALUATION OF THE INTEGRALS FOR THE	
WAVE FRONTS	98
Cagniard's Method	101
Regular Wave Fronts	104
Head Waves and Two Sided Shear Waves	105
Rayleigh Waves	109
The Saddle Point Method	114
D. MODIFICATIONS FOR CYLINDRICAL	
SYMMETRY	119
The Point Force	120
The Circular Rod	123
E. RAY THEORY	124
Geometry of the Rays	129
Divergence Factor	131
The Source	133
Multiply Reflected Rays	135
V. RESULTS FROM WAVE FRONT THEORY	142
A. WAVE FRONT LOCATIONS	142
B. WAVE FRONT AMPLITUDES	148
Time Dependence	148
Amplitudes	150
The Source	160
Reflection at Grazing Incidence	162
Head Waves	169

Effects of Divergence, Reflection, and Cylindrical Symmetry	170
C. WAVE FRONTS IN THE MODAL EXPANSION	171
D. EXACT SOLUTIONS FOR LIMITED TIME INTERVALS	182
REFERENCES	190

I. INTRODUCTION

Transient wave propagation in semi-infinite elastic rods and plates has been studied from two viewpoints. Most of the literature has been devoted to the study of the low frequency - long wave response. These studies quite accurately explain phenomena observed at long times after the application of the load and at long distances from the end of the rod or edge of the plate. Attention has also been given to the high frequency character of the response with the purpose of finding the displacements and strains near to the load. This thesis is divided into two main parts; sections II and III deal mainly with low frequencies while sections IV and V are concerned with high frequencies.

Low frequency behavior is most conveniently studied by examining the modes of wave propagation, branches of the frequency equation and associated displacements for all wave lengths. The most important mathematical tool employed is Kelvin's method of stationary phase. The associated concept of group velocity plays an important role. On the other hand, the high frequency response is most easily investigated by means of ray theory. Though special mathematical techniques are employed, Cagniard's method and the saddle point method, the essential concept is that of rays and wave fronts.

The literature on the theory of the low frequency response is based on two different methods of approach. The first method used is to develop "approximate" theories. These are equations of motion which incorporate the essential physics of the "exact

theory" (three dimensional linear elasticity) and the simplifying features of the elementary theory--one dimensionality, plane sections remain plane, etc. Approximate theories govern the motion accurately provided the frequencies are low enough and the wave lengths long enough. Approximate theories may be solved exactly as Miklowitz (1, 2) has done with the Mindlin-Herrmann (3, 4) equations governing compressional waves in a circular rod. The second method of approach is to write a formal solution to the equations of motion from the linear theory of elasticity by using double transforms. Skalak (5) and Folk, Fox, Shook, and Curtis (6) have done this for problems of compressional waves in a circular rod. The formal solutions are evaluated approximately by asymptotic methods and are valid for large time and the far field.

The solutions from approximate and exact theories are both written in terms of modes of propagation. As an example, solutions to the Mindlin-Herrmann theory are written in terms of two modes, which model the lowest two modes of the exact (Pochhammer) theory for the circular rod. Miklowitz (7) has shown that the lowest frequency waves of both his solution of the Mindlin-Herrmann theory and the exact theory solution given by Skalak and Folk et al. behave in the same way. This behavior and like phenomena for higher modes will be found for a noncircular rod in the present work.

Wave propagation in rods of arbitrary cross section has received little attention due to difficulties in the mathematics.

Love (Reference 8, p. 428) gave a simple approximate theory and frequency equation valid for low frequencies. Further work was hampered by two difficulties. Little is known about the exact theory modes of propagation and frequency equation, which were the bases of most mathematical analyses of the circular rod. Furthermore, the differential equations for the double transforms of the exact theory solution were not solved. However, one can use these differential equations to write the double transforms formally in terms of the modes of propagation, as is shown in section II of this thesis. Experience has shown that one needs only to know the modes of propagation at certain critical points, where the group velocity is a maximum or minimum. This fact is used in section III to evaluate asymptotically for long time the formal solution from the double transforms. The forms of the modes of propagation are determined only in so far as is needed for the approximate evaluation.

The differential equations for the double transforms of the exact theory solutions for a rod may be found by using a method developed by Folk, Fox, Shook, and Curtis (6). This method, unfortunately, cannot be used to solve the case of nonmixed boundary conditions on the end of the rod or edge of the plate, e.g. the end pressure shock problem, step axial stress, zero shear stress. In section III of this thesis the boundary conditions of the pressure shock problem are assumed and some conclusions are drawn.

Wave fronts may be found from the double transforms either

by means of Cagniard's method (an ingenious method for inverting the Laplace transform) or the saddle point method. Cagniard's method has been used by Mencher (9), Broberg (10), and Davids (11). The saddle point method has been used by Knopoff (12) and Knopoff and Gilbert (13). Either way the double transforms are first expanded into terms, each representing the disturbance following a single wave front. Wave front information is then extracted from each term.

The axially symmetric plate problems studied in papers (9) to (13) are closely related to the rod and plate problems of interest here. Those papers gave results which are only for restricted regions of the plate. Mencher studied the displacement at the epicenter of an infinite plate with a step point source of pressure at its center. Papers (10) to (13) considered an infinite plate with a transient point force applied normally to one surface. Broberg and Davids considered displacements and stresses on the axis of symmetry only. Knopoff and Gilbert studied the displacement on the face of the plate opposite the load. The present work studies the strains and displacements throughout the interior of a plate to which is applied a normal point force. Also, the circular rod is studied. Here, two different transient compressional loads on the end are considered. The analysis is aided by working with the plane strain equivalents of the problems first.

A physical understanding of the equations for wave fronts is achieved through a study of ray theory. Karal and Keller (14)

and Babich and Alekseev (15) have developed a general ray theory of elastic wave fronts. The fundamental idea is that elastic waves may be studied through a geometric theory in much the same way as light waves are. The general ideas are explained at the beginning of section IV, and the ray theory is used in both sections IV and V as a partial substitute for Cagniard's method and the saddle point method. It is most satisfying that the formulas found by the three methods, the saddle point method, Cagniard's method, and the ray theory, are in complete agreement.

II. MODES OF PROPAGATION

Most solutions to wave propagation problems have been written in terms of modes of propagation. Such solutions to the linear theory of elasticity have been given only for simple geometries, circular rods and plane strain or stress. This suggests that one ought to be able to write similar solutions to problems of transient propagation in infinite cylinders of arbitrary cross section in terms of modes of propagation. One would expect to build up a solution by proving some orthogonality properties and using them in much the same way as the orthogonality properties of modes of vibration are used to solve transient vibration problems. Just such a solution is derived below. It contributes to a further understanding of previously published solutions for the circular rod and is evaluated in section III for certain features of wave propagation in noncircular rods.

The starting point for the mathematics is to transform two variables, time and the spatial variable in the direction of propagation. Laplace and Fourier transforms were used by Skalak (5) and Folk, Fox, Shook, and Curtis (6) to derive their solutions for a rod of circular cross section. Explicit expressions for the double transforms were found. Skalak and Folk et al. then used inversion integrals, evaluating the first by residue theory with each mode of propagation contributing one pole. A similar method will be used here. However, the double transforms in the present case cannot be given in an explicit, closed form. They are found by making an expansion based on orthogonality properties

of the modes. The general method of making the expansion is given in textbooks on the mathematics of linear equations, such as Courant and Hilbert (16).

A. THEORY OF ELASTICITY, MODES OF VIBRATION

The mathematics and governing laws used here to investigate the modes of propagation are quite similar to those which are used to discuss modes of vibration. The equations for the modes of propagation are long. Certain steps in the derivations may be carried out more easily by drawing the analogy with vibration. Therefore, it is convenient to discuss modes of vibration first, writing the equations in a concise form by means of variable indices.

Consider a finite, homogeneous, isotropic, linearly elastic solid upon which no work producing forces are acting. A harmonic time dependence, $e^{i\omega t}$, is assumed in order to study the free vibrations. The governing laws may be expressed by setting equal to zero the variation of an integral which is similar to twice the Lagrangian in Hamilton's principle for arbitrary time dependence for elastic bodies with no external work producing forces, (see reference 8, pp. 166-167)

$$\delta L = \delta \iiint \left[\rho \omega^2 u_i u_i - \frac{1}{2} \sigma_{ij} \left(\frac{\partial u_i}{\partial x_j} + \frac{\partial u_j}{\partial x_i} \right) \right] dV = 0. \quad (1)$$

In equation 1 the $u_i(k_i)$ are the Cartesian displacements, ρ the density, the integration is over the volume of the solid, repeated indices imply summation, and the stresses $\sigma_{ij}(x_k)$ are defined linearly in terms of the strains through the constants K_{ijkl} by

$$\sigma_{ij} = K_{ijkl} \left(\frac{\partial u_k}{\partial x_l} + \frac{\partial u_l}{\partial x_k} \right). \quad (2)$$

There are three symmetry conditions on the K_{ijkl} :

$$K_{ijkl} = K_{klij}, \quad K_{ijkl} = K_{jikl}, \quad \text{and} \quad K_{ijkl} = K_{ijlk}. \quad (3)$$

The integrand of equation 1 is a bilinear form which is symmetric on account of the first of equations 3. Because of the symmetry it is only necessary to take the variation of the second member of each term in equation 1 and to multiply by two. Thus, equation 1 may be written as

$$\delta L = 2 \iiint \left[\rho \omega^2 u_i \delta u_i - \frac{1}{2} \sigma_{ij} \left(\frac{\partial}{\partial x_j} \delta u_i + \frac{\partial}{\partial x_i} \delta u_j \right) \right] dV = 0. \quad (4)$$

Then, by virtue of the second of equations 3, which represents the symmetry of the stress tensor,

$$\delta L = 2 \iiint \left[\rho \omega^2 u_i \delta u_i - \sigma_{ij} \frac{\partial}{\partial x_j} \delta u_i \right] dV = 0. \quad (5)$$

The next step is to integrate by parts and apply the divergence theorem. There result two integrals which are required to be zero.

The first is a volume integral, the second a surface integral,

$$\iiint \left(\rho \omega^2 u_i + \frac{\partial \sigma_{ij}}{\partial x_j} \right) \delta u_i dV = 0 \quad (6)$$

$$\iint \delta u_i (\sigma_{ij} dn_j) = 0. \quad (7)$$

In equation 7 dn_j is a vector proportional to the differential element

of area and normal to the surface. If the boundaries of the solid are rigidly held, then we restrict the variations in equation 1 by requiring $\delta u_i = 0$ at the surface and look for an extremum of L . Then equation 7 holds. If the boundaries are not rigidly held, then the δu_i are not restricted and equation 7 holds only if $\sigma_{ij} dn_j$ vanishes everywhere on the surface. Thus, the stress, (as defined by equation 2) acting on the surface is required by the variational principle to be zero. It is possible to have mixed boundary conditions requiring some components of the displacement to be zero and some components of the force to be zero. By the usual arguments of the calculus of variations, the equations of motion are found by setting equal to zero the coefficients of each of the δu_i in equation 6;

$$\rho \omega^2 u_i + \frac{\partial \sigma_{ij}}{\partial x_j} = 0. \quad (8)$$

The solutions to the equations of motion, equations 8, and the boundary conditions represent the modes of vibration of an elastic body. Let $u_i^{(n)}$ be the displacements and $\sigma_{ij}^{(n)}$ be the stresses of the n^{th} mode, and let ω_n be the associated frequency of vibration. Then the orthogonality relation may be derived from the symmetric integral

$$I = - \iiint \frac{1}{2} \sigma_{ij}^{(n)} \left(\frac{\partial u_i^{(m)}}{\partial x_j} + \frac{\partial u_j^{(m)}}{\partial x_i} \right) dV. \quad (9)$$

As in deriving equation 6 from equation 4, we may use the symmetry of the stress tensor, integrate by parts, and use the divergence theorem and the boundary conditions on equation 9 to show that

$$I = \iiint \frac{\partial \sigma_{ij}^{(n)}}{\partial x_j} u_i^{(m)} dV. \quad (10)$$

Equations 8 are then substituted into equation 10 to show that

$$I = -\rho\omega_n^2 \iiint u_i^{(n)} u_i^{(m)} dV. \quad (11)$$

Because I is symmetric under interchange of n and m , we may deduce from equation 11 the orthogonality relation

$$(\omega_m^2 - \omega_n^2) \iiint u_i^{(n)} u_i^{(m)} dV = 0. \quad (12)$$

If ω_n and ω_m are not equal, the integral in equation 12 must be zero. If ω_n and ω_m are equal, but the functions $u_i^{(n)}$ and $u_i^{(m)}$ are linearly independent, the Gram-Schmidt orthogonalization process may be used to form from them two orthogonal modes with the same natural frequency. The modes are then a set of functions for which

$$\iiint u_i^{(n)} u_i^{(m)} dV = \begin{cases} 0 & m \neq n \\ 1 \text{ (say) } & m = n. \end{cases} \quad (13)$$

These orthogonal modes are used to express the solutions to forced or free vibration problems and initial value problems.

B. DOUBLE TRANSFORMS

Laplace and Fourier transforms aid in deriving a solution in terms of harmonic wave trains. Folk, Fox, Shook and Curtis (6) have developed the technique of using double transforms for problems of elastic wave propagation in semi-infinite cylinders. Essentially, their method is used here to derive the differential equations for the double transforms.

The rod and the Cartesian coordinate system are shown in figure 1. Initially the rod is at rest. At time $t = 0$ forces or displacements are applied at $z = 0$, the end of the semi-infinite rod. The boundary conditions along the lateral boundary are consistent with an equation such as 7. In particular, it will be assumed in section III that the lateral surfaces are stress free.

The stress equations of motion are (see equation 8)

$$\frac{\partial \sigma_{zz}}{\partial z} + \frac{\partial \sigma_{yz}}{\partial y} + \frac{\partial \sigma_{xz}}{\partial x} - \rho \frac{\partial^2 u_z}{\partial t^2} = 0 \quad (14a)$$

$$\frac{\partial \sigma_{xx}}{\partial x} + \frac{\partial \sigma_{xy}}{\partial y} + \frac{\partial \sigma_{xz}}{\partial z} - \rho \frac{\partial^2 u_x}{\partial t^2} = 0 \quad (14b)$$

$$\frac{\partial \sigma_{yy}}{\partial y} + \frac{\partial \sigma_{xy}}{\partial x} + \frac{\partial \sigma_{yz}}{\partial z} - \rho \frac{\partial^2 u_y}{\partial t^2} = 0 ,$$

where the stresses are given by (see equation 2)

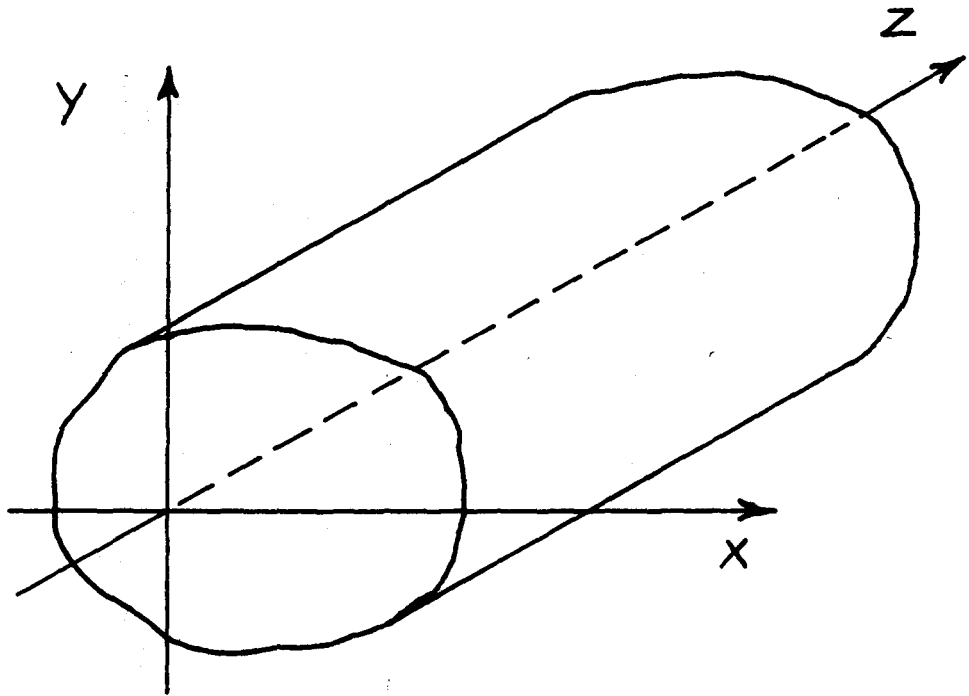
$$\sigma_{zz} = \lambda \left(\frac{\partial u_x}{\partial x} + \frac{\partial u_y}{\partial y} \right) + (\lambda + 2\mu) \frac{\partial u_z}{\partial z} \quad (14c)$$

$$\sigma_{xx} = \lambda \left(\frac{\partial u_y}{\partial y} + \frac{\partial u_z}{\partial z} \right) + (\lambda + 2\mu) \frac{\partial u_x}{\partial x} \quad (14d)$$

$$\sigma_{yy} = \lambda \left(\frac{\partial u_x}{\partial x} + \frac{\partial u_z}{\partial z} \right) + (\lambda + 2\mu) \frac{\partial u_y}{\partial y}$$

$$\sigma_{xy} = \mu \left(\frac{\partial u_x}{\partial y} + \frac{\partial u_y}{\partial x} \right) \quad (14e)$$

$$\sigma_{xz} = \mu \left(\frac{\partial u_x}{\partial z} + \frac{\partial u_z}{\partial x} \right) \quad \sigma_{yz} = \mu \left(\frac{\partial u_y}{\partial z} + \frac{\partial u_z}{\partial y} \right) , \quad (14f)$$



ROD AND COORDINATE SYSTEM

Figure 1

where λ and μ are Lamé's constants. The Laplace transform of these equations is taken by multiplying them by e^{-pt} and integrating over t from zero to infinity. Since it is assumed that the rod is initially at rest, it is only necessary to replace $\frac{\partial}{\partial t}$ in equations 14 by p and indicate transformed variables by a bar. The definition of the Laplace transform of any function, φ , and its inversion integral are

$$\bar{\varphi}(x, y, z, p) = \int_0^{\infty} \varphi(x, y, z, t) e^{-pt} dt \quad (15a)$$

$$\varphi(x, y, z, t) = \frac{1}{2\pi i} \int_{Br_1} \bar{\varphi}(x, y, z, p) e^{pt} dp, \quad (15b)$$

where Br_1 is the Bromwich contour, which is located in the right half p plane to the right of all singularities.

Next, sine and cosine transforms of equations 14 are taken.

The double transforms are defined here as

$$\left. \begin{aligned} \text{(sine)} \quad \bar{\bar{\varphi}}(x, y, \kappa, p) &= -i \int_0^{\infty} \bar{\varphi}(x, y, z, p) \sin \kappa z dz \\ \text{(cosine)} \quad \bar{\bar{\varphi}}(x, y, \kappa, p) &= \int_0^{\infty} \bar{\varphi}(x, y, z, p) \cos \kappa z dz. \end{aligned} \right\} (16a)$$

For either type of transform the single inversion integral,

$$\bar{\varphi}(x, y, z, p) = \frac{1}{\pi} \int_{-\infty}^{\infty} \bar{\bar{\varphi}}(x, y, \kappa, p) e^{i\kappa z} d\kappa, \quad (16b)$$

is correct. The important thing about Folk, Fox, Shook and Curtis' method is that it is possible to take sine and cosine transforms of

equations 14 such that each variable appears as either a sine or cosine transform, but not both. Two schemes may be used, and they are outlined in table 1.

TABLE 1*		
	Scheme 1	Scheme 2
Equations Laplace-cosine transformed	14a, 14f	14b, 14c 14d, 14e
Equations Laplace-sine transformed	14b, 14c 14d, 14e	14a, 14f
Variables Laplace-cosine transformed	$u_z, \sigma_{xz}, \sigma_{yz}, \psi$	$u_x, u_y, \sigma_{xy}, \sigma_{xx}, \sigma_{yy}, \sigma_{zz}, \varphi$
Variables Laplace-sine transformed	$u_x, u_y, \sigma_{xy}, \sigma_{xx}, \sigma_{yy}, \sigma_{zz}, \varphi$	$u_z, \sigma_{xz}, \sigma_{yz}, \psi$
Boundary conditions asked for at $z = 0$	$\sigma_{zz}, u_x, u_y, \varphi, \partial\psi/\partial z$	$u_z, \sigma_{xz}, \sigma_{yz}, \psi, \partial\varphi/\partial z$

The equations for the double transforms are

$$\left. \begin{aligned}
 ik \bar{\sigma}_{zz} + \frac{\partial \bar{\sigma}}{\partial y} yz + \frac{\partial \bar{\sigma}}{\partial x} xz - \rho p^2 \bar{u}_z &= \left[\begin{array}{c} \bar{\sigma}_{zz} |_{z=0} \\ 0 \end{array} \right] \\
 \frac{\partial \bar{\sigma}}{\partial x} xx + \frac{\partial \bar{\sigma}}{\partial y} xy + ik \bar{\sigma}_{xz} - \rho p^2 \bar{u}_x &= \left[\begin{array}{c} 0 \\ \bar{\sigma}_{xz} |_{z=0} \end{array} \right] \\
 \frac{\partial \bar{\sigma}}{\partial y} yy + \frac{\partial \bar{\sigma}}{\partial x} xy + ik \bar{\sigma}_{yz} - \rho p^2 \bar{u}_y &= \left[\begin{array}{c} 0 \\ \bar{\sigma}_{yz} |_{z=0} \end{array} \right]
 \end{aligned} \right\} (17a)$$

* φ and ψ are the displacement potentials defined and used in sections IV and V.

$$\left. \begin{aligned}
 \sigma_{zz} &= \lambda \left(\frac{\partial \bar{u}_x}{\partial x} + \frac{\partial \bar{u}_y}{\partial y} \right) + (\lambda + 2\mu) i\kappa \bar{u}_z - \left[\begin{array}{c} 0 \\ (\lambda + 2\mu) \bar{u}_z \end{array} \right]_{z=0} \\
 \sigma_{xx} &= \lambda \left(\frac{\partial \bar{u}_y}{\partial y} + i\kappa \bar{u}_z \right) + (\lambda + 2\mu) \frac{\partial \bar{u}_x}{\partial x} - \left[\begin{array}{c} 0 \\ \lambda \bar{u}_z \end{array} \right]_{z=0} \\
 \sigma_{yy} &= \lambda \left(\frac{\partial \bar{u}_x}{\partial x} + i\kappa \bar{u}_z \right) + (\lambda + 2\mu) \frac{\partial \bar{u}_y}{\partial y} - \left[\begin{array}{c} 0 \\ \lambda \bar{u}_z \end{array} \right]_{z=0} \\
 \sigma_{xy} &= \mu \left(\frac{\partial \bar{u}_x}{\partial y} + \frac{\partial \bar{u}_y}{\partial x} \right) \\
 \sigma_{xz} &= \mu \left(\frac{\partial \bar{u}_z}{\partial x} + i\kappa \bar{u}_x \right) - \left[\begin{array}{c} \mu \bar{u}_x \\ 0 \end{array} \right]_{z=0} \\
 \sigma_{yz} &= \mu \left(\frac{\partial \bar{u}_z}{\partial y} + i\kappa \bar{u}_y \right) - \left[\begin{array}{c} \mu \bar{u}_y \\ 0 \end{array} \right]_{z=0}
 \end{aligned} \right\} (17b)$$

They are derived by taking the Laplace transforms of equations 14 and then multiplying by either $\cos \kappa z$ or $-i \sin \kappa z$ and integrating over z from zero to infinity. The boundary terms are different according to the two schemes of table 1 and are given in brackets with scheme 1 above and scheme 2 below. Notice that the two schemes ask for different boundary conditions at the end of the rod. Both schemes ask for mixed boundary conditions, which involve both stresses and displacements. This is a serious

shortcoming of equations 17, for nonmixed boundary conditions are known in the very important pressure shock problem.

C. SOLUTION USING MODES OF PROPAGATION

Orthogonality Properties

The analogy between vibration problems and propagation problems may now be made clear. Equations 17 should be compared to equations 8. In equations 17 the terms in brackets are the forcing functions. The remaining terms constitute the homogeneous equations for the modes. The eigen parameter is p^2 . The eigen value problem must be solved for all values of κ . Letting the superscript, (n), represent the nth mode, for which the eigen value is $p_n(\kappa)$, the equations for the modes are

$$\left. \begin{aligned} ik\sigma_{zz}^{(n)} + \frac{\partial\sigma_{yz}^{(n)}}{\partial y} + \frac{\partial\sigma_{xz}^{(n)}}{\partial x} - \rho p_n^2 u_z^{(n)} &= 0 \\ \frac{\partial\sigma_{xx}^{(n)}}{\partial x} + \frac{\partial\sigma_{xy}^{(n)}}{\partial y} + ik\sigma_{xz}^{(n)} - \rho p_n^2 u_x^{(n)} &= 0 \end{aligned} \right\} (18a)$$

$$\left. \begin{aligned} \frac{\partial\sigma_{yy}^{(n)}}{\partial y} + \frac{\partial\sigma_{xy}^{(n)}}{\partial x} + ik\sigma_{yz}^{(n)} - \rho p_n^2 u_y^{(n)} &= 0 \\ \sigma_{zz}^{(n)} &= \lambda \left(\frac{\partial u_x^{(n)}}{\partial x} + \frac{\partial u_y^{(n)}}{\partial y} \right) + (\lambda + 2\mu) i\kappa u_z^{(n)} \\ \sigma_{xx}^{(n)} &= \lambda \left(\frac{\partial u_y^{(n)}}{\partial y} + i\kappa u_z^{(n)} \right) + (\lambda + 2\mu) \frac{\partial u_x^{(n)}}{\partial x} \\ \sigma_{yy}^{(n)} &= \lambda \left(\frac{\partial u_x^{(n)}}{\partial x} + i\kappa u_z^{(n)} \right) + (\lambda + 2\mu) \frac{\partial u_y^{(n)}}{\partial y} \\ \sigma_{xy}^{(n)} &= \mu \left(\frac{\partial u_x^{(n)}}{\partial y} + \frac{\partial u_y^{(n)}}{\partial x} \right) \\ \sigma_{xz}^{(n)} &= \mu \left(\frac{\partial u_z^{(n)}}{\partial x} + i\kappa u_x^{(n)} \right) \quad \sigma_{yz}^{(n)} = \mu \left(\frac{\partial u_z^{(n)}}{\partial y} + i\kappa u_y^{(n)} \right) \end{aligned} \right\} (18b)$$

A variational principle similar to equation 1 will aid in investigating the properties of certain modes. The correct form is

$$\delta L = \delta \int \int_A \left[-\rho p_n^2 (u_x^{(n)} u_x^{(n)*} + u_y^{(n)} u_y^{(n)*} + u_z^{(n)} u_z^{(n)*}) - \sigma_{xx}^{(n)} \frac{\partial u_x^{(n)*}}{\partial x} - \sigma_{yy}^{(n)} \frac{\partial u_y^{(n)*}}{\partial y} - \sigma_{zz}^{(n)} (iku_z^{(n)})^* - \sigma_{xy}^{(n)} \left(\frac{\partial u_x^{(n)}}{\partial y} + \frac{\partial u_y^{(n)}}{\partial x} \right) - \sigma_{xz}^{(n)} \left(iku_x^{(n)} + \frac{\partial u_z^{(n)*}}{\partial x} \right) - \sigma_{yz}^{(n)} \left(iku_y^{(n)} + \frac{\partial u_z^{(n)*}}{\partial y} \right) \right] dx dy = 0, \quad (19)$$

where the integration is over the area of the rod and the * represents complex conjugation. The equations of motion, equations 18a, can be derived from equation 19 by inspection. It is only necessary to notice that equation 19 contains a Hermitian form* and that it can be integrated by parts using the boundary conditions on the lateral surfaces. The terms in equation 19 can be matched one by one with the terms in equations 18a. The detailed steps are the same as those used to derive equations 8 from equation 1.

The orthogonality relation is derived by writing an integral similar to the one in equation 9. The correct bilinear form is

$$I = \iint_A \left[-\sigma_{xx}^{(n)} \frac{\partial u_x^{(m)*}}{\partial x} - \sigma_{yy}^{(n)} \frac{\partial u_y^{(m)*}}{\partial y} - \sigma_{zz}^{(n)} (iku_z^{(m)})^* - \sigma_{xy}^{(n)} \left(\frac{\partial u_x^{(m)}}{\partial y} + \frac{\partial u_y^{(m)}}{\partial x} \right) \right] \quad (20)$$

*The Hermitian form is the extension to complex functions of the symmetric form used in section IIA.

$$\begin{aligned}
 & -\sigma_{xz}^{(n)} \left(iku_x^{(m)} + \frac{\partial u_z^{(m)}}{\partial x} \right)^* \\
 & -\sigma_{yz}^{(n)} \left(iku_y^{(m)} + \frac{\partial u_z^{(m)}}{\partial y} \right)^* \Big] dx dy . \tag{20}
 \end{aligned}$$

(cont'd)

I is integrated by parts, again using the boundary conditions, to find the form analogous to equation 10;

$$\begin{aligned}
 I = \iint_A & \left[\frac{\partial \sigma_{xx}^{(n)}}{\partial x} u_x^{(m)*} + \frac{\partial \sigma_{yy}^{(n)}}{\partial y} u_y^{(m)*} + i\kappa \sigma_{zz}^{(n)} u_z^{(m)*} \right. \\
 & + \frac{\partial \sigma_{xy}^{(n)}}{\partial y} u_x^{(m)*} + \frac{\partial \sigma_{xy}^{(n)}}{\partial x} u_y^{(m)*} + i\kappa \sigma_{xz}^{(n)} u_x^{(m)*} \\
 & \left. + \frac{\partial \sigma_{xz}^{(n)}}{\partial x} u_z^{(m)*} + i\kappa \sigma_{yz}^{(n)} u_y^{(m)*} + \frac{\partial \sigma_{yz}^{(n)}}{\partial y} u_z^{(m)*} \right] dx dy . \tag{21}
 \end{aligned}$$

Then, the equations of motion for the modes, equations 18a, are substituted to find (see equation 11)

$$I = \rho p_n^2 \iint_A \left[u_x^{(n)} u_x^{(m)*} + u_y^{(n)} u_y^{(m)*} + u_z^{(n)} u_z^{(m)*} \right] dx dy . \tag{22}$$

I is real and negative when $n = m$, according to the definition, equation 20. Then, letting $n = m$ in equation 22, it may be concluded that p_n^2 must be real and negative. That is, the frequencies of the modes of propagation are real when the wave number, κ , is real*.

* It is known for the circular rod that there are modes of propagation with real frequency and complex wave number.

Physically, this represents a lack of dissipation and a stable solution.

Interchanging n and m in equation 22, it follows that (see equation 12)

$$(p_n^2 p_m^2) \iint_A \left[u_x^{(n)} u_x^{(m)*} + u_y^{(n)} u_y^{(m)*} + u_z^{(n)} u_z^{(m)*} \right] dx dy = 0. \quad (23)$$

The integral in equation 23 must be zero if p_n^2 and p_m^2 are unequal. If, at a particular value of κ , there are linearly independent modes with the same value of the eigen parameter p^2 , they may be combined by means of the Gram-Schmidt orthogonalization process (reference 16, p. 50) into modes for which the integral in equation 23 does vanish. Thus, associated with the homogeneous equations 18 are the modes of propagation among which one may write the orthogonality relation (see equation 13)

$$\iint_A \left[u_x^{(n)} u_x^{(m)*} + u_y^{(n)} u_y^{(m)*} + u_z^{(n)} u_z^{(m)*} \right] dx dy = \begin{cases} 0 & n \neq m \\ 1 \text{ (say)} & n = m \end{cases} \quad (24)$$

According to equations 24, the modes of propagation are a set of orthonormal functions.

Expansion in Terms of Modes

The orthogonality relation makes it possible to solve equations 17 by writing the double transforms as an expansion in terms of the modes of propagation. We assume that there exist functions of κ , $\Gamma_n(\kappa, p)$, such that the double transforms can be represented

by the sums

$$\bar{u}_i(x, y, \kappa, p) = \sum_m \Gamma_m(\kappa, p) u_i^{(m)}(x, y; \kappa), \quad (25)$$

where $i = x, y, z$.

Following a common procedure, the three equations 25 are multiplied by $u_x^{(n)*}$, $u_y^{(n)*}$, and $u_z^{(n)*}$, respectively, added together, and integrated over the area of the rod. Equation 24 guarantees that only one term in the sum over m is nonzero. Then,

$$\Gamma_n = \iint_A \left[\bar{u}_x u_x^{(n)*} + \bar{u}_y u_y^{(n)*} + \bar{u}_z u_z^{(n)*} \right] dx dy \quad (26)$$

can be used to determine the Γ_n .

Consider the appropriate, nearly Hermitian integral,

$$\begin{aligned} I' = \iint_A \left[-\sigma_{xx}^{(n)} \frac{\partial \bar{u}_x}{\partial x} - \sigma_{yy}^{(n)} \frac{\partial \bar{u}_y}{\partial y} - \sigma_{zz}^{(n)} (i\kappa \bar{u}_z)^* - \sigma_{xy}^{(n)} \left(\frac{\partial \bar{u}_x}{\partial y} + \frac{\partial \bar{u}_y}{\partial x} \right)^* \right. \\ \left. - \sigma_{xz}^{(n)} \left(i\kappa \bar{u}_x + \frac{\partial \bar{u}_z}{\partial x} \right)^* - \sigma_{yz}^{(n)} \left(i\kappa \bar{u}_y + \frac{\partial \bar{u}_z}{\partial y} \right)^* \right] dx dy. \quad (27a) \end{aligned}$$

I' is not Hermitian because the definitions of the double transforms of the stresses, equations 17b, contain some of the forcing terms. The forcing terms must be included in the second equation, for I'^* ,

$$\begin{aligned}
 I^* = \iint_A & \left\{ - \left(\sigma_{xx}^{(n)} + \begin{bmatrix} 0 \\ \lambda \bar{u}_z |_{z=0} \end{bmatrix} \right) \frac{\partial u_x^{(n)*}}{\partial x} - \left(\sigma_{yy}^{(n)} + \begin{bmatrix} 0 \\ \lambda \bar{u}_z |_{z=0} \end{bmatrix} \right) \frac{\partial u_y^{(n)*}}{\partial y} \right. \\
 & - \left(\sigma_{zz}^{(n)} + \begin{bmatrix} 0 \\ (\lambda + 2\mu) \bar{u}_z |_{z=0} \end{bmatrix} \right) (iku_z^{(n)*} - \sigma_{xy}^{(n)} \left(\frac{\partial u_x^{(n)*}}{\partial y} + \frac{\partial u_y^{(n)*}}{\partial x} \right)) \\
 & - \left(\sigma_{xz}^{(n)} + \begin{bmatrix} \mu \bar{u}_x |_{z=0} \\ 0 \end{bmatrix} \right) \left(iku_x^{(n)*} + \frac{\partial u_z^{(n)*}}{\partial x} \right) \\
 & \left. - \left(\sigma_{yz}^{(n)} + \begin{bmatrix} \mu \bar{u}_y |_{z=0} \\ 0 \end{bmatrix} \right) \left(iku_y^{(n)*} + \frac{\partial u_z^{(n)*}}{\partial y} \right) \right\} dx dy.
 \end{aligned} \tag{27b}$$

First, I' is evaluated by integrating equation 27a by parts and using the boundary conditions at the rod lateral surfaces. The result is

$$\begin{aligned}
 I' = \iint_A & \left[\frac{\partial \sigma_{xx}^{(n)}}{\partial x} \bar{u}_x^* + \frac{\partial \sigma_{yy}^{(n)}}{\partial y} \bar{u}_y^* + ik\sigma_{zz}^{(n)} \bar{u}_z^* + \frac{\partial \sigma_{xy}^{(n)}}{\partial y} \bar{u}_x^* \right. \\
 & + \frac{\partial \sigma_{xy}^{(n)}}{\partial x} \bar{u}_y^* + ik\sigma_{xz}^{(n)} \bar{u}_x^* + \frac{\partial \sigma_{xz}^{(n)}}{\partial x} \bar{u}_z^* + ik\sigma_{yz}^{(n)} \bar{u}_y^* \\
 & \left. + \frac{\partial \sigma_{yz}^{(n)}}{\partial y} \bar{u}_z^* \right] dx dy.
 \end{aligned} \tag{28}$$

Substituting equations 18a we find

$$I' = \rho p_n^2 \iint_A (u_x^{(n)} \bar{u}_x^* + u_y^{(n)} \bar{u}_y^* + u_z^{(n)} \bar{u}_z^*) dx dy. \quad (29)$$

Next, I'^* is evaluated by writing equation 27b as two integrals. One integral is integrated by parts using the boundary conditions and the second integral (corresponding to the bracketed terms in equation 27b) is simplified by substituting the definitions of $\sigma_{zz}^{(n)}$, $\sigma_{xz}^{(n)}$, and $\sigma_{yz}^{(n)}$ from equations 18b. The result is

$$\begin{aligned} I'^* = & \iint_A \left[\frac{\partial \bar{\sigma}_{xx}}{\partial x} u_x^{(n)*} + \frac{\partial \bar{\sigma}_{yy}}{\partial y} u_y^{(n)*} + i k \bar{\sigma}_{zz} u_z^{(n)*} + \frac{\partial \bar{\sigma}_{xy}}{\partial y} u_x^{(n)*} \right. \\ & + \frac{\partial \bar{\sigma}_{xy}}{\partial x} u_y^{(n)*} + i k \bar{\sigma}_{xz} u_x^{(n)*} + \frac{\partial \bar{\sigma}_{xz}}{\partial x} u_z^{(n)*} + i k \bar{\sigma}_{yz} u_y^{(n)*} \\ & \left. + \frac{\partial \bar{\sigma}_{yz}}{\partial y} u_z^{(n)*} \right] dx dy \\ & - \iint_A \left\{ \begin{bmatrix} 0 \\ \bar{u}_z |_{z=0} \end{bmatrix} \sigma_{zz}^{(n)*} + \begin{bmatrix} \bar{u}_x |_{z=0} \\ 0 \end{bmatrix} \sigma_{xz}^{(n)*} + \begin{bmatrix} \bar{u}_y |_{z=0} \\ 0 \end{bmatrix} \sigma_{yz}^{(n)*} \right\} dx dy. \end{aligned} \quad (30)$$

Equations 17a are then substituted into equation 30 to give

$$\begin{aligned} I'^* = & \rho p_n^2 \iint_A \left[\bar{u}_x u_x^{(n)*} + \bar{u}_y u_y^{(n)*} + \bar{u}_z u_z^{(n)*} \right] dx dy \\ & + \iint_A \left\{ \begin{bmatrix} \bar{\sigma}_{zz} |_{z=0} \\ 0 \end{bmatrix} u_z^{(n)*} + \begin{bmatrix} 0 \\ \bar{\sigma}_{xz} |_{z=0} \end{bmatrix} u_x^{(n)*} + \begin{bmatrix} 0 \\ \bar{\sigma}_{yz} |_{z=0} \end{bmatrix} u_y^{(n)*} \right\} dx dy \quad (31) \end{aligned}$$

$$\left. \begin{aligned} & \left[\begin{array}{c} 0 \\ \bar{u}_z|_{z=0} \end{array} \right] \sigma_{zz}^{(n)*} - \left[\begin{array}{c} \bar{u}_x|_{z=0} \\ 0 \end{array} \right] \sigma_{xz}^{(n)*} - \left[\begin{array}{c} \bar{u}_y|_{z=0} \\ 0 \end{array} \right] \sigma_{yz}^{(n)*} \end{aligned} \right\} dx dy. \quad (31)$$

Equations 26, 29, and 31 can be combined easily to find the expansion coefficients;

scheme 1,

$$\Gamma_n = \frac{1}{\rho(p_n^2 - p^2)} \iint_A \left[\bar{\sigma}_{zz}|_{z=0} u_z^{(n)*} - \bar{u}_x|_{z=0} \sigma_{xz}^{(n)*} - \bar{u}_y|_{z=0} \sigma_{yz}^{(n)*} \right] dx dy; \quad (32a)$$

scheme 2,

$$\Gamma_n = \frac{1}{\rho(p_n^2 - p^2)} \iint_A \left[-\bar{u}_z|_{z=0} \sigma_{zz}^{(n)*} + \bar{\sigma}_{xz}|_{z=0} u_x^{(n)*} + \bar{\sigma}_{yz}|_{z=0} u_y^{(n)*} \right] dx dy. \quad (32b)$$

Together, equations 25 and 32 are the solutions for the double transforms in terms of the modes of propagation.

Inversion of the Transforms

The displacements are found from their double transforms by using the inversion theorems, equations 15b and 16b. Because $p_n^2 - p^2$ appears in equations 32 for the Γ_n , it is convenient to invert

the Laplace transform over time first. It will be necessary to interchange the order of certain integrals and summations. The required uniform convergence of the integrals and sums will be assumed.

In accordance with the definition of the Laplace transform, equation 15a, $\sigma_{zz}|_{z=0}(x, y, p)$, for example, is replaced by

$$\int_0^{\infty} \sigma_{zz}|_{z=0}(x, y, \tau) e^{-p\tau} d\tau.$$

Then the inversion integrals, equations 15b and 16b, are applied to the double transform for u_i , equations 25 and 32, to give the formal solution for scheme 1

$$u_i(x, y, z, t) = \frac{1}{2\pi^2 i} \int_{-\infty}^{\infty} d\kappa e^{i\kappa z} \int_{Br_1} dp e^{pt} \sum_n \frac{u_i^{(n)}(x, y; \kappa)}{\rho[p_n^2(\kappa) - p^2]} \iint_A d\xi d\eta \int_0^{\infty} d\tau e^{-p\tau} \left[\sigma_{zz}|_{z=0}(\xi, \eta, \tau) u_z^{(n)*}(\xi, \eta; \kappa) - u_x|_{z=0}(\xi, \eta, \tau) \sigma_{xz}^{(n)*}(\xi, \eta; \kappa) - u_y|_{z=0}(\xi, \eta, \tau) \sigma_{yz}^{(n)*}(\xi, \eta; \kappa) \right]. \quad (33)$$

with a similar expression for scheme 2.

The inversion integral over p can be carried out using Cauchy's residue theorem. The Bromwich contour is to the right of all singularities in the p plane. For $t < \tau$ the contour is completed to the right where there are no singularities, and for $t > \tau$ the contour is completed to the left around the singularities at $p = +p_n$ and

$p = -p_n$. The integral over p is

$$\int_{Br_1} \frac{e^{p(t-\tau)}}{(p_n-p)(p_n+p)} dp = \begin{cases} 2\pi i \left[-\frac{e^{p_n(t-\tau)}}{2p_n} + \frac{e^{-p_n(t-\tau)}}{2p_n} \right] & t > \tau \\ 0 & t < \tau \end{cases} \quad (34)$$

The integration over τ in equation 33 is carried only up to the value t because of equation 34. Letting $p_n = i\omega_n$, equation 34 is then substituted into equation 33. The results for the displacement u_i are for scheme 1

$$u_i = \frac{-1}{2\pi i} \sum_n \int_{-\infty}^{\infty} d\kappa \frac{e^{i\kappa z}}{\omega_n(\kappa)} \frac{u_i^{(n)}(x, y; \kappa)}{\omega_n(\kappa)} \int_0^t d\tau \left(\frac{e^{i\omega_n(\kappa)(t-\tau)} - e^{-i\omega_n(\kappa)(t-\tau)}}{-e^{-i\omega_n(\kappa)(t-\tau)}} \right) \iint_A d\xi d\eta \quad (35a)$$

$$\left[\sigma_{zz} \Big|_{z=0} (\xi, \eta, \tau) u_z^{(n)*}(\xi, \eta; \kappa) - u_x \Big|_{z=0} (\xi, \eta, \tau) \sigma_{xz}^{(n)*}(\xi, \eta; \kappa) - u_y \Big|_{z=0} (\xi, \eta, \tau) \sigma_{yz}^{(n)*}(\xi, \eta; \kappa) \right]$$

For scheme 2* the expression in brackets in equation 35a is replaced by

*The boundary conditions asked for by scheme 2 correspond to the longitudinal impact problem.

$$\left[-u_z \Big|_{z=0} \sigma_{zz}^{(n)*} + \sigma_{xz} \Big|_{z=0} u_x^{(n)*} + \sigma_{yz} \Big|_{z=0} u_y^{(n)*} \right] \quad (35b)$$

In equations 35 the integral over τ is a convolution integral. The infinite sum and the integral over κ show that the response is composed of contributions from all parts of all modes. The inner double integral over the area gives the magnitude of the contribution from each part of each mode. This magnitude depends on the distribution of the load over the end of the rod. The two exponentials represent harmonic waves travelling to the left and to the right, respectively.

When the load has a simple form and the modes are known explicitly, the integrals over the area and over τ can be carried out explicitly. The double transform solutions found by Skalak (5) and Folk, Fox, Shook, and Curtis (6) took forms similar to equation 35. Lloyd (18) has pointed out an essential difference in form between the solutions given by Folk et al. and the solutions given by Skalak and equation 35. Folk et al. found their solutions by integrating over κ first. The result includes modes for which κ is complex, but only those real modes with group velocities such that the waves move toward the right. In the present and Skalak's solution wave groups travelling to both the right and left are found, but complex modes are not used unless κ is extended to complex values through contour integration as pointed out by Miklowitz (17). Lloyd (18) discussed in detail the similarities between the two types of solutions.

The solution in equation 35 might be used in two ways. First, solutions for complicated end loads on circular rods and flat plates might be found. The modes are known in explicit form, and so the inner integrals can be carried out. In particular, one could study the effects of a load applied to a circular area centered on the end of a circular rod. The second way of using the above equations is to study the noncircular rod. That is the purpose of the following section.

III. LONG WAVES IN A NONCIRCULAR ROD

Through the use of the method of stationary phase Skalak (5) showed that the large disturbance at long times after the application of an axial load to the end of a circular semi-infinite rod came from the low frequency, long waves of the lowest compressional mode. The longest waves from the higher modes trail far behind the head of the pulse and are easily detected as Miklowitz and Nisewanger (2, 19) noted, because they travel with group velocities approaching zero. Knowledge of the longest waves of the higher modes of the exact theory has also proved useful, as Mindlin and Herrmann showed, for improving the accuracy of approximate theories. This background and the fact that the higher mode, long wave response can also be approximated by the method of stationary phase provide reasons for investigating equations 18 for the modes by a perturbation scheme for long wave lengths, i. e., small κ .

In the work below the investigation of the modes at small κ is followed by a related approximation of the exact theory solution, equation 35. The approximation gives the contribution to the response from the longest waves. Then, an approximate theory with five modes is developed. The approximate theory is similar to the three mode theory given by Mindlin and McNiven (20) for the circular rod. The difference in number of modes required for an approximate theory of a noncircular rod provides an interesting contrast. The exact theory is used as a guide for discussing the approximate theory.

Only a little work has been done previously on the noncircular rod. Love (reference 8, p. 428) gave a single mode approximate theory. Chree (21) and Gazis and Mindlin (22) studied the longest waves and derived approximate frequency equations. These three works are discussed in greater detail and compared to the present work following equation 51 below. Volterra (23) derived a more complex approximate theory by his method of internal constraints and has studied the resulting frequency equation. Mindlin and Fox (24) have used the exact theory to find modes of propagation in a rectangular rod, but only for certain wave numbers and certain ratios of width to thickness.

A. THE PERTURBATION SCHEME

The solution to equations 18 for the modes is now assumed in the form of a Taylor series at κ equal to zero. The frequency is written as

$$-p_n^2 = \omega_n^2 = \Omega_n^2 + (i\kappa)^2 C_n + (i\kappa)^4 D_n + \dots \quad (36)$$

There are no odd powers of $i\kappa$ in equation 36 since the frequency should not depend on the sign of κ . The Ω_n are cut off frequencies, i. e. frequencies for which $\kappa = 0$. For the first compressional mode, Ω_0 is zero and $-C_0$ is the square of the velocity of propagation of the longest waves, $\sqrt{\frac{E}{\rho}}$, where E is Young's modulus.

Writing the displacements in a series in all powers of $i\kappa$ and substituting into equations 18, there is a separation of terms

so that there are two separate problems and two sets of modes.

For the first set of modes the expansion

$$\left. \begin{aligned} u_x^{(n)}(x,y;k) &= iku_{x1}^{(n)}(x,y) + (ik)^3 u_{x2}^{(n)}(x,y) + \dots \\ u_y^{(n)} &= iku_{y1}^{(n)} + (ik)^3 u_{y2}^{(n)} + \dots \\ u_z^{(n)} &= u_{z0}^{(n)} + (ik)^2 u_{z1}^{(n)} + (ik)^4 u_{z2}^{(n)} + \dots \end{aligned} \right\} (37a)$$

holds. For the second set of modes we write a slightly different form,

$$\left. \begin{aligned} u_x^{(n)} &= u_{x1}^{(n)} + (ik)^2 u_{x2}^{(n)} + \dots \\ u_y^{(n)} &= u_{y1}^{(n)} + (ik)^2 u_{y2}^{(n)} + \dots \\ u_z^{(n)} &= iku_{z1}^{(n)} + (ik)^3 u_{z2}^{(n)} + \dots \end{aligned} \right\} (37b)$$

with u_{z0} equal to zero. Obviously, all of the governing equations for the two sets of modes are the same except for the normalization condition in equation 24. Equations 37 are substituted into equation 24 with n equal to m so that equation 24 can be expanded according to powers of ik for either set of modes. The resulting normalization conditions are, respectively, for the two sets of modes

$$\left. \begin{aligned} \iint_A u_{z0}^2 dx dy = 1 \quad \iint_A (2u_{z0}u_{z1} - u_{x1}^2 - u_{y1}^2) dx dy = 0 \\ \iint_A (2u_{z0}u_{z2} - 2u_{x1}u_{x2} - 2u_{y1}u_{y2} + u_{z1}^2) dx dy = 0 \quad \text{etc.} \end{aligned} \right\} (38a)$$

Note at the top of page 31

$$\left. \begin{aligned} \iint_A (u_{x1}^2 + u_{y1}^2) dx dy &= 1 \quad (u_{z0} = 0) \\ \iint (2u_{x1} u_{x2} + 2u_{y1} u_{y2} - u_{z1}^2) dx dy &= 0 \quad \text{etc.} \end{aligned} \right\} (38b)$$

where the superscript (n) is omitted.

The assumed expansions, equations 37, are substituted into equations 18b defining the stresses to find definitions for the perturbed stresses. The results are

$$\begin{aligned} \sigma_{xx} &= i\kappa \sigma_{xx1} + (i\kappa)^3 \sigma_{xx2} + \dots & \sigma_{yy} &= i\kappa \sigma_{yy1} + (i\kappa)^3 \sigma_{yy2} + \dots \\ \sigma_{zz} &= i\kappa \sigma_{zz1} + (i\kappa)^3 \sigma_{zz2} + \dots & \sigma_{xy} &= i\kappa \sigma_{xy1} + (i\kappa)^3 \sigma_{xy2} + \dots \\ \sigma_{xz} &= \sigma_{xzo} + (i\kappa)^2 \sigma_{xz1} + (i\kappa)^4 \sigma_{xz2} + \dots & \sigma_{yz} &= \sigma_{yzo} + (i\kappa)^2 \sigma_{yz1} + (i\kappa)^4 \sigma_{yz2} + \dots \end{aligned} \quad (39a)$$

Divide the right hand sides of equations 39a

by $i\kappa$ and set $\sigma_{xzo} = \sigma_{yzo} = 0$.

where

$$\left. \begin{aligned} \sigma_{xx1} &= \lambda \left(\frac{\partial u_{y1}}{\partial y} + u_{z0} \right) + (\lambda + 2\mu) \frac{\partial u_{x1}}{\partial x} & \sigma_{xx2} &= \lambda \left(\frac{\partial u_{y2}}{\partial y} + u_{z1} \right) + (\lambda + 2\mu) \frac{\partial u_{x2}}{\partial x} \\ \sigma_{yy1} &= \lambda \left(\frac{\partial u_{x1}}{\partial x} + u_{z0} \right) + (\lambda + 2\mu) \frac{\partial u_{y1}}{\partial y} & \sigma_{yy2} &= \lambda \left(\frac{\partial u_{x2}}{\partial x} + u_{z1} \right) + (\lambda + 2\mu) \frac{\partial u_{y2}}{\partial y} \\ \sigma_{zz1} &= \lambda \left(\frac{\partial u_{x1}}{\partial x} + \frac{\partial u_{y1}}{\partial y} \right) + (\lambda + 2\mu) u_{z0} & \sigma_{zz2} &= \lambda \left(\frac{\partial u_{x2}}{\partial x} + \frac{\partial u_{y2}}{\partial y} \right) + (\lambda + 2\mu) u_{z1} \\ \sigma_{xy1} &= \mu \left(\frac{\partial u_{x1}}{\partial y} + \frac{\partial u_{y1}}{\partial x} \right) & \sigma_{xy2} &= \mu \left(\frac{\partial u_{x2}}{\partial y} + \frac{\partial u_{y2}}{\partial x} \right) \end{aligned} \right\} (40)$$

$$\left. \begin{aligned} \sigma_{xzo} &= \mu \frac{\partial u_{zo}}{\partial x} & \sigma_{xz1} &= \mu \left(u_{x1} + \frac{\partial u_{z1}}{\partial x} \right) & \sigma_{xz2} &= \mu \left(u_{x2} + \frac{\partial u_{z2}}{\partial x} \right) \\ \sigma_{yzo} &= \mu \frac{\partial u_{zo}}{\partial y} & \sigma_{yz1} &= \mu \left(u_{y1} + \frac{\partial u_{z1}}{\partial y} \right) & \sigma_{yz2} &= \mu \left(u_{y2} + \frac{\partial u_{z2}}{\partial y} \right) \end{aligned} \right\} \begin{array}{l} (40) \\ (\text{cont'd}) \end{array}$$

The stress free boundary conditions must hold for each level of perturbation.

The differential equations for the perturbations are derived by substituting equations 36, 37, and 39 into the differential equations 18a. The coefficients of the separate powers of iK are set equal to zero. The results are easily seen to be for the first set of modes

$$\frac{\partial \sigma_{xzo}}{\partial x} + \frac{\partial \sigma_{yzo}}{\partial y} + \rho \Omega^2 u_{zo} = \mu \left(\frac{\partial^2 u_{zo}}{\partial x^2} + \frac{\partial^2 u_{zo}}{\partial y^2} \right) + \rho \Omega^2 u_{zo} = 0 \quad (41)$$

$$\frac{\partial \sigma_{xx1}}{\partial x} + \frac{\partial \sigma_{xy1}}{\partial y} + \sigma_{xzo} + \rho \Omega^2 u_{x1} = 0 \quad (42a)$$

$$\frac{\partial \sigma_{yy1}}{\partial y} + \frac{\partial \sigma_{xy1}}{\partial x} + \sigma_{yzo} + \rho \Omega^2 u_{y1} = 0 \quad (42b)$$

$$\sigma_{zz1} + \frac{\partial \sigma_{xz1}}{\partial x} + \frac{\partial \sigma_{yz1}}{\partial y} + \rho \Omega^2 u_{z1} + \rho C u_{zo} = 0 \quad (42c)$$

$$\frac{\partial \sigma_{xx2}}{\partial x} + \frac{\partial \sigma_{xy2}}{\partial y} + \sigma_{xz1} + \rho \Omega^2 u_{x2} + \rho C u_{x1} = 0 \quad (43a)$$

$$\frac{\partial \sigma_{yy2}}{\partial y} + \frac{\partial \sigma_{xy2}}{\partial x} + \sigma_{yz1} + \rho \Omega^2 u_{y2} + \rho C u_{y1} = 0 \quad (43b)$$

$$\sigma_{zz2} + \frac{\partial \sigma_{xz2}}{\partial x} + \frac{\partial \sigma_{yz2}}{\partial y} + \rho \Omega^2 u_{z2} + \rho C u_{z1} + \rho D u_{zo} = 0. \quad (43c)$$

Equations 41, 42c, and 43c are the coefficients of 1, $(i\kappa)^2$, and $(i\kappa)^4$, respectively, in equations 18a, while equations 42a and 42b are the coefficients of $i\kappa$ and equations 43a and 43b are the coefficients of $(i\kappa)^3$ in equations 18a. Equations 41, 42, and 43 also hold for the second set of modes, but u_{zo} , σ_{xzo} , and σ_{yzo} must be set equal to zero.

A variational principle for the above equations can be developed by substituting equations 37 and 39 into the integral L in equation 19. Terms are collected according to powers of $i\kappa$ so that for the two sets of modes, respectively,

$$L = L_0 + (i\kappa)^2 L_1 + (i\kappa)^4 L_2 + \dots$$

and $L = L_1 + (i\kappa)^2 L_2 + \dots$

There are no odd powers of $i\kappa$ because of the Hermitian property of L. If the variation of L is to be zero for all values of $i\kappa$, then the variations of L_0 , L_1 , and L_2 must all be zero. L_0 and L_1 are

$$\begin{aligned} L_0 &= \iint_A \left[\rho \Omega^2 u_{zo} u_{zo} - \sigma_{xzo} \frac{\partial u_{zo}}{\partial x} - \sigma_{yzo} \frac{\partial u_{zo}}{\partial y} \right] dx dy \\ L_1 &= \iint_A \left[\rho \Omega^2 (-u_{xl} u_{xl} - u_{yl} u_{yl} + u_{zo} u_{zl} + u_{zl} u_{zo}) + \rho C u_{zo} u_{zo} \right. \\ &+ \sigma_{xxl} \frac{\partial u_{xl}}{\partial x} + \sigma_{yy1} \frac{\partial u_{yl}}{\partial y} + \sigma_{zzl} u_{zo} + \sigma_{xyl} \left(\frac{\partial u_{xl}}{\partial y} + \frac{\partial u_{yl}}{\partial x} \right) \\ &\left. - \sigma_{xzl} \frac{\partial u_{zo}}{\partial x} - \sigma_{xzo} \left(u_{xl} + \frac{\partial u_{zl}}{\partial x} \right) - \sigma_{yzl} \frac{\partial u_{zo}}{\partial y} - \sigma_{yzo} \left(u_{yl} + \frac{\partial u_{zl}}{\partial y} \right) \right] dx dy. \end{aligned} \quad (44)$$

where u_{zo} , σ_{xzo} , and σ_{yzo} are zero in L_1 for the set of modes

governed by equations 38b. L_0 , L_1 , and L_2 are all bilinear and symmetric. Table 2 shows the way the differential equations 41 through 43 are derived from the variational principle. Notice that in certain cases the equations for the higher order unknown are derived by varying the lower order unknowns. For instance, using L_2 , the equation for u_{z2} is derived by varying u_{z0} .

TABLE 2

Equation	Variables	Variables varied in		
		L_0	L_1	L_2
41	$\Omega^{**}; u_{z0}^*$	u_{z0}^*	u_{z1}	u_{z2}
42a	$\Omega ; u_{z0}^*, u_{x1}, u_{y1}$	-	u_{x1}	u_{x2}
42b	$\Omega ; u_{z0}^*, u_{x1}, u_{y1}$	-	u_{y1}	u_{y2}
42c	$C^* \Omega ; u_{z0}^*, u_{x1}, u_{y1}, u_{z1}$	-	u_{z0}^*	u_{z1}
43a	$C, \Omega ; u_{z0}^*, u_{x1}, u_{y1}, u_{z1}, u_{x2}, u_{y2}$	-	-	u_{x1}
43b	$C, \Omega ; u_{z0}^*, u_{x1}, u_{y1}, u_{z1}, u_{x2}, u_{y2}$	-	-	u_{y1}
43c	$D^* C, \Omega ; u_{z0}^*, u_{x1}, u_{y1}, u_{z1}, u_{x2}, u_{y2}, u_{z2}$	-	-	u_{z0}^*

Equations 41, 42, and 43 must be solved under the alternative normalization conditions, equations 38a and 38b. Using equations 38a and setting u_{z0} equal to a constant, we will find the first compressional mode, for which Ω equals zero. The remaining

* If equations 38b govern, u_{z0} is not a variable, nor can it be varied to derive equations 41 through 43.

** Does not appear if equation 38b governs.

compressional modes consistent with equations 38a have nonzero cut off frequencies and will be referred to as "longitudinal shear modes". The modes found by using equations 38b will be called "radial modes". The flexural and torsional modes will not be discussed, although they too are governed by the above equations.

B. THE FIRST MODE

For the first compressional mode $u_{z0}^{(0)}$ is taken as a constant. Equations 41 and 42 can then be solved easily for the conditions of zero force acting on the boundary as follows. To do this, it is assumed that in addition to equation 41 and 42 there are the conditions

$$\left. \begin{aligned} \sigma_{xxl}^{(0)} &= \lambda \left(\frac{\partial u_{yl}^{(0)}}{\partial y} + u_{z0}^{(0)} \right) + (\lambda + 2\mu) \frac{\partial u_{xl}^{(0)}}{\partial x} = 0 \\ \sigma_{yy1}^{(0)} &= \lambda \left(\frac{\partial u_{xl}^{(0)}}{\partial x} + u_{z0}^{(0)} \right) + (\lambda + 2\mu) \frac{\partial u_{yl}^{(0)}}{\partial y} = 0 \\ \sigma_{xyl}^{(0)} &= \mu \left(\frac{\partial u_{xl}^{(0)}}{\partial y} + \frac{\partial u_{yl}^{(0)}}{\partial x} \right) = 0 \\ \sigma_{xzl}^{(0)} &= \mu \left(u_{xl}^{(0)} + \frac{\partial u_{zl}^{(0)}}{\partial x} \right) = 0 \\ \sigma_{yzl}^{(0)} &= \mu \left(u_{yl}^{(0)} + \frac{\partial u_{zl}^{(0)}}{\partial y} \right) = 0, \end{aligned} \right\} (45)$$

where equations 40 defining the perturbed stresses are used. Thus, the boundary is force free because all of the stresses appearing in the boundary conditions also appear in equations 45. Equations 41, 42, and 45 can all be satisfied provided Ω_0 is zero and $-C_0$ takes

on the value

$$-C_0 = \frac{\mu(3\lambda + 2\mu)}{\rho(\lambda + \mu)} = \frac{E}{\rho} = c_0^2, \quad (46)$$

which is the correct value for the square of the speed of propagation of infinitely long waves of the first compressional mode. The solution for the first mode is written with two undetermined constants of integration, x_0 and y_0 , as

$$\left. \begin{aligned} u_{z0}^{(0)} &= \frac{1}{\sqrt{A}} & u_{x1}^{(0)} &= -\frac{\nu}{\sqrt{A}}(x-x_0) & u_{y1}^{(0)} &= -\frac{\nu}{\sqrt{A}}(y-y_0) \\ u_{z1}^{(0)} &= \frac{\nu}{2\sqrt{A}} [(x-x_0)^2 + (y-y_0)^2] - \frac{\nu(\lambda+2\mu)}{4(\lambda+\mu)\sqrt{A}} (I_x + I_y), \end{aligned} \right\} (47)^*$$

where A is the area of the rod, $\nu = \frac{\lambda}{2(\lambda+\mu)}$ is Poisson's ratio, and I_x and I_y are the moments of inertia (divided by the area),

$$I_x = \frac{1}{A} \iint_A (x-x_0)^2 dx dy \quad I_y = \frac{1}{A} \iint_A (y-y_0)^2 dx dy.$$

In equations 47 some of the constants of integration have been determined by applying equations 38a. These results depend on the shape of the rod only through the moments of inertia. The transverse displacements are coupled to the axial displacement by Poisson's ratio.

* That equations 47 satisfy equations 41, 42, and 45 can easily be seen. For instance, the first two of equations 45 determine $\frac{\partial u_{x1}}{\partial x}$ and $\frac{\partial u_{y1}}{\partial y}$ and the last two of equations 45 relate u_{z1} to u_{x1} and u_{y1} . Equations 41, 42a, and 42b are satisfied trivially.

Equations 43 are difficult to solve; the solution depends on the shape of the rod. However, it is possible to find D_0 , which determines the dispersion of the longest waves. Integrating equation 43a over the area of the rod and using equations 47, one finds (Ω_0 and σ_{xz1} are zero.)

$$\frac{\nu \rho c^2}{\sqrt{A}} \iint_A (x-x_0) dx dy = \int \sigma_{xx2} \Big|_{x(y)} dy + \int \sigma_{xy2} \Big|_{y(x)} dx,$$

where the superscript (o) is omitted. The boundary conditions require that the two boundary terms add up to zero. Equation 43b can be integrated in a similar manner. This shows that x_0 and y_0 are the coordinates of the centroid of the rod.

The unknown, D_0 , is contained in equation 43c, which is integrated over the area using the first of equations 47 to give

$$\rho D_0 \sqrt{A} = \rho c_0^2 \iint_A u_{z1} dx dy - \iint \sigma_{zz2} dx dy - \int \sigma_{xz2} \Big|_{x(y)} dy - \int \sigma_{yz2} \Big|_{y(x)} dx \quad (48)$$

The boundary terms must vanish for the surface to be force free. To evaluate the integral with σ_{zz2} , one must first use the identity, found from equations 40 and 46,

$$\sigma_{zz2} = \rho c_0^2 u_{z1} + \nu (\sigma_{xx2} + \sigma_{yy2}). \quad (49)$$

Then, equation 43a is multiplied by $x-x_0$ and equation 43b is multiplied by $y-y_0$ and they are integrated over the area using equations 46 and 47 to give

$$\begin{aligned}
 \rho c_o^2 \frac{\nu}{\sqrt{A}} \iint_A (x-x_o)^2 dx dy &= - \iint_A (x-x_o) \left(\frac{\partial \sigma_{xx}}{\partial x} + \frac{\partial \sigma_{xy}}{\partial y} \right) dx dy \\
 &= \iint_A \sigma_{xx} dx dy - \int (x-x_o) \sigma_{xx} \Big|_{x(y)} dy - \int (x-x_o) \sigma_{xy} \Big|_{y(x)} dx \\
 \rho c_o^2 \frac{\nu}{\sqrt{A}} \iint_A (y-y_o)^2 dx dy &= \iint_A \sigma_{yy} dx dy \\
 &\quad - \int (y-y_o) \sigma_{yy} \Big|_{y(x)} dx - \int (y-y_o) \sigma_{xy} \Big|_{x(y)} dy
 \end{aligned} \tag{50}$$

Again, the boundary terms vanish. Equations 49 and 50 are then used in equation 48 to find D_o as

$$D_o = -\nu^2 c_o^2 (I_x + I_y) \tag{51}$$

$I_x + I_y$ is the polar moment of inertia of the area about its centroid.

Equations 46, 47, and 51 together give the behavior of the longest waves of the first compressional mode. Together with equation 36 they are an expansion of the frequency equation for the first mode. This expansion,

$$\omega^2 \approx c_o^2 \kappa^2 - \nu^2 c_o^2 (I_x + I_y) \kappa^4 \tag{52}$$

is like the approximate frequency equations found by Chree (21) and by Love (reference 8, p. 428) and is similar to an expansion found by Gazis and Mindlin (22). Chree expanded the displacements in powers of x and y and then neglected the higher powers of x and y rather than expanding on κ as was done here. Love developed a

single mode approximate theory more accurate than the elementary theory (one dimensional wave equation) by taking into account the radial inertia. The frequency equation for that approximate theory can be expanded for small κ and equation 52 results. The approaches used by Chree and by Love do not guarantee that the resulting frequency equation is a valid expansion for the first compressional mode of the exact theory. It is the exact theory which is of interest here; in particular, an exact value for the constant D_0 is desired. Gazis and Mindlin derived a frequency equation for the thin rectangular rod by using an approximate theory for thin plates given by Kane and Mindlin (25). Their approximate frequency equation is identical with equation 52 provided the rectangular rod is thin enough so that I_y can be neglected with respect to I_x , where the x direction is parallel to the width dimension of the rod. The inaccuracy for thicker rods can be blamed on the approximate theory used to derive the frequency equation.

C. HIGHER MODES

Longitudinal Shear Modes

The behavior of the longitudinal shear modes near $\kappa = 0$ is governed by equations 38a and 41 through 43. Equation 41 for u_{z0} must be solved under boundary conditions on $\sigma_{xz0} = \mu \frac{\partial u_{z0}}{\partial x}$ and $\sigma_{yz0} = \mu \frac{\partial u_{z0}}{\partial y}$. The boundary condition in terms of u_{z0} is a well known problem leading to discrete eigen values, $\frac{\rho}{\mu} \Omega_n^2$. The important features of the longitudinal shear modes near their cut

off frequencies are contained in the $u_{zo}^{(n)}$, Ω_n , and C_n . The following paragraphs contain a means of calculating the C_n from the known solutions for the $u_{zo}^{(n)}$ and Ω_n .

A useful expression is found by multiplying equation 42c by u_{zo} and integrating over the area of the rod;

$$\iint_A \left[\rho C u_{zo}^2 + \rho \Omega^2 u_{zl} u_{zo} + \sigma_{zzl} u_{zo} + \frac{\partial \sigma_{xzl}}{\partial x} u_{zo} + \frac{\partial \sigma_{y zl}}{\partial y} u_{zo} \right] dx dy = 0.$$

Integrating by parts and then setting the sum of the boundary terms equal to zero leads to the equation,

$$\iint_A \left[\rho C u_{zo}^2 + \rho \Omega^2 u_{zl} u_{zo} + \sigma_{zzl} u_{zo} - \sigma_{xzl} \frac{\partial u_{zo}}{\partial x} - \sigma_{y zl} \frac{\partial u_{zo}}{\partial y} \right] dx dy = 0.$$

The definitions of σ_{xzo} , σ_{yzo} , σ_{xzl} , and $\sigma_{y zl}$ are substituted to give

$$\iint_A \left[\rho C u_{zo}^2 + \rho \Omega^2 u_{zl} u_{zo} + \sigma_{zzl} u_{zo} - \sigma_{xzo} \left(u_{xl} + \frac{\partial u_{zl}}{\partial x} \right) - \sigma_{yzo} \left(u_{yl} + \frac{\partial u_{zl}}{\partial y} \right) \right] dx dy = 0.$$

This is integrated by parts, again using the boundary conditions to show that the boundary terms add up to zero, with the result

$$\iint_A \left[\rho C u_{zo}^2 + \rho \Omega^2 u_{zl} u_{zo} + \sigma_{zzl} u_{zo} - \sigma_{xzo} u_{xl} + u_{zl} \frac{\partial \sigma_{xzo}}{\partial x} - \sigma_{yzo} u_{yl} + u_{zl} \frac{\partial \sigma_{yzo}}{\partial y} \right] dx dy = 0.$$

Equations 41 and the first of 38a are then substituted to show that

$$\rho C = \iint_A \left[u_{xo} \sigma_{xzo} + u_{yl} \sigma_{yzo} - u_{zo} \sigma_{zxl} \right] dx dy. \quad (53)$$

Thus, u_{zl} is eliminated from the equations.

In order to use equation 53, it is necessary to determine u_{zo} , u_{xl} , and u_{yl} . An approximate solution for u_{xl} and u_{yl} will be found by using the Rayleigh-Ritz method. Notice in table 2 that equations 42a and 42b for u_{xl} and u_{yl} are found by varying u_{xl} and u_{yl} in the integral L_1 given in equation 44. We assume an approximate form for the unknowns,

$$u_{xl} = a_1 x \quad u_{yl} = a_2 y, \quad (54)$$

where the origin of coordinates is at the centroid of the area. L_1 is then a function of a_1 and a_2 , $\tilde{L}_1(a_1, a_2)$. The terms in \tilde{L}_1 containing a_1 and a_2 are

$$\begin{aligned} \frac{1}{A} \tilde{L}_1(a_1, a_2) = & -\rho\Omega^2 I_x a_1^2 - \rho\Omega^2 I_y a_2^2 + \lambda(a_1 + a_2)^2 \\ & + 2\lambda(a_1 + a_2) \frac{1}{A} \iint_A u_{zo} dx dy + 2\mu (a_1^2 + a_2^2) \\ & - \frac{2a_1}{A} \iint_A x\sigma_{xzo} dx dy - \frac{2a_2}{A} \iint_A y\sigma_{yzo} dx dy \end{aligned}$$

Then \tilde{L}_1 is made stationary with respect to variations of u_{xl} and u_{yl} by means of the conditions

$$0 = \frac{1}{2A} \frac{\partial \tilde{L}_1}{\partial a_1} = (\lambda + 2\mu - \rho\Omega^2 I_x) a_1 + \lambda a_2 + \frac{1}{A} \iint_A (\lambda u_{z0} - x\sigma_{xzo}) dx dy$$

$$0 = \frac{1}{2A} \frac{\partial \tilde{L}_1}{\partial a_2} = \lambda a_1 + (\lambda + 2\mu - \rho\Omega^2 I_y) a_2 + \frac{1}{A} \iint_A (\lambda u_{z0} - y\sigma_{yzo}) dx dy .$$

These equations are then solved for a_1 and a_2 :

$$a_1 = \frac{1}{A\Delta} \left[(\lambda + 2\mu - \rho\Omega^2 I_y) \iint_A (x\sigma_{xzo} - \lambda u_{z0}) dx dy + \lambda \iint_A (\lambda u_{z0} - y\sigma_{yzo}) dx dy \right] \quad (55)$$

$$a_2 = \frac{1}{A\Delta} \left[(\lambda + 2\mu - \rho\Omega^2 I_x) \iint_A (y\sigma_{yzo} - \lambda u_{z0}) dx dy + \lambda \iint_A (\lambda u_{z0} - x\sigma_{xzo}) dx dy \right]$$

$$\text{where } \Delta = I_x I_y (\rho\Omega^2)^2 - (\lambda + 2\mu)(I_x + I_y)\rho\Omega^2 + 4\mu(\lambda + \mu) .$$

Equations 53, 54, and 55 are an approximate solution for the C_n provided the $u_{z0}^{(n)}$ are known. The accuracy is limited by the form chosen in equation 54. The exact solution for the circular rod shows that for the higher modes u_{x1} and u_{y1} oscillate rapidly with x and y *. Therefore, the present solution is expected to be accurate only for the lowest one or two modes.

Radial Modes

The radial modes are governed by more complicated equations than the longitudinal shear modes. An exact solution of equations 42a and 42b for the cut off frequencies is difficult. Apparently, only numerical methods work except in special cases.

* The exact solution of Pochhammer is written in terms of Bessel functions of large argument.

The important constants are the Ω_n and the C_n . Table 2 shows that C is found by using equations 43a and 43b. Below, a formula for C is derived so that equations 43a and 43b do not have to be solved.

Equations 42a, 42b, 43a, and 43b are multiplied by u_{x2} , u_{y2} , $-u_{x1}$, and $-u_{y1}$, respectively, added together, and integrated over the area. Then, equations 38b are used to find

$$\iint_A \left[u_{x2} \left(\frac{\partial \sigma_{xx1}}{\partial x} + \frac{\partial \sigma_{xy1}}{\partial y} \right) + u_{y2} \left(\frac{\partial \sigma_{yy1}}{\partial y} + \frac{\partial \sigma_{xy1}}{\partial x} \right) - u_{x1} \left(\frac{\partial \sigma_{xx2}}{\partial x} + \frac{\partial \sigma_{xy2}}{\partial y} + \sigma_{xz1} \right) - u_{y1} \left(\frac{\partial \sigma_{yy2}}{\partial y} + \frac{\partial \sigma_{xy2}}{\partial x} + \sigma_{yz1} \right) \right] dx dy \quad (56)$$

$$-\rho C = 0.$$

Equation 56 is then integrated by parts using boundary conditions with the result

$$\rho C = \iint_A \left[-\sigma_{xx1} \frac{\partial u_{x2}}{\partial x} - \sigma_{yy1} \frac{\partial u_{y2}}{\partial y} + \sigma_{xx2} \frac{\partial u_{x1}}{\partial x} + \sigma_{yy2} \frac{\partial u_{y1}}{\partial y} - \sigma_{xy1} \left(\frac{\partial u_{x2}}{\partial y} + \frac{\partial u_{y2}}{\partial x} \right) + \sigma_{xy2} \left(\frac{\partial u_{x1}}{\partial y} + \frac{\partial u_{y1}}{\partial x} \right) - \sigma_{xz1} u_{x1} - \sigma_{yz1} u_{y1} \right] dx dy .$$

The definitions of the stresses, equations 40, are used to show that several terms cancel and to produce the final result

$$\rho C = \iint_A \left[\lambda u_{z1} \left(\frac{\partial u_{x1}}{\partial x} + \frac{\partial u_{y1}}{\partial y} \right) - \sigma_{xz1} u_{x1} - \sigma_{yz1} u_{y1} \right] dx dy. \quad (57)$$

D. THE LONG TIME RESPONSE

The modal solution given in equation 35 will now be evaluated approximately by using the forms for the modes found by means of the perturbation scheme. The integrand of equation 35 will be approximated in the neighborhood of $\kappa = 0$. Thus, the response due to the longest waves will be found. It will be shown that the longest waves of the first mode give rise to the head of the pulse measured at long distances from the end of the rod. The parts of both the upper longitudinal shear and radial modes near cut off cause vibration like motions long after the head of the pulse has passed. Similar vibrations would be expected from cut off frequencies where κ is not zero but the $\omega_n(\kappa)$ have minima. However, those cut off frequencies are more difficult to study.

We consider the pressure shock problem. The boundary conditions on the end of the rod are that a normal compressional stress σ_{zz} is applied suddenly at $t = 0$ and the shear stresses σ_{xz} and σ_{yz} are zero. Notice that the right hand side is not known completely in either equation 35a or equation 35b.

The importance of the longest waves of the first compressional mode can be seen as follows. The solution given in equations 35 is of the type to which the method of stationary phase can be applied for large t and fixed x/t . The largest contributions to the integral over κ come from the points of stationary phase provided the integrand is sufficiently smooth. Such contributions are of order $1/\sqrt{t}$ for large t . (See reference 26, pp. 51-52. The theorem is strictly true only for finite limits of integration, but

only wave fronts come from infinite κ .) The only larger contributions must come from places where the integrand is infinite, and that can only be where $\omega_n(\kappa)$ is zero in equations 35a or 35b. Now, for compressional disturbances ω goes to zero only for the first compressional mode and when κ goes to zero. Therefore, we can expect the major compressional disturbance at long time and large distances from the end of the rod to come from that mode from the vicinity of $\kappa = 0$.

In accordance with the above arguments we consider first the contribution to equation 35a from the part of the first compressional mode with κ very small. In equation 35a the second two terms are negligible with respect to the first because $\sigma_{xz}^{(0)}$ and $\sigma_{yz}^{(0)}$ vanish as κ goes to zero, which can be seen by examining the expansions, equations 37a and 39a, and recalling that $\sigma_{xzo}^{(0)}$ and $\sigma_{yzo}^{(0)}$ are zero. According to equation 37a, u_z may be approximated by u_{zo} , which is given as $1/\sqrt{A}$ in equation 47. Then, the innermost integral of equation 35a can be carried out. The integral of $\sigma_{zz}|_{z=0}$ over the area is written as $-AP$, in which P is the average pressure over the end face. In place of equation 35a we then write

$$u_i \approx \frac{P\sqrt{A}}{2\pi\rho l} \int_{-\epsilon}^{\epsilon} \int_0^t \left(e^{i\omega_0(t-\tau)+i\kappa z} - e^{-i\omega_0(t-\tau)+i\kappa z} \right) \frac{u_i^{(0)}(x,y)}{\omega_0} d\tau d\kappa + \int_{\epsilon}^{\infty} \tilde{F}(\kappa) d\kappa + \int_{-\infty}^{-\epsilon} \tilde{F}(\kappa) d\kappa ; \quad (58)$$

where ϵ is small and positive and the integrals containing $\tilde{F}(\kappa)$

are of the stationary phase type. Those integrals give a contribution which dies out as $\frac{1}{\sqrt{t}}$ for large t and can be neglected. The integration over τ is carried out first and ω_0 approximated, using equation 36 and letting $C = -c_0^2$, as

$$\omega_0 \approx c_0 k + \frac{D_0}{2c_0} k^3. \quad (59)$$

Then,

$$u_i \approx \frac{P\sqrt{A}}{\pi \rho c_0 z} \int_{-\infty}^{\infty} \left[\cos\left(c_0 k + \frac{D_0}{2c_0} k^3\right) t - 1 \right] e^{ikz} u_i^{(0)} \frac{dk}{k^2}, \quad (60)$$

where the limits of integration have been extended to infinity; in so doing a stationary phase contribution of order $\frac{1}{\sqrt{t}}$ for large t is neglected.

The first term of the expansion for $u_i^{(0)}(x, y)$ from equations 37a and 47 is then substituted into equation 60. To find the strain $\epsilon_z = \partial u_z / \partial z$ one must differentiate equation 60 with respect to z within the integral sign, thus bringing down the factor ik . Then,

$$\epsilon_z \approx -\frac{u_x}{\nu(x-x_0)} \approx -\frac{u_y}{\nu(y-y_0)} \approx \quad (61)$$

$$i \frac{P}{\pi \rho c_0 z} \int_{-\infty}^{\infty} \left[\cos\left(c_0 k + \frac{D_0}{2c_0} k^3\right) t - 1 \right] e^{ikz} \frac{dk}{k}.$$

The longitudinal strain and the lateral displacements are coupled by Poisson's ratio. Noting that an odd function of k will integrate to zero and using a trigonometric identity, equation 61 becomes

$$\epsilon_z \approx -\frac{u_x}{v(x-x_0)} \approx -\frac{u_y}{v(y-y_0)} \approx$$

$$\frac{P}{\rho c_0^2} \int_0^\infty \left\{ 2 \sin k z - \sin \left[\left(c_0 k + \frac{D_0}{2c_0} k^3 \right) t + k z \right] \right. \quad (62)$$

$$\left. + \sin \left[\left(c_0 k + \frac{D_0}{2c_0} k^3 \right) t - k z \right] \right\} \frac{dk}{k} .$$

The first term is a well known integral. The second term may be approximated, provided z or t is large, by neglecting the term in k^3 in the argument of the sine function. The result is the same as the first term except for a factor of 2 and is independent of z or t . The last term is conveniently written with a change of variables so that

$$\epsilon_z \approx -\frac{u_x}{v(x-x_0)} \approx -\frac{u_y}{v(y-y_0)} \approx -\frac{P}{\rho c_0^2} \left\{ \frac{1}{2} - \frac{1}{\pi} \int_0^\infty \sin \left[(z - c_0 t) \left(\frac{2c_0}{3|D_0|t} \right)^{1/3} \eta + \frac{\eta^3}{3} \right] \frac{d\eta}{\eta} \right\}$$

(63)

The solution is a function of τ_1 , where

$$\tau_1 = (c_0 t - z) \left(\frac{2c_0}{3|D_0|t} \right)^{1/3} \approx \left(t - \frac{z}{c_0} \right) \left(\frac{2c_0^5}{3|D_0|z} \right)^{1/3} .$$

Equation 63 is the same solution that was found for the circular rod by Skalak (5) and by Folk, Fox, Shook, and Curtis (6) in their exact theory and also by Miklowitz (7) in related approximate theory work. They showed that the right hand side of equation 63 could be written as the integral of the Airy function,

$$-\frac{P_0}{\rho c_0^2} \left[\frac{1}{3} + \int_0^{\tau_1} \text{Ai}(-x) dx \right],$$

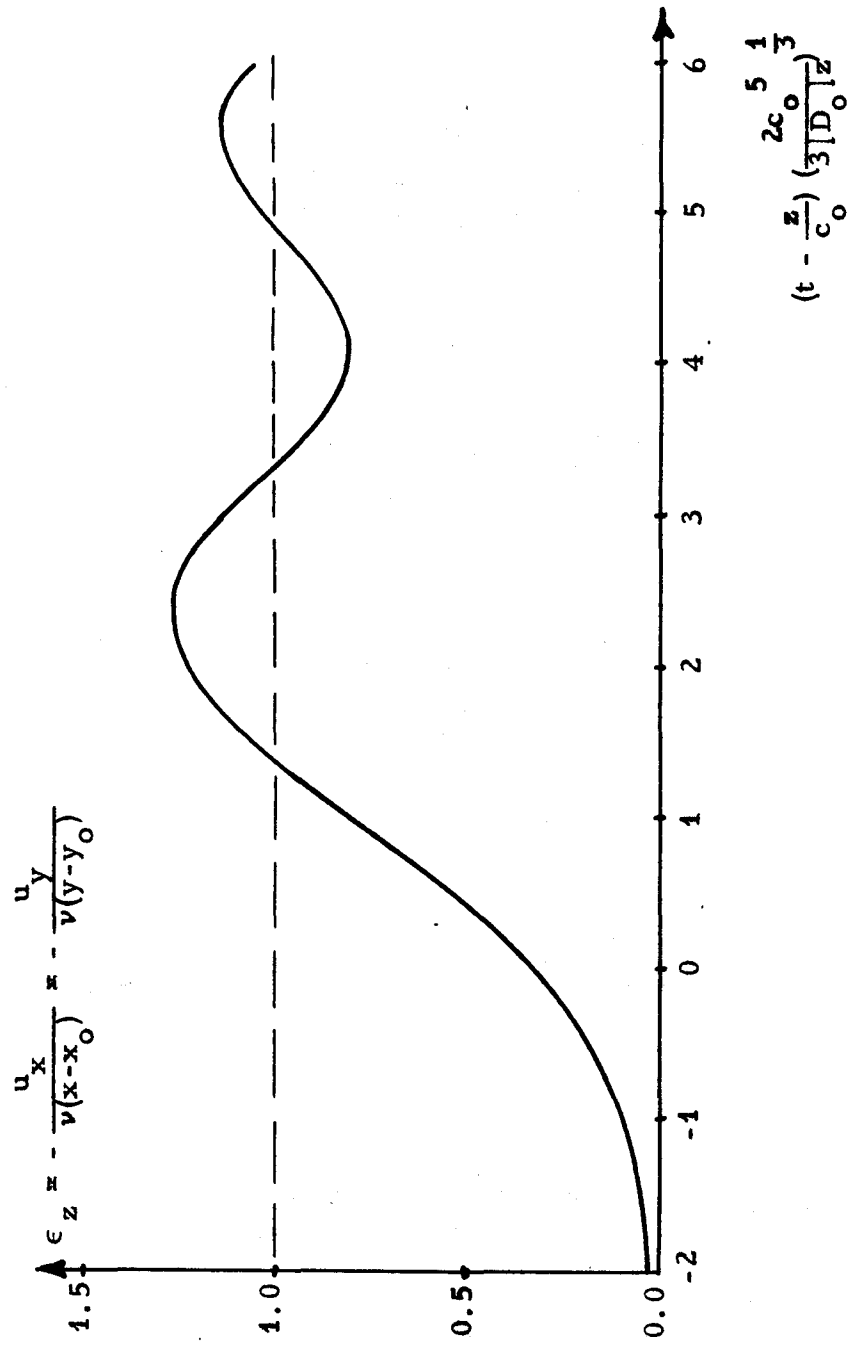
where the constant, $\frac{1}{3}$, is found by setting τ_1 equal to zero in equation 63, a well known integral resulting. The integral of the Airy function has been tabulated by Curtis (27). Figure 2 illustrates the form of the solution.

The contributions from the vicinity of the cut off frequencies of the higher modes can also be found from equation 35a. However, since u_x and u_y are unknown at $z = 0$, some constants in the solution must remain unevaluated. The integral over the area in equation 35a can be approximated for small κ by using the expansions in equations 37 and 39. For the shear modes and radial modes the results are, respectively,

$$G_n(\tau) = \iint_A \left[\sigma_{zz}|_{z=0} u_{z0}^{(n)}(\xi, \eta) - u_x|_{z=0} \sigma_{xz0}^{(n)} - u_y|_{z=0} \sigma_{yz0}^{(n)} \right] d\xi d\eta \quad (64)$$

$$i\kappa G_n(\tau) = i\kappa \iint_A \left[\sigma_{zz}|_{z=0} u_{zl}^{(n)} - u_x|_{z=0} \sigma_{xzl}^{(n)} - u_y|_{z=0} \sigma_{yzl}^{(n)} \right] d\xi d\eta,$$

where the $G_n(\tau)$ are different for longitudinal shear and radial modes. For any mode $G_n(\tau)$ approaches a constant for large τ because σ_{zz} , u_x , and u_y at $z = 0$ approach constant values at long time. The results to follow are incomplete because the $G_n(\tau)$ are unknown. If mixed boundary conditions were specified on the end of the rod, then



RESPONSE FOR LONG TIME AND LARGE z

Figure 2

the $G_n(\tau)$ would be known through either equation 35a or equation 35b.

An approximate expression for the time derivative of the displacements is found by differentiating equation 35a with respect to time and using the first of equations 64. The differentiation is carried out to avoid certain difficulties which will be mentioned. Two terms arise; the first, found by evaluating the integrand at the upper limit of the integral over τ , is zero; and the second term, found by differentiating the integrand, is

$$\frac{\partial u_i}{\partial t} \approx -\frac{1}{\rho p} \int_{-\infty}^{\infty} u_i^{(n)} e^{iKz} \int_0^t G_n(\tau) \cos \omega_n (t-\tau) d\tau dK \quad (65)$$

for the n^{th} shear mode. For the radial modes there is an additional factor iK .

The integration over τ can be approximated for large t by writing the integration in two parts;

$$\begin{aligned} & \int_0^t \cos \omega_n (t-\tau) G_n(\tau) d\tau \\ &= \cos \omega_n t \int_0^t \cos \omega_n \tau G_n(\tau) d\tau + \sin \omega_n t \int_0^t G_n(\tau) \sin \omega_n \tau d\tau. \quad (66) \end{aligned}$$

Since t is large, each of the integrals on the right hand side of equation 66 can be written as two integrals, one from zero to t_0 and the other from t_0 to t , where t_0 is a large number less than t . The integrals from zero to t_0 are independent of t . The integrals from t_0 to t are evaluated approximately by setting $G_n(\tau)$ equal to constant, $G_n(\infty)$. The two terms which are found in that

manner are*

$$\frac{G_n(\infty)}{\omega_n} (-\cos \omega_n t \sin \omega_n t_0 + \sin \omega_n t \cos \omega_n t_0).$$

It is then seen that the right hand side of equation 66 reduces to the form

$$\begin{aligned} \int_0^t \cos \omega_n (t-\tau) G_n(\tau) d\tau &\approx \text{constant} \cdot \cos \omega_n t + \text{constant} \cdot \sin \omega_n t \\ &= A_n \cos (\omega_n t + \varphi_n). \end{aligned} \quad (67)$$

A_n and φ_n are undetermined constants.

Equation 67 is substituted into equation 65 to show that

$$\frac{\partial u_i}{\partial t} \approx -\frac{A_n}{\pi \rho} \int_{-\infty}^{\infty} u_i^{(n)} \cos (\omega_n t + \varphi_n) e^{ikz} dk. \quad (68)$$

The first term of the expansion in equation 37a is used to approximate $u_x^{(n)}$, for example, and the first two terms of equation 36 are used to approximate ω_n with the result for the n^{th} longitudinal shear mode

$$\frac{\partial u_x}{\partial t} \approx -\frac{A_n u_{x1}^{(n)}(x, y)}{\pi \rho} \int_{-\infty}^{\infty} ik \cos \left[\left(\Omega_n - \frac{C_n}{2\Omega_n} k^2 \right) t + \varphi_n \right] e^{ikz} dk. \quad (69)$$

For the radial modes exactly the same equation holds. (Equations 37b and the second of equations 64 are used.) Equation 69 is evaluated for large t and fixed z/t by the method of stationary phase (reference 26, p. 51) with the points of stationary phase being found at

* This dependence on t is the reason for working with $\partial u_i / \partial t$ rather than u_i . For u_i there would be an additive constant, independent of t . That constant would cause the integral in the equation analogous to equation 68 to be divergent.

$$\kappa = + \frac{\Omega_n z}{C_n t} \quad (70)$$

Since approximations have been made for κ small, the results are valid only for large t/z . The result for u_x is

$$\frac{\partial u_x}{\partial t} \approx \frac{A_n}{\rho} \sqrt{\frac{2\Omega_n}{|C_n| \pi t}} \frac{\Omega_n z}{C_n t} \sin\left(\Omega_n t + \frac{\Omega_n z^2}{2C_n t} + \varphi_n - \frac{C_n}{|C_n|} \frac{\pi}{4}\right) u_{xl}^{(n)}(x, y). \quad (71)$$

Equation 71 cannot be integrated exactly to find the displacement.

However, we have the approximate relation,

$$u_x \approx - \frac{A_n}{\rho} \sqrt{\frac{2\Omega_n}{|C_n| \pi t}} \frac{z}{C_n t} \cos\left(\Omega_n t + \frac{\Omega_n z^2}{2C_n t} + \varphi_n - \frac{C_n}{|C_n|} \frac{\pi}{4}\right) u_{xl}^{(n)}(x, y). \quad (72)$$

The time derivative of equation 72 is equation 71 provided t/z is large as had already been assumed. u_y is similar to u_x . Similarly, for the shear modes one finds for ϵ_z

$$\epsilon_z \approx - \frac{A_n}{\rho} \sqrt{\frac{2\Omega_n}{|C_n| \pi t}} \frac{z}{C_n t} \cos\left(\Omega_n t + \frac{\Omega_n z^2}{2C_n t} + \varphi_n - \frac{C_n}{|C_n|} \frac{\pi}{4}\right) u_{zo}^{(n)}(x, y). \quad (73)$$

For the radial modes $u_{zo}^{(n)}$ is replaced by $u_{zl}^{(n)}$ and the right hand side of equation 73 is multiplied by $(i\kappa)^2$ evaluated at the point of stationary phase, that is, by

$$- \frac{\Omega_n^2 z^2}{C_n^2 t^2}.$$

Both the shear and radial modes cause vibrations which die out as t increases. The magnitudes and phases of the vibrations are not given by equations 72 and 73, for the A_n and φ_n are unknown. The longitudinal strain of the radial modes dies out more quickly

than the other variables calculated above. Such vibrations for the circular rod were pointed out by Miklowitz (2) in the approximate theory work and by Miklowitz and Nisewanger (19) in their experimental response records. These vibrations occur for all z at long times after the head of the pulse has passed. Similar vibrations would be expected from places in the frequency spectrum where the wave length is not infinite but the frequency is a minimum.

E. APPROXIMATE THEORY

Problems too difficult for the exact theory are often tractable by approximate equations of motion. Mindlin and McNiven (20) have recently developed an approximate theory for compressional waves in a circular rod. A forerunner is the less accurate but more easily solved two mode approximate theory of Mindlin and Herrmann (3,4). Volterra (23) has developed a three mode theory for the rectangular rod. A five mode theory for compressional waves in rods of arbitrary cross section is developed below. It is based on the same physical approximations as the Mindlin-McNiven theory, but the present theory allows for the asymmetry of a noncircular rod. Following Mindlin and McNiven, the frequency equations of the approximate and exact theories are compared near their cut off frequencies.

The starting point is Hamilton's principle for time dependent problems;

$$\delta L = \delta \int_{t_1}^{t_2} \int_{z_1}^{z_2} \iint_A \left\{ \rho \left[\left(\frac{\partial u_x}{\partial t} \right)^2 + \left(\frac{\partial u_y}{\partial t} \right)^2 + \left(\frac{\partial u_z}{\partial t} \right)^2 \right] \right. \\ \left. - \lambda \left(\frac{\partial u_x}{\partial x} + \frac{\partial u_y}{\partial y} + \frac{\partial u_z}{\partial z} \right)^2 - 2\mu \left[\left(\frac{\partial u_x}{\partial x} \right)^2 + \left(\frac{\partial u_y}{\partial y} \right)^2 + \left(\frac{\partial u_z}{\partial z} \right)^2 \right] \right. \\ \left. - \mu \left(\frac{\partial u_x}{\partial y} + \frac{\partial u_y}{\partial x} \right)^2 - \mu \left(\frac{\partial u_x}{\partial z} + \frac{\partial u_z}{\partial x} \right)^2 - \mu \left(\frac{\partial u_y}{\partial z} + \frac{\partial u_z}{\partial y} \right)^2 \right\} dx dy dz dt, \quad (74)$$

where L is twice the Lagrangian. The variations of the displacements are zero at t equal to t_1 and t_2 . Appropriate boundary conditions must be given at z equal to z_1 and z_2 and on the longitudinal surfaces of the rod.

Equation 74 is used by first assuming for the displacements the forms

$$u_z = w_1(z, t) + x^2 w_2(z, t) + y^2 w_3(z, t) \\ u_x = x u_1(z, t) \quad u_y = y u_2(z, t). \quad (75)$$

The integration over the area in equation 74 is performed and the variational principle gives partial differential equations in z and t. The accuracy of the result depends on the accuracy of equations 75. The dependences on x and y chosen in equations 75 are similar to those chosen by Mindlin and McNiven for the circular rod. They did not allow for differences between the x and y co-ordinates because they only considered waves which are symmetric about the axis of the rod. In the present case there is no symmetry and w_2 and u_1 are assumed to be independent of w_3 and

u_2 . (With symmetry $w_2 = w_3$ and $u_1 = u_2$.) All that follows is a natural consequence of equations 75. For instance, no modes of flexure or torsion will result because the motions assumed in equations 75 are not bending or torsional in nature. Equation 74 is valid for several possible boundary conditions on the longitudinal surfaces. The approximate forms in equation 75 were chosen with stress free surfaces in mind. If the boundaries were rigidly held, equation 75 would not be appropriate.

Having substituted equations 75 into equation 74, the integration over the area is easy. The results are expressed in terms of the moments of inertia

$$I_x = \frac{1}{A} \iint_A x^2 dx dy \qquad I_y = \frac{1}{A} \iint_A y^2 dx dy$$

$$I_{xx} = \frac{1}{A} \iint_A x^4 dx dy \quad I_{xy} = \frac{1}{A} \iint_A x^2 y^2 dx dy \quad I_{yy} = \frac{1}{A} \iint_A y^4 dx dy.$$

Letting a dot represent $\frac{\partial}{\partial t}$ and a prime $\frac{\partial}{\partial z}$,

$$\begin{aligned} \frac{L}{A} = & \int_{t_1}^{t_2} \int_{z_1}^{z_2} \left\{ \rho \left[I_x \dot{u}_1^2 + I_y \dot{u}_2^2 + \dot{w}_1^2 + I_{xx} \dot{w}_2^2 + I_{yy} \dot{w}_3^2 \right. \right. \\ & \left. \left. + I_x (\dot{w}_1 \dot{w}_2 + \dot{w}_2 \dot{w}_1) + I_y (\dot{w}_1 \dot{w}_3 + \dot{w}_3 \dot{w}_1) + I_{xy} (\dot{w}_2 \dot{w}_3 + \dot{w}_3 \dot{w}_2) \right] \right. \\ & - \lambda \left[(u_1 u_2 + u_2 u_1) + (u_1 + u_2)(w_1' + I_x w_2' + I_y w_3') \right. \\ & \left. + (w_1' + I_x w_2' + I_y w_3') (u_1 + u_2) \right] - (\lambda + 2\mu) \left[u_1^2 + u_2^2 + w_1'^2 \right. \\ & \left. + I_{xx} w_2'^2 + I_{yy} w_3'^2 + I_x (w_1' w_2' + w_2' w_1') + I_y (w_1' w_3' + w_3' w_1') \right. \\ & \left. + I_{xy} (w_2' w_3' + w_3' w_2') \right] - \mu I_x (u_1' + 2w_2')^2 - \mu I_y (u_2' + 2w_3')^2 \left. \right\} dz dt. \end{aligned} \tag{76}$$

It is easy to take the variation of L because it contains a symmetric bilinear form. Only the second member of each term need be varied. The variations are taken by the usual method.

A term \dot{u}^2 is varied and integrated by parts to give

$$\frac{1}{2} \delta \int_{t_1}^{t_2} \dot{u}^2 dt = - \int_{t_1}^{t_2} \ddot{u} \delta u dt.$$

A term $wu' + u'w$ is varied and integrated by parts to give

$$\frac{1}{2} \delta \int_{z_1}^{z_2} (wu' + u'w) dz = \int_{z_1}^{z_2} (-w' \delta u + u' \delta w) dz + w \delta u \Big|_{z_1}^{z_2}.$$

The last term on the right hand side is used to determine the boundary conditions. Since there are five dependent variables, there are five displacement equations of motion and five boundary conditions as follows:

$$\left. \begin{aligned} & -\rho \ddot{w}_1 + (\lambda + 2\mu) w_1'' - \rho I_x \ddot{w}_2 + (\lambda + 2\mu) I_x w_2'' - \rho I_y \ddot{w}_3 \\ & \quad + (\lambda + 2\mu) I_y w_3'' + \lambda u_1' + \lambda u_2' = 0 \\ & -\rho I_x \ddot{w}_1 + (\lambda + 2\mu) I_x w_1'' - \rho I_{xx} \ddot{w}_2 + (\lambda + 2\mu) I_{xx} w_2'' - 4\mu I_x w_2 \\ & -\rho I_{xy} \ddot{w}_3 + (\lambda + 2\mu) I_{xy} w_3'' + \lambda I_x u_1' - 2\mu I_x u_1' + \lambda I_x u_2' = 0 \\ & -\rho I_y \ddot{w}_1 + (\lambda + 2\mu) I_y w_1'' - \rho I_{xy} \ddot{w}_2 + (\lambda + 2\mu) I_{xy} w_2'' - \rho I_{yy} \ddot{w}_3 \\ & + (\lambda + 2\mu) I_{yy} w_3'' - 4\mu I_y w_3' + \lambda I_y u_1' - \lambda I_y u_2' - 2\mu I_y u_2' = 0 \\ & -\lambda w_1' - \lambda I_x w_2' + 2\mu I_x w_2' - \lambda I_y w_3' - \rho I_x \ddot{u}_1 - (\lambda + 2\mu) u_1 \\ & \quad + \mu I_x u_1'' - \lambda u_2 = 0 \\ & -\lambda w_1' - \lambda I_x w_2' - \lambda I_y w_3' + 2\mu I_y w_3' - \lambda u_1 - \rho I_y \ddot{u}_2 \\ & \quad - (\lambda + 2\mu) u_2 + \mu I_y u_2'' = 0. \end{aligned} \right\} (77a)$$

At $z = z_1, z_2,$

$$\left. \begin{aligned} \delta w_1 [\lambda(u_1+u_2) + (\lambda+2\mu)(w_1'+I_x w_2'+I_y w_3')] &= 0 \\ \delta w_2 [\lambda I_x(u_1+u_2) + (\lambda+2\mu)(I_{xx} w_2'+I_x w_1'+I_{xy} w_3')] &= 0 \\ \delta w_3 [\lambda I_y(u_1+u_2) + (\lambda+2\mu)(I_{yy} w_3'+I_y w_1'+I_{xy} w_2')] &= 0 \\ \delta u_1 [I_x(u_1'+2w_2)] &= 0 \\ \delta u_2 [I_y(u_2'+2w_3)] &= 0. \end{aligned} \right\} (77b)$$

Equations 77a are a tenth order set of partial differential equations governing approximately the motions of a noncircular rod.

Equations 77a are not invariant under a rotation of the x and y axes.

Letting $u_1 = u_2$ and $w_2 = w_3$, equations 77 reduce to the homogeneous Mindlin-McNiven equations and boundary conditions for the circular rod with all correction factors in the latter equations set equal to unity. Volterra's* equations for the rectangular rod are derived by setting $w_2 = w_3 = 0$ in equations 77. Finally, letting $u_1 = u_2$ and $w_2 = w_3 = 0$ in equations 77, one finds the homogeneous Mindlin-Herrmann equations and boundary conditions with all correction factors unity. In the same way the assumed approximations in equations 75 reduce to the assumed forms used

*There is no apparent reason why Volterra's equations cannot be considered as valid for arbitrary cross section. They are expressed in terms of I_x and I_y as are equations 77.

by the earlier authors. This correspondence between the assumed forms of the displacements and the resulting differential equations holds here despite the fact that Mindlin's derivation is different from the derivation by Hamilton's principle used here and by Volterra. Evidently, the derivations are equivalent. Notice that the Mindlin-Herrmann equations are the symmetric form of Volterra's equations and that the Mindlin-McNiven equations are the symmetric form of the present approximate theory. Also, notice that Volterra's equations are derived from equations 77 by dropping the w_2 and w_3 which will be seen to lead to the important longitudinal shear modes.

The boundary conditions need to be studied. The stresses on the end of the rod are

$$\begin{aligned}\sigma_{zz} &\equiv \lambda \left(\frac{\partial u_x}{\partial x} + \frac{\partial u_y}{\partial y} \right) + (\lambda + 2\mu) \frac{\partial u_z}{\partial z} \\ &\approx \lambda (u_1 + u_2) + (\lambda + 2\mu) (w_1' + x^2 w_2 + y^2 w_3') \\ \sigma_{xz} &\equiv \mu \left(\frac{\partial u_x}{\partial z} + \frac{\partial u_z}{\partial x} \right) \approx x\mu (u_1' + 2w_2) \\ \sigma_{yz} &\equiv \mu \left(\frac{\partial u_y}{\partial z} + \frac{\partial u_z}{\partial y} \right) \approx y\mu (u_2' + 2w_3),\end{aligned}\tag{78}$$

where the approximations are found by using equations 75. By comparing equations 78 to equations 77b, the boundary conditions are interpreted. Each boundary condition* in equations 77b requires that in general either a displacement (or corresponding

*The boundary conditions could be incorporated into the derivation through Hamilton's extended principle (see reference 8, pp. 166-167.).

velocity) or a "bar stress" be specified as a function of time, where the bar stresses are, respectively,

$$\iint_A \sigma_{zz} dx dy, \quad \iint_A x^2 \sigma_{zz} dx dy, \quad \iint_A y^2 \sigma_{zz} dx dy,$$
$$\iint_A x \sigma_{xz} dx dy, \quad \text{and} \quad \iint_A y \sigma_{yz} dx dy.$$

The five modes of propagation of the approximate theory will be compared to the corresponding modes of the exact theory. The comparison provides a physical understanding of the modes and is a criterion for judging the accuracy of the approximate equations. In Mindlin's work there was an additional reason for such a comparison. Correction factors were introduced by Mindlin into the approximate theory and were adjusted to make the approximate theory approach the exact theory more closely in the long wave region (κ small). According to Herrmann (4), the correction factors must be introduced into the theory in such a way that the bilinear form in equation 76 remains symmetric as in the exact theory. There are many ways of introducing correction factors under that condition. One can multiply any term or symmetric pair of terms in equation 76 by an unevaluated constant. According to Mindlin and McNiven, the constants should be adjusted so that the frequency equations of the approximate and exact theories are the same for long wave lengths. Since no exact formulas for general cross sections have been given for the Ω_n and C_n for the noncircular rod, it appears fruitless to

introduce the correction factors in the present work. The correction factors could be introduced profitably if a particular cross section were being considered. Then, the Ω_n and C_n for the lowest modes could be calculated to the accuracy desired, numerically if necessary.

To develop the frequency equation, we substitute into the differential equations 77a the travelling wave solutions

$$\begin{aligned} w_1 &= A_1 e^{i(\omega t + \kappa z)} & w_2 &= A_2 e^{i(\omega t + \kappa z)} & w_3 &= A_3 e^{i(\omega t + \kappa z)} \\ u_1 &= A_4 e^{i(\omega t + \kappa z)} & u_2 &= A_5 e^{i(\omega t + \kappa z)}. \end{aligned} \quad (79)$$

The resulting linear equations for the A_n are

$$\begin{pmatrix} a_{11} & a_{12} & a_{13} & ia_{14} & ia_{15} \\ a_{12} & a_{22} & a_{23} & ia_{24} & ia_{25} \\ a_{13} & a_{23} & a_{33} & ia_{34} & ia_{35} \\ -ia_{14} & -ia_{24} & -ia_{34} & a_{44} & a_{45} \\ -ia_{15} & -ia_{25} & -ia_{35} & a_{45} & a_{55} \end{pmatrix} \begin{pmatrix} A_1 \\ A_2 \\ A_3 \\ A_4 \\ A_5 \end{pmatrix} = \begin{pmatrix} 0 \\ 0 \\ 0 \\ 0 \\ 0 \end{pmatrix}, \quad (80)$$

where

$$\begin{aligned} a_{11} &= \rho\omega^2 - (\lambda + 2\mu)\kappa^2 & a_{12} &= I_x [\rho\omega^2 - (\lambda + 2\mu)\kappa^2] \\ a_{22} &= I_{xx} [\rho\omega^2 - (\lambda + 2\mu)\kappa^2] - 4\mu I_x & a_{13} &= I_y [\rho\omega^2 - (\lambda + 2\mu)\kappa^2] \\ a_{33} &= I_{yy} [\rho\omega^2 - (\lambda + 2\mu)\kappa^2] - 4\mu I_y & a_{23} &= I_{xy} [\rho\omega^2 - (\lambda + 2\mu)\kappa^2] \end{aligned}$$

$$\begin{aligned}
 a_{44} &= I_x(\rho\omega^2 - \mu\kappa^2) - (\lambda + 2\mu) & a_{55} &= I_y(\rho\omega^2 - \mu\kappa^2) - (\lambda + 2\mu) \\
 a_{14} &= a_{15} = \lambda\kappa & a_{45} &= -\lambda & a_{24} &= I_x(\lambda - 2\mu)\kappa \\
 a_{25} &= I_x\lambda\kappa & a_{34} &= I_y\lambda\kappa & a_{35} &= I_y(\lambda - 2\mu)\kappa
 \end{aligned}$$

The frequency equation is found by setting the determinant of the Hermitian matrix in equation 80 equal to zero.

To study the cut off frequencies, Ω , we let κ go to zero in equation 80 and replace ω with Ω . The matrix elements a_{14} , a_{15} , a_{24} , a_{25} , a_{34} , and a_{35} are zero. Then, equation 80 separates into two equations, one equation for A_1 , A_2 , and A_3 , the other for A_4 and A_5 . The equations are

$$\begin{pmatrix} \rho\Omega^2 & I_x\rho\Omega^2 & I_y\rho\Omega^2 \\ I_x\rho\Omega^2 & I_{xx}\rho\Omega^2 - 4\mu I_x & I_{xy}\rho\Omega^2 \\ I_y\rho\Omega^2 & I_{xy}\rho\Omega^2 & I_{yy}\rho\Omega^2 - 4\mu I_y \end{pmatrix} \begin{pmatrix} A_1 \\ A_2 \\ A_3 \end{pmatrix} = \begin{pmatrix} 0 \\ 0 \\ 0 \end{pmatrix} \quad (81a)$$

$$\begin{pmatrix} I_x\rho\Omega^2 - (\lambda + 2\mu) & -\lambda \\ -\lambda & I_y\rho\Omega^2 - (\lambda + 2\mu) \end{pmatrix} \begin{pmatrix} A_4 \\ A_5 \end{pmatrix} = \begin{pmatrix} 0 \\ 0 \end{pmatrix} \quad (81b)$$

Three cut off frequencies are found from equation 81a. One of them is zero and comes from the first mode. The other two are related closely to the longitudinal shear modes of the exact theory. Equation 81b yields two cut off frequencies, both related to the radial modes of the exact theory.

To see that equations 81a and 81b are directly related to the exact theory, we consider the variational principle formulation

of the equations for the cut off frequencies of the exact theory. The Rayleigh-Ritz method is used on the integrals L_0 and L_1 given in equations 44 and equations 81a and 81b result. In L_0 we try the approximate form

$$u_{z0} = A_1 + A_2 x^2 + A_3 y^2, \quad (82a)$$

while in L_1 we let $u_{z0} = 0$ and try

$$u_{x1} = A_4 x \quad u_{y1} = A_5 y. \quad (82b)$$

Equations 82 are intentionally made to resemble equations 75 and 79 without the dependence on z and t .

To carry out the Rayleigh-Ritz method, equations 82 are substituted into equations 44 and the integrations are carried out. The results are written in terms of the moments of inertia. Then, the "variations" of L_0 and L_1 are set equal to zero by requiring

$$\frac{\partial L_0}{\partial A_1} = \frac{\partial L_0}{\partial A_2} = \frac{\partial L_0}{\partial A_3} = 0 \quad \frac{\partial L_1}{\partial A_4} = \frac{\partial L_1}{\partial A_5} = 0. \quad (83)$$

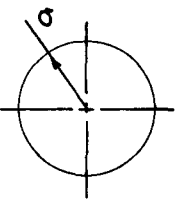
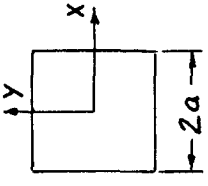
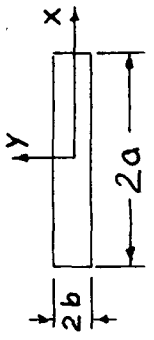
The resulting linear equations are precisely equations 81a and 81b. This is not surprising in view of the fact that the physical assumptions, equations 82, which went into the approximate calculation on the exact theory were the same as the assumptions that went into writing the approximate theory. We are now assured that the five modes of the approximate theory correspond approximately to five of the lower modes of the exact theory. The

first mode of both the approximate and exact theories is a compressional mode with a velocity of c_0 for infinitely long waves.

Figure 3 makes a comparison between the solutions of the exact and approximate theories at cut off. The approximate theory solutions come directly from equations 75, 79, and 81. The exact theory solutions for the longitudinal shear modes at cut off are known through an analogy with a problem in electromagnetic wave propagation. The H (TE) modes of propagation of electromagnetic waves in a waveguide of arbitrary cross section are governed by the same boundary value problem and the solutions are given in reference (28). The boundary value problem for the radial modes is more complex. The exact theory solution for the circular cross section given in figure 3 comes from Pochhammer's solution. The lower radial mode in the approximate theory for the circle is not axially symmetric, and, therefore, there is no comparable Pochhammer mode. The solutions of the exact theory for radial modes for the thin rectangular cross section come from assuming plane strain for the higher mode or plane stress* for the lower mode. The formulas for the modes are not normalized.

An idea of the accuracy of the approximate theory can be gathered by comparing the cut off frequencies of the exact and approximate theories as given in figure 3. Similarly, the

*For plane stress $\sigma_{yy} = \sigma_{xy} = 0$ for the coordinates of figure 3. u_y is determined by setting $\sigma_{yy} = 0$.

CROSS SECTION	LONGITUDINAL SHEAR	RADIAL	u_x	u_y	
CIRCLE  $x = r \cos \theta$ $y = r \sin \theta$ $u_r = r$ DIS- PLACEMENT		$\Omega a \sqrt{\mu}$	u_x	u_y	
	APPROX	3.46	$x^2 - y^2$	x	$-y$
		4.90	$1 - 2 \left(\frac{r}{a}\right)^2$	x	y
	EXACT	3.05	$J_2 \left(3.05 \frac{r}{a}\right) \cos 2\theta$	—	—
SQUARE 		$\Omega a \sqrt{\mu}$	$x \sqrt{\frac{\lambda+2\mu}{\mu}}$	$u_r = J_1 \left(x \frac{r}{a}\right)$	
	APPROX.	3.87	$1 - 3 \left(\frac{x}{a}\right)^2$	x	$-y$
		3.87	$1 - 3 \left(\frac{y}{a}\right)^2$	x	y
	EXACT	3.14	$\cos \frac{\pi x}{a}$ or $\cos \frac{\pi y}{a}$	—	—
RECTANGLE 		$\Omega a \sqrt{\mu}$	—	—	
	APPROX.	3.87	$1 - 3 \left(\frac{x}{a}\right)^2$	x	$-\frac{\lambda}{\lambda+2\mu} y$
		$3.87 \frac{a}{b}$	$1 - 3 \left(\frac{y}{b}\right)^2$	0	y
	EXACT	3.14	$\cos \frac{\pi x}{a}$	$\sin \frac{\pi x}{2a}$	$-\left(\frac{\lambda}{\lambda+2\mu}\right) \left(\frac{\pi}{2a}\right) y \cos \frac{\pi x}{2a}$
		$3.14 \frac{a}{b}$	$\cos \frac{\pi y}{b}$	0	$\sin \frac{\pi y}{2b}$

APPROXIMATE AND EXACT THEORY MODES AT CUT OFF. FIGURE 3

forms of the displacements in the two theories can be compared. For the radial mode in the circle, χ is 2.126 when Poisson's ratio is 0.3.

It can be seen in figure 3 that there is a definite correspondence between the modes of the approximate theory and the modes of the exact theory. The contrast between the square and the circle is most interesting. According to the exact theory, there is a doubly degenerate asymmetric lower longitudinal shear mode while the symmetric higher longitudinal shear mode for either cross section is not degenerate. In the circle the approximate theory has one mode corresponding to the lower longitudinal shear mode of the exact theory and one mode for the higher longitudinal shear mode of the exact theory. But, in the square the approximate theory has two modes which have equal cut off frequencies. These two modes seem from the form of the displacements to correspond to the two degenerate modes of the exact theory.

The limitations of the approximate theory can be deduced from figure 3. A criterion suggested by Mindlin and McNiven is to limit the solution to long wave lengths and to frequencies below the lowest* frequency of the lowest exact theory mode omitted by the approximate theory. For the thin rectangle the

*The lowest frequency of some modes of both the exact and approximate theories is a little lower than the long wave cut off frequencies discussed here.

higher shear mode and the higher radial mode of the approximate theory both have very high cut off frequencies. Those two modes are coupled to the smaller dimension of the cross section. But, the exact theory has many modes coupled to the larger dimension which would have lower cut off frequencies than the two high modes of the approximate theory. Those two modes should then be eliminated from the approximate theory or ignored for the thin rectangle or any other thin shape.

It can easily be seen from the frequency equation (the determinant of equation 80 set equal to zero) that three modes have a limiting high frequency, short wave velocity of $c_d = \sqrt{\frac{\lambda + 2\mu}{\rho}}$, while the other two modes go to the velocity $c_s = \sqrt{\frac{\mu}{\rho}}$ in the same limit.

It is clear that the present approximate theory models the exact theory near the cut off frequencies. Furthermore, the frequency equation of the Mindlin-McNiven theory, which is a special case of the present approximate theory, was shown by Mindlin and McNiven (20) to have solutions similar to the exact theory provided only longer wave lengths are considered. Therefore, it seems reasonable to expect the present approximate theory to model the exact theory for all wave lengths longer than, say, the largest transverse dimension of the rod. Solution of the approximate theory for harmonic wave trains would indicate the behavior of the exact theory in the neighborhood of long waves. Such a solution would be valuable as the exact theory is extremely

difficult to solve. From the approximate theory one can learn, for instance, the form of the modes with complex wave numbers (such as exist in the circular rod). In addition, solutions to difficult transient problems can be attempted with the present approximate theory.

IV. THEORY OF WAVE FRONT AMPLITUDES AND LOCATIONS

The concept of wave front is associated with hyperbolic partial differential equations with $N + 1$ independent variables-- N space variables and one time variable. The time plays a role distinct from that of the space variables. In this $N + 1$ space a characteristic surface is defined to be any N dimensional surface across which any derivative of the dependent variable can be discontinuous. Wave fronts are associated with characteristic surfaces and can be visualized either by considering stationary observers or by considering the situation at a particular time.

A stationary observer detects the variation of the disturbance, the dependent variable, with time at some fixed location in space. A strain gage placed on an elastic rod is a stationary observer. At certain times, depending on the location and called the times of arrival, τ , the stationary observer detects discontinuities in the disturbance or its time derivatives. The magnitudes of the discontinuities are called the amplitudes of the wave fronts at that location.

At a particular time, t_0 , consider the disturbance as it varies in space. This corresponds to taking a picture of the disturbance. The $N - 1$ dimensional surfaces across which the disturbance has discontinuous space derivatives are the wave fronts at that particular time. The equations of the wave fronts at time t_0 are found by setting the time of arrival as a function of the N space variables

equal to t_0 , i. e. $\tau = t_0$. Viewed at successive times, the wave fronts are seen to move. The speed of the motion measured along a line perpendicular to a wave front at a point is the speed of propagation at that point and can be determined from the governing partial differential equation. The trajectories perpendicular to the wave fronts are called rays.

Letting t be the time, y and z be the space variables, and $H(x)$ the Heaviside step function, one can write the wave front expansion as

$$\sum_n \left\{ \sum_l A_{nl}(y, z) [t - \tau_n(y, z)]^l \right\} H[t - \tau_n(y, z)] . \quad (84)$$

where $l = 0, 1, 2, \dots$ or $l = -1/2, 1/2, 3/2, 5/2, \dots$ * In the outer sum the n^{th} term is identically zero before the time of arrival, $\tau_n(y, z)$, for that term. The inner sum is similar to a Taylor series for the disturbance with the coefficients depending on the space variables. The coefficient, $A_{nl}(y, z)$, of the first non-zero term of the inner expansion is the wave front amplitude which, along with the time of arrival, is the object of the calculations of this section.

A useful form of the wave front expansion can be found by taking its Laplace transform, which is written as

$$\sum_n \left[\sum_l \frac{l!}{p^{l+1}} A_{nl}(y, z) \right] e^{-p\tau_n(y, z)} . \quad (85)$$

* Karal and Keller (14) and Babich and Alekseev (15) have given a more general form, but only these two forms are of interest here.

The following work is based to a large extent on two observations about the transform in equation 85. First, the time of arrival is found in exponential functions. Second, the inner expansion is in the form of an asymptotic expansion for large values of the transform variable p . The first term of the expansion is the wave front amplitude.

In this section the wave front amplitudes are found for the displacement potentials ϕ and $\bar{\psi}$ in Lamé's well known general solution of the displacement equations of motion from linear elasticity,

$$\bar{u} = \bar{\nabla} \phi + \bar{\nabla} \times \bar{\psi} .$$

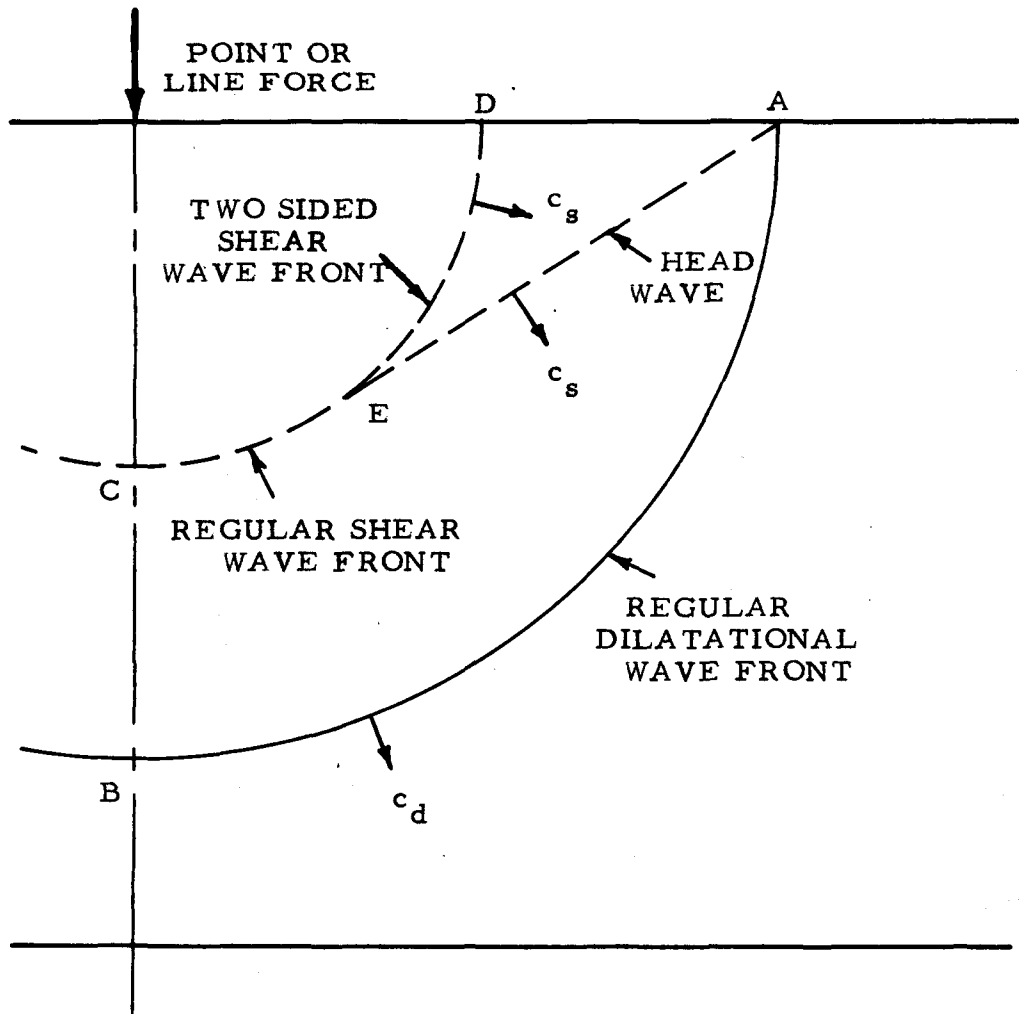
Wave fronts found from ϕ are called P or dilatational wave fronts because the displacement field is irrotational. Wave fronts found from $\bar{\psi}$ are called S or shear wave fronts because the displacement field is equivoluminal. (These are the SV and SH waves of reference 29. Here $\bar{\psi}$ will have only one component and the shear waves will be SV waves.) The wave front amplitude for ϕ is proportional to the wave front amplitude of longitudinal strain measured in a direction perpendicular to a P wave front. Similarly $\bar{\psi}$ measures shear strain along the direction of an S wave front. Published works have previously calculated wave front amplitudes of displacements or stresses along fixed directions (9-13). But then the answer includes a factor dependent upon the angle the wave front makes with the arbitrarily chosen fixed direction.

In the following work the wave fronts are first found by work-

ing with the transforms. Two inversion methods are used. The first, Cagniard's method, is patterned here after the work done by Mencher (9), Broberg (10), and Davids (11), who calculated a limited number of wave front amplitudes in a plate. The second, the saddle point method, is used here in a manner similar to that of Knopoff and Gilbert (13), who also calculated some of the wave front amplitudes in a plate. In the following work all of the wave fronts and their amplitudes are found from the transforms. The time dependences of the potentials at the wave fronts are clearly displayed. The mathematics of the transform method somewhat obscures the dependences on the space coordinates and on the integers n and m identifying the wave fronts. Therefore, ray theory is used to study the wave fronts.

The ray theory has one distinct advantage over the transform methods; it is able to provide a transparent and meaningful interpretation to the formulas which were also found by use of the transforms. However, ray theory is not used here to find all of the answers, the most notable lack being the time dependence. The results of ray theory and of the transform methods will both be written in terms of the same symbols. The symbols will be defined differently for the two methods. What is notable is that the definitions and formulas found by the two methods are equivalent.

It is convenient at this time to discuss the different types of wave fronts which will be found. All types develop immediately after the load is applied. Figure 4 shows the wave fronts in a plate under a point (or line) force suddenly applied at time $t = 0$. The wave fronts



BASIC WAVE FRONT TYPES

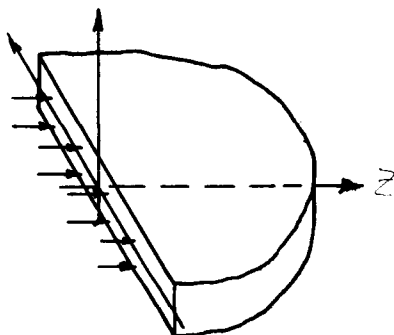
Figure 4

are drawn to geometric scale for a time, t , before any reflections have occurred. The dilatational waves move at the speed c_d and the shear waves move at the speed c_s . The spherical (cylindrical) wave front indicated by the solid line AB is a regular dilatational or P wave front, which is at a distance $c_d t$ from the applied force. At the same time there is a regular shear or S wave front, CE , at a radius $c_s t$. The line AE indicates a head wave. It is created by the dilatational wave front moving along the boundary similarly to the way a Mach wave is created in the supersonic flow of fluids. The part ED of the spherical (cylindrical) shear wave between the free surface and the head wave is not a regular wave front; it is called here a two sided shear wave. The time dependence of the two sided shear waves, as will be shown, is distinctly different from that of the head waves and the regular waves.

A. DERIVATION OF THE DOUBLE TRANSFORMS

The wave fronts will be found by working with double transforms of the displacement potentials. The several steps in deriving the double transforms for six problems of interest are carried out below. First, the governing partial differential equations and boundary conditions are written in terms of the potentials. Next, all of these equations are transformed twice by Laplace and Fourier transforms. The resulting ordinary differential equations and boundary conditions for the double transforms are then easily solved.

Figure 5 shows the six problems to be studied and the coordinate systems. In each case, z is the coordinate in the direction of wave

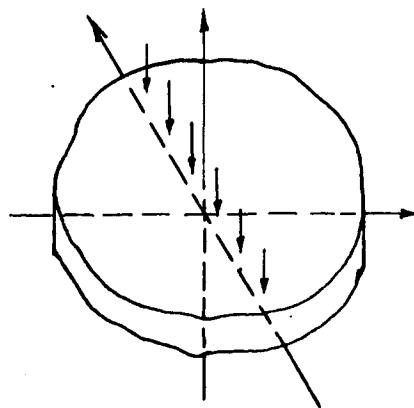


PLATE, END LOADS

i) STEP VELOCITY

ii) STEP PRESSURE

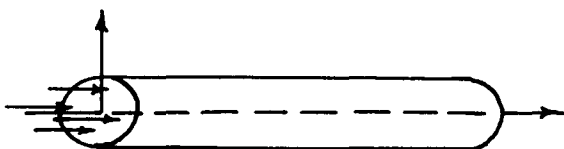
CARTESIAN COORDINATES



PLATE

iii) NORMAL LINE FORCE

CARTESIAN COORDINATES

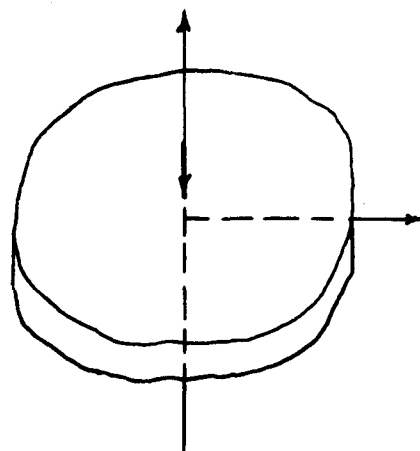


ROD, END LOADS

iv) STEP VELOCITY

v) STEP PRESSURE

CYLINDRICAL COORDINATES



PLATE

vi) NORMAL POINT FORCE

CYLINDRICAL COORDINATES

PHYSICAL PROBLEMS

Figure 5

propagation and y is the transverse coordinate. Similarly, in each case the boundary conditions on y are specified at $y = \pm a$. Problems i, ii, and iii are the easier to solve plane strain problems. Problems iv, v, and vi are the analogous and more difficult problems with cylindrical symmetry. The small Roman numerals next to the equation numbers in this section will refer to the applicable problems.

The boundary conditions are all expressed in terms of a source magnitude, Z , as follows:

Problems i and iv, (Longitudinal impact problems)

$$\text{At } z = 0, u_z = Zc_d t H(t) \text{ and } \sigma_{yz} = 0; \text{ at } y = \pm a, \sigma_{yy} = \sigma_{yz} = 0.$$

Problems ii and v, (Pressure step problems)

$$\text{At } z = 0, \sigma_{zz} = -Z(\lambda + 2\mu)H(t) \text{ and } u_y = 0; \text{ at } y = \pm a, \sigma_{yy} = \sigma_{yz} = 0.$$

Problem iii, (Line force problem)

$$\text{At } z = 0, u_z = \partial u_y / \partial z = 0 \text{ by symmetry; } \sigma_{yz} = 0 \text{ at } y = \pm a, \\ \sigma_{yy} = 0 \text{ at } y = -a, \sigma_{yy} = -Z\mu a \delta(z) H(t) \text{ at } y = +a, \text{ where for}$$

$$\text{any positive } \epsilon, \int_{-\epsilon}^{\epsilon} \delta(z) dz = 1.$$

Problem vi, (Point force problem)

$$\text{At } z = 0, \text{ continuity of displacements required; } \sigma_{yz} = 0 \text{ at } \\ y = \pm a, \sigma_{yy} = 0 \text{ at } y = -a, \sigma_{yy} = -Z\mu a^2 \frac{\delta(z)}{z} H(t) \text{ at } y = +a,$$

$$\text{where for any positive } \epsilon, 2 \int_0^{\epsilon} \delta(z) dz = 1.$$

Each of these boundary conditions is mixed on the end surface, $z = 0$.

Therefore, schemes 1 and 2 of section II will work.

The two scalar displacement potentials are defined by

$$u_z = \frac{\partial \varphi}{\partial z} - \frac{\partial \psi}{\partial y} \qquad u_y = \frac{\partial \varphi}{\partial y} + \frac{\partial \psi}{\partial z} \qquad (86i, ii, iii)$$

$$u_z = \frac{\partial \varphi}{\partial z} - \frac{1}{y} \frac{\partial}{\partial y} (y\psi) \qquad u_y = \frac{\partial \varphi}{\partial y} + \frac{\partial \psi}{\partial z} \qquad (86iv, v)$$

$$u_z = \frac{\partial \varphi}{\partial z} - \frac{\partial \psi}{\partial y} \qquad u_y = \frac{\partial \varphi}{\partial y} + \frac{1}{z} \frac{\partial}{\partial z} (z\psi) . \qquad (86vi)$$

φ gives rise to an irrotational displacement field, ψ to an equivo-luminal displacement field. The potentials are all defined in a similar way so that the plane strain problems can easily be compared to the cylindrically symmetric problems.

The expressions for the stresses and the derivations of the equations of motion in terms of the potentials are given in Ewing, Jardetzky, and Press (29), pp. 6-8 and 306-308. The equations of motion are the wave equations

$$\left. \begin{aligned} \frac{\partial^2 \varphi}{\partial z^2} + \frac{\partial^2 \varphi}{\partial y^2} - \frac{1}{c_d^2} \frac{\partial^2 \varphi}{\partial t^2} &= 0 \\ \frac{\partial^2 \psi}{\partial z^2} + \frac{\partial^2 \psi}{\partial y^2} - \frac{1}{c_s^2} \frac{\partial^2 \psi}{\partial t^2} &= 0 \end{aligned} \right\} (87i, ii, iii)$$

$$\left. \begin{aligned} \frac{\partial^2 \varphi}{\partial z^2} + \frac{1}{y} \frac{\partial}{\partial y} (y \frac{\partial \varphi}{\partial y}) - \frac{1}{c_d^2} \frac{\partial^2 \varphi}{\partial t^2} &= 0 \\ \frac{\partial^2 \psi}{\partial z^2} + \frac{\partial}{\partial y} [\frac{1}{y} \frac{\partial}{\partial y} (y\psi)] - \frac{1}{c_s^2} \frac{\partial^2 \psi}{\partial t^2} &= 0 \end{aligned} \right\} (87iv, v)$$

$$\left. \begin{aligned} \frac{1}{z} \frac{\partial}{\partial z} (z \frac{\partial \varphi}{\partial z}) + \frac{\partial^2 \varphi}{\partial y^2} - \frac{1}{c_d^2} \frac{\partial^2 \varphi}{\partial t^2} &= 0 \\ \frac{\partial}{\partial z} \left[\frac{1}{z} \frac{\partial}{\partial z} (z \psi) \right] + \frac{\partial^2 \psi}{\partial y^2} - \frac{1}{c_s^2} \frac{\partial^2 \psi}{\partial t^2} &= 0 \end{aligned} \right\} (87vi)$$

The stresses which are involved in the boundary conditions are

$$\left. \begin{aligned} \sigma_{zz} &= \lambda \frac{\partial^2 \varphi}{\partial y^2} - 2\mu \frac{\partial^2 \psi}{\partial y \partial z} + (\lambda + 2\mu) \frac{\partial^2 \varphi}{\partial z^2} \\ \sigma_{yy} &= \lambda \frac{\partial^2 \varphi}{\partial z^2} + 2\mu \frac{\partial^2 \psi}{\partial y \partial z} + (\lambda + 2\mu) \frac{\partial^2 \varphi}{\partial y^2} \\ \sigma_{yz} &= \mu \left(2 \frac{\partial^2 \varphi}{\partial y \partial z} + \frac{\partial^2 \psi}{\partial z^2} - \frac{\partial^2 \psi}{\partial y^2} \right) \end{aligned} \right\} (88i, ii, iii)$$

$$\left. \begin{aligned} \sigma_{zz} &= \frac{\lambda}{y} \frac{\partial}{\partial y} (y \frac{\partial \varphi}{\partial y}) - \frac{2\mu}{y} \frac{\partial}{\partial y} (y \frac{\partial \psi}{\partial z}) + (\lambda + 2\mu) \frac{\partial^2 \varphi}{\partial z^2} \\ \sigma_{yy} &= \lambda \frac{\partial^2 \varphi}{\partial z^2} + 2\mu \frac{\partial^2 \psi}{\partial y \partial z} + \frac{\lambda}{y} \frac{\partial}{\partial y} (y \frac{\partial \varphi}{\partial y}) + 2\mu \frac{\partial^2 \varphi}{\partial y^2} \\ \sigma_{yz} &= \mu \left\{ 2 \frac{\partial^2 \varphi}{\partial y \partial z} + \frac{\partial^2 \psi}{\partial z^2} - \frac{\partial}{\partial y} \left[\frac{1}{y} \frac{\partial}{\partial y} (y \psi) \right] \right\} \end{aligned} \right\} (88iv, v)$$

$$\left. \begin{aligned} \sigma_{zz} &= \lambda \frac{\partial^2 \varphi}{\partial y^2} - 2\mu \frac{\partial^2 \psi}{\partial y \partial z} + \frac{\lambda}{z} \frac{\partial}{\partial z} (z \frac{\partial \varphi}{\partial z}) + 2\mu \frac{\partial^2 \varphi}{\partial z^2} \\ \sigma_{yy} &= \frac{\lambda}{z} \frac{\partial}{\partial z} (z \frac{\partial \varphi}{\partial z}) + \frac{2\mu}{z} \frac{\partial}{\partial z} (z \frac{\partial \psi}{\partial y}) + (\lambda + 2\mu) \frac{\partial^2 \varphi}{\partial y^2} \\ \sigma_{yz} &= \mu \left\{ 2 \frac{\partial^2 \varphi}{\partial y \partial z} + \frac{\partial}{\partial z} \left[\frac{1}{z} \frac{\partial}{\partial z} (z \psi) \right] - \frac{\partial^2 \psi}{\partial y^2} \right\} \end{aligned} \right\} (88vi)$$

Initially the rod or plate is at rest. The initial conditions which are prescribed for the potentials are

$$\varphi = \frac{\partial \varphi}{\partial t} = \psi = \frac{\partial \psi}{\partial t} = 0 . \quad (t = 0) \quad (89)$$

Equations 89 do two things. First, they guarantee that the rod or plate is at rest initially. Second, equations 89 eliminate unwanted solutions which could arise because equations 86 do not define the potentials uniquely. For instance, in equations 86i, ii, iii any pair of functions φ and ψ satisfying the Cauchy-Riemann equations would not cause any displacements u_y or u_z and would not be of interest. If such a pair of functions were independent of time, they would satisfy the boundary conditions and the governing differential equations but not the initial conditions in equations 89.

To express the boundary conditions at $z = 0$ in terms of the potentials in a simple way, we proceed as follows. For the plane strain impact problem, problem i, the two conditions on u_z and σ_{yz} can be expressed in terms of $\frac{\partial \varphi}{\partial z}$ and ψ by using the differential equations 87i and 88i;

$$\left. \begin{aligned} 2 \frac{\partial}{\partial y} \left(\frac{\partial \varphi}{\partial z} \right) + \frac{1}{c_s^2} \frac{\partial^2 \psi}{\partial t^2} - 2 \frac{\partial^2 \psi}{\partial y^2} &= 0 \\ \frac{\partial \varphi}{\partial z} - \frac{\partial \psi}{\partial y} &= Z c_d t H(t) . \end{aligned} \right\} (z = 0) \quad (\underline{a})$$

Equations a are a pair of differential equations with independent variables y and t . With this in mind we differentiate the second of equations a with respect to y and substitute into the first with

the result

$$\frac{\partial^2 \psi}{\partial t^2} = 0 \quad (z = 0) \quad (b)$$

Equation b is a simple differential equation which is solved with the help of the initial conditions, equations 89, to find that ψ is zero at $z = 0$. Then, equation a gives $\frac{\partial \varphi}{\partial z}$. The impact problem in the rod, problem iv, is worked in the same manner; and we have the boundary conditions

$$\frac{\partial \varphi}{\partial z} = Z c_d t H(t) \quad \psi = 0. \quad (z = 0) \quad (90i, iv)$$

For the problem of the pressure step on the plate, problem ii, the two boundary conditions on σ_{zz} and u_y become conditions on φ and $\frac{\partial \psi}{\partial z}$;

$$-2\mu \frac{\partial^2 \varphi}{\partial y^2} + \frac{\lambda+2\mu}{c_d^2} \frac{\partial^2 \varphi}{\partial t^2} - 2\mu \frac{\partial}{\partial y} \left(\frac{\partial \psi}{\partial z} \right) = -Z(\lambda+2\mu)H(t) \quad (z = 0) \quad (c)$$

$$\frac{\partial \varphi}{\partial y} + \frac{\partial \psi}{\partial z} = 0 .$$

The second of equations c is differentiated with respect to y and substituted into the first to show that

$$\frac{\partial^2 \varphi}{\partial t^2} = -Z c_d^2 H(t) . \quad (z = 0) \quad (d)$$

The differential equation d is easy to solve with the initial conditions, equations 89, and then the second of equations c requires that $\frac{\partial \psi}{\partial z}$ be zero. The results for the rod are similar. Then, the

boundary conditions at $z = 0$ for the pressure step problems are

$$\varphi = -Zc_d^2 \frac{t^2}{2} H(t) \quad \frac{\partial \psi}{\partial z} = 0 \quad (z = 0) \quad (90ii, v)$$

For the line force problem the symmetry conditions that u_z and $\partial u_y / \partial z$ be zero are reflected in the two conditions

$$\frac{\partial \varphi}{\partial z} = \psi = 0 \quad (z = 0) \quad (90iii)$$

For the point force problem we only require that φ and ψ remain finite as z goes to zero.

To take the Laplace transforms, the governing differential equations, equations 87, are multiplied by $e^{-pt} dt$ and integrated over t from zero to infinity. In the same way we transform the boundary conditions on the edge of the plate or the end of the rod, equations 90, and the boundary conditions at $y = \pm a$. The Laplace transform has the definition given in equation 15a. Because the initial conditions are zero, the equations are transformed easily by putting bars over φ and ψ and replacing $\frac{\partial}{\partial t}$ by p . The resulting differential equations and boundary conditions are written below. For convenience second derivatives with respect to z are eliminated from the boundary conditions at $y = \pm a$. This is done by substituting the governing differential equations. The Laplace transformed equations are

$$\frac{\partial^2 \bar{\varphi}}{\partial z^2} + \frac{\partial^2 \bar{\varphi}}{\partial y^2} - \frac{p^2}{c_d^2} \bar{\varphi} = 0 \quad \frac{\partial^2 \bar{\psi}}{\partial z^2} + \frac{\partial^2 \bar{\psi}}{\partial y^2} - \frac{p^2}{c_s^2} \bar{\psi} = 0 \quad (91i, ii, iii)$$

$$\left. \begin{aligned} \frac{\partial^2 \bar{\varphi}}{\partial z^2} + \frac{1}{y} \frac{\partial}{\partial y} (y \frac{\partial \bar{\varphi}}{\partial y}) - \frac{p^2}{c_d^2} \bar{\varphi} &= 0 \\ \frac{\partial^2 \bar{\Psi}}{\partial z^2} + \frac{\partial}{\partial y} [\frac{1}{y} \frac{\partial}{\partial y} (y \bar{\Psi})] - \frac{p^2}{c_s^2} \bar{\Psi} &= 0 \end{aligned} \right\} (91iv, v)$$

$$\left. \begin{aligned} \frac{1}{z} \frac{\partial}{\partial z} (z \frac{\partial \bar{\varphi}}{\partial z}) + \frac{\partial^2 \bar{\varphi}}{\partial y^2} - \frac{p^2}{c_d^2} \bar{\varphi} &= 0 \\ \frac{\partial}{\partial z} [\frac{1}{z} \frac{\partial}{\partial z} (z \bar{\Psi})] + \frac{\partial^2 \bar{\Psi}}{\partial y^2} - \frac{p^2}{c_s^2} \bar{\Psi} &= 0 \end{aligned} \right\} (91vi)$$

$$\left. \begin{aligned} 2 \frac{\partial^2 \bar{\varphi}}{\partial y^2} + \frac{\lambda p^2}{\mu c_d^2} \bar{\varphi} + 2 \frac{\partial^2 \bar{\Psi}}{\partial y \partial z} &= \begin{cases} -\frac{Za}{p} \delta(z) & \text{iii, (y=+a)} \\ 0 & \text{(elsewhere)} \end{cases} \\ 2 \frac{\partial^2 \bar{\varphi}}{\partial y \partial z} - 2 \frac{\partial^2 \bar{\Psi}}{\partial y^2} + \frac{p^2}{c_s^2} \bar{\Psi} &= 0 \end{aligned} \right\} \begin{matrix} (y=\pm a) \\ (92i, ii, iii) \end{matrix}$$

$$\left. \begin{aligned} 2 \frac{\partial^2 \bar{\varphi}}{\partial y^2} + \frac{\lambda}{\mu} \frac{p^2}{c_d^2} \bar{\varphi} + 2 \frac{\partial^2 \bar{\Psi}}{\partial y \partial z} &= 0 \\ 2 \frac{\partial^2 \bar{\varphi}}{\partial y \partial z} - 2 \frac{\partial}{\partial y} [\frac{1}{y} \frac{\partial}{\partial y} (y \bar{\Psi})] + \frac{p^2}{c_s^2} \bar{\Psi} &= 0 \end{aligned} \right\} (y = +a) (92iv, v)$$

$$\left. \begin{aligned} 2 \frac{\partial^2 \bar{\varphi}}{\partial y^2} + \frac{\lambda}{\mu} \frac{p^2}{c_d^2} \bar{\varphi} + \frac{2}{z} \frac{\partial}{\partial z} (z \frac{\partial \bar{\Psi}}{\partial y}) &= \begin{cases} -\frac{Za^2}{pz} \delta(z) & (y=+a) \\ 0 & (y=-a) \end{cases} \\ 2 \frac{\partial^2 \bar{\varphi}}{\partial y \partial z} - 2 \frac{\partial^2 \bar{\Psi}}{\partial y^2} + \frac{p^2}{c_s^2} \bar{\Psi} &= 0 \end{aligned} \right\} (92vi) \quad (y=\pm a)$$

$$\frac{\partial \bar{\varphi}}{\partial z} = \frac{Zc_d}{p^2} \quad \bar{\Psi} = 0 \quad (z=0) \quad (93i, iv)$$

$$\bar{\varphi} = -\frac{Zc_d^2}{p^3} \quad \frac{\partial \bar{\Psi}}{\partial z} = 0 \quad (z=0) \quad (93ii, v)$$

$$\frac{\partial \bar{\phi}}{\partial x} = \bar{\psi} = 0 \quad (x=0). \quad (93iii)$$

Next, sine and cosine transforms of equations 91i, ii, iii, iv, v and 92i, ii, iii, iv, v are taken by multiplying the equations by either $\cos Kz dz$ or $-i \sin Kz dz$ and integrating over z from zero to infinity. Table 1 indicates which variables are sine transformed and which variables are cosine transformed. The choice of schemes is determined by what boundary conditions are given at $x = 0$. Problems ii and v fit into scheme 1 and problems i, iii, and iv fit into scheme 2. In each case the boundary conditions at the end of the rod or plate asked for by the transforming procedure are the same as the boundary conditions that are known. The definitions of the double transforms and the inversion theorem for the sine and cosine transforms are given in equations 16. The results are

$$\frac{d^2 \bar{\phi}}{dy^2} - \kappa_d^2 \bar{\phi} = \begin{cases} \frac{Zc_d}{p^2} \\ -\frac{Zi\kappa_c^2 d}{p^3} \\ 0 \end{cases} \quad \frac{d^2 \bar{\psi}}{dy^2} - \kappa_s^2 \bar{\psi} = \begin{cases} 0 \\ 0 \\ 0 \end{cases} \quad \begin{matrix} (94i) \\ (94ii) \\ (94iii) \end{matrix}$$

$$\frac{1}{y} \frac{d}{dy} \left(y \frac{d \bar{\phi}}{dy} \right) - \kappa_d^2 \bar{\phi} = \begin{cases} \frac{Zc_d}{p^2} \\ -\frac{Zi\kappa_c^2 d}{p^3} \end{cases} \quad \begin{matrix} (94iv) \\ (94v) \end{matrix}$$

$$\frac{d}{dy} \left[\frac{1}{y} \frac{d}{dy} (y \bar{\psi}) \right] - \kappa_s^2 \bar{\psi} = \begin{cases} 0 \\ 0 \end{cases}, \quad \begin{matrix} (94iv) \\ (94v) \end{matrix}$$

where $\kappa_d^2 = \frac{p^2}{c_d^2} + \kappa^2$ and $\kappa_s^2 = \frac{p^2}{c_s^2} + \kappa^2$.

$$\left. \begin{aligned}
 2 \frac{d^2 \bar{\varphi}}{dy^2} + \frac{\lambda}{\mu} \frac{p^2}{c_d^2} \bar{\varphi} + 2i\kappa \frac{d\bar{\psi}}{dy} &= \begin{cases} -\frac{Za}{2p} & (y=+a), \text{iii} \\ 0 & (\text{otherwise}) \end{cases} \\
 2i\kappa \frac{d\bar{\varphi}}{dy} - 2 \frac{d^2 \bar{\psi}}{dy^2} + \frac{p^2}{c_s^2} \bar{\psi} &= 0
 \end{aligned} \right\} \begin{matrix} (y=\pm a) \\ (95i, \text{ii}, \text{iii}) \end{matrix}$$

$$\left. \begin{aligned}
 2 \frac{d^2 \bar{\varphi}}{dy^2} + \frac{\lambda}{\mu} \frac{p^2}{c_d^2} \bar{\varphi} + 2i\kappa \frac{d\bar{\psi}}{dy} &= 0 \\
 2i\kappa \frac{d\bar{\varphi}}{dy} - 2 \frac{d}{dy} \left[\frac{1}{y} \frac{d}{dy} (y \bar{\psi}) \right] + \frac{p^2}{c_s^2} \bar{\psi} &= 0
 \end{aligned} \right\} \begin{matrix} (y=+a) \\ (95iv, v) \end{matrix}$$

Hankel transforms are used for the point force problem because of the cylindrical symmetry in the direction of propagation, z . To keep a similarity between the line force and point force problems, the Hankel transforms are defined here as

$$\left. \begin{aligned}
 \bar{\varphi}(y, \kappa, p) &= \int_0^\infty \frac{z}{a} \bar{\varphi}(y, z, p) J_0(\kappa z) dz \\
 \bar{\psi}(y, \kappa, p) &= -i \int_0^\infty \frac{z}{a} \bar{\psi}(y, z, p) J_1(\kappa z) dz
 \end{aligned} \right\} (96a)$$

The inversion integrals are (30, p. 342)

$$\left. \begin{aligned}
 \bar{\varphi}(y, z, p) &= a \int_0^\infty \kappa \bar{\varphi}(y, \kappa, p) J_0(\kappa z) d\kappa \\
 \bar{\psi}(y, z, p) &= ia \int_0^\infty \kappa \bar{\psi}(y, \kappa, p) J_1(\kappa z) d\kappa
 \end{aligned} \right\} (96b)$$

Equations 91vi and 92vi are then transformed by multiplying them

by $(z/a)J_0(\kappa z) dz$ or $-(iz/a)J_1(\kappa z) dz$ and integrating over z from zero to infinity. The terms with z derivatives are integrated by parts, the boundary terms at $z = 0$ vanishing provided $\bar{\varphi}$ and $\bar{\psi}$ are bounded as z goes to zero. The results are

$$\frac{d^2 \bar{\varphi}}{dy^2} - \kappa_d^2 \bar{\varphi} = 0 \quad \frac{d^2 \bar{\psi}}{dy^2} - \kappa_s^2 \bar{\psi} = 0 \quad (94vi)$$

$$2 \frac{d^2 \bar{\varphi}}{dt^2} + \frac{\lambda}{\mu} \frac{P}{c_d} \frac{d^2 \bar{\varphi}}{dt^2} + 2i\kappa \frac{d\bar{\psi}}{dy} = \begin{cases} -\frac{Za}{Zp} & (y=+a) \\ 0 & (y=-a) \end{cases} \quad (95vi)$$

$$2i\kappa \frac{d\bar{\varphi}}{dy} - 2 \frac{d^2 \bar{\psi}}{dy^2} + \frac{P}{c_s} \frac{d^2 \bar{\psi}}{dy^2} = 0 \quad (y=\pm a).$$

Important comparisons can be made between the problems. Equations 94vi and 95vi are exactly the same as equations 94iii and 95iii. Therefore, the double transforms for the line force are exactly the same as the double transforms for the point force. Only the inversion theorems, equations 96b and 16b, are different. Furthermore, the nonhomogeneous terms in equations 94 for problems ii and v differ from the same terms for problems i and iv only by the factor $-i\kappa c_d/p$. Therefore, the two pressure step problems will differ from the impact problems only because of that one factor and through the difference between the definitions of Z .

Equations 94 and 95 are easily solved. The solutions to the differential equations 94 are

$$\begin{aligned}
 \bar{\phi} &= K_1 \cosh \kappa_d y + K_2 \sinh \kappa_d y - \frac{Z c_d}{\kappa_d^2} & \left. \begin{aligned} & \\ & \end{aligned} \right\} (97i) \\
 \bar{\psi} &= K_3 \sinh \kappa_s y + K_4 \cosh \kappa_s y & \\
 \bar{\phi} &= K_1 \cosh \kappa_d y + K_2 \sinh \kappa_d y & \left. \begin{aligned} & \\ & \end{aligned} \right\} (97iii) \\
 \bar{\psi} &= K_3 \sinh \kappa_s y + K_4 \cosh \kappa_s y & \\
 \bar{\phi} &= K_1 I_0(\kappa_d y) - \frac{Z c_d}{\kappa_d^2} & \bar{\psi} = K_3 I_1(\kappa_s y), & (97iv)
 \end{aligned}$$

where the K_i are independent of y and $I_0(x)$ and $I_1(x)$ are modified Bessel functions of the first kind. Equations 97 are the complete solutions of the differential equations for the double transforms.

Equation 97iv omits the solutions which are irregular at $y = 0$. The double transforms for the other three problems are similar to the double transforms given above.

The boundary conditions, equations 95, are applied directly to equations 97 to find the K_i . Four linear algebraic equations result, two equations for $y = +a$ and two equations for $y = -a$, except that for the circular rod there are no equations for $y = -a$. The forcing terms in the four equations come from the constant terms in equations 97i, ii, iv, v and for the line and point force problem directly from the boundary conditions, equations 95iii, vi. The two equations for K_1 and K_3 for the rod have the determinant

$$\begin{aligned}
 F &= \left(\frac{P}{c_s} + 2\kappa^2 \right)^2 I_0(\kappa_d a) I_1(\kappa_s a) - 4\kappa^2 \kappa_d \kappa_s I_1(\kappa_d a) I_0(\kappa_s a) \\
 &\quad - \frac{2P}{ac_s} \kappa_d I_1(\kappa_d a) I_1(\kappa_s a). & (98a)
 \end{aligned}$$

The equation $F = 0$ is the Pochhammer-Chree frequency equation for the circular frequency, $\omega = -ip$, as a function of the wave number, κ . The four equations for the plate problems can be separated into two pairs of equations. One pair is for symmetric or compressional waves and has the determinant

$$F_g = \left(\frac{P}{Z} + 2\kappa^2 \right) \frac{2}{c_s} \cosh \kappa_d a \sinh \kappa_s a - 4\kappa^2 \kappa_d \kappa_s \sinh \kappa_d a \cosh \kappa_s a. \quad (98b)$$

The other pair of equations is for the antisymmetric or flexural waves and has the determinant

$$F_u = \left(\frac{P}{Z} + 2\kappa^2 \right) \frac{2}{c_s} \sinh \kappa_d a \cosh \kappa_s a - 4\kappa^2 \kappa_d \kappa_s \cosh \kappa_d a \sinh \kappa_s a. \quad (98c)$$

The equations $F_g = 0$ and $F_u = 0$ are the Rayleigh-Lamb frequency equations for the symmetric and antisymmetric waves in a plate.

Having solved for the K_1 , the results for the double transforms are as follows:

Plate, impact,

$$\left. \begin{aligned} \bar{\varphi} &= \frac{Z\lambda}{\mu c_d \kappa_d^2 F_g} \left(\frac{P}{Z} + 2\kappa^2 \right) \frac{2}{c_s} \sinh \kappa_s a \cosh \kappa_d y - \frac{Zc_d}{\kappa_d^2 p} \\ \bar{\psi} &= \frac{2Z\lambda i \kappa}{\mu c_d \kappa_d^2 F_g} \sinh \kappa_d a \sinh \kappa_s y. \end{aligned} \right\} (99i)$$

Plate, pressure step,

$$\text{Replace } Z \text{ in equations 99i by } -i \frac{c_d \kappa}{p} Z. \quad (99ii)$$

Plate, line and point force,

$$\bar{\phi} = - \frac{Za \left(\frac{p^2}{c_s^2} + 2\kappa^2 \right)}{2p} \left[\frac{\sinh \kappa_s a \cosh \kappa_d y}{2F_g} + \frac{\cosh \kappa_s a \sinh \kappa_d y}{2F_u} \right]$$

$$\bar{\psi} = \frac{-Za i \kappa \kappa_d}{p} \left[\frac{\sinh \kappa_d a \sinh \kappa_s y}{2F_g} + \frac{\cosh \kappa_d a \cosh \kappa_s y}{2F_u} \right]. \quad (99iii, vi)$$

Rod, impact,

$$\bar{\phi} = \frac{Z\lambda \left(\frac{p^2}{c_s^2} + 2\kappa^2 \right)}{\mu c_d \kappa_d^2 F} I_1(\kappa_s a) I_0(\kappa_d y) - \frac{Z c_d}{\kappa_d^2 p^2}$$

(99iv)

$$\bar{\psi} = \frac{2Z\lambda i \kappa}{\mu c_d \kappa_d F} I_1(\kappa_d a) I_1(\kappa_s y).$$

Rod, pressure step,

$$\text{Replace } Z \text{ in equations 99iv by } -i \frac{c_d \kappa}{p} Z. \quad (99v)$$

B. EXPANSION OF THE TRANSFORMS FOR PLANE STRAIN

The wave front expansion for plane strain is derived in several steps. The exponential functions, which, according to equation 85, are associated with the times of arrival, are contained in the hyperbolic sine and cosine functions in the double transforms, equations 99i, ii, iii. The exponential functions in F_g and F_u are brought to the numerator by using a binomial expansion. It is only necessary to look at F_g or F_u as a binomial consisting of one large term, the largest of the exponentials, and one small term, the rest of F_g or F_u . In addition, notice that the double transforms, aside from the exponential parts, are homogeneous in κ/p . This suggests the substitution, $\kappa = sp/c_d$, giving a new variable $s = \kappa c_d/p$. Then $\kappa_d = \frac{p}{c_d} \sqrt{1+s^2}$ and $\kappa_s = \frac{p}{c_d} \sqrt{k^2+s^2}$, where $k = c_d/c_s$. The quantities

$$\frac{c_d^4}{p^4} F_g = (k^2 + 2s^2)^2 \cosh \kappa_d a \sinh \kappa_s a - 4s^2 \sqrt{(1+s^2)(k^2+s^2)} \sinh \kappa_d a \cosh \kappa_s a \quad (100a)$$

and

$$\frac{c_d^4}{p^4} F_u = (k^2 + 2s^2)^2 \sinh \kappa_d a \cosh \kappa_s a - 4s^2 \sqrt{(1+s^2)(k^2+s^2)} \cosh \kappa_d a \sinh \kappa_s a \quad (100b)$$

must be expanded by the binomial expansion. Thus, in each case the first inversion integral, equation 16b, becomes an integral along the real axis of s :

Plate, impact,

$$\bar{\varphi} = -\frac{Zc_d^2}{\pi p^3} \int_{-\infty}^{\infty} \frac{e^{i(p/c_d)sz}}{(1+s^2)} ds$$

$$+ \frac{Z\lambda c_d^2}{\pi \mu p^3} \int_{-\infty}^{\infty} \frac{(k^2+2s^2) \sinh \kappa_s a \cosh \kappa_d y}{(1+s^2) \left(\frac{c_d}{p}\right)^4 F_g} e^{i(p/c_d)sz} ds$$

$$\bar{\psi} = \frac{2Z\lambda c_d^2}{\pi \mu p^3} \int_{-\infty}^{\infty} \frac{is \sinh \kappa_d a \sinh \kappa_s y}{\sqrt{(1+s^2)} \left(\frac{c_d}{p}\right)^4 F_g} e^{i(p/c_d)sz} ds$$
} (1011)

Plate, pressure step,

Replace Z in equation 1011 by -isZ (1011i)

Plate, line force,

$$\bar{\varphi} = -\frac{Zac_d}{4\pi p^2} \int_{-\infty}^{\infty} (k^2+2s^2) \left[\frac{\sinh \kappa_s a \cosh \kappa_d y}{\left(\frac{c_d}{p}\right)^4 F_g} + \frac{\cosh \kappa_s a \sinh \kappa_d y}{\left(\frac{c_d}{p}\right)^4 F_u} \right] e^{i(p/c_d)sz} ds$$

$$\bar{\psi} = -\frac{Zac_d}{2\pi p^2} \int_{-\infty}^{\infty} is \sqrt{1+s^2} \left[\frac{\sinh \kappa_d a \sinh \kappa_s y}{\left(\frac{c_d}{p}\right)^4 F_g} + \frac{\cosh \kappa_d a \cosh \kappa_s y}{\left(\frac{c_d}{p}\right)^4 F_u} \right] e^{i(p/c_d)sz} ds$$
} (1011ii)

It is now necessary to choose a branch of the square root function for what follows. The above integrations are along the real s axis and hence $\sqrt{1+s^2}$ and $\sqrt{k^2+s^2}$ must be real numbers, either positive or negative. We will choose the positive square

roots to be meant by either of the radicals when s is real. Under that choice $e^{-K_d a} = e^{-\frac{pa}{c_d} \sqrt{1+s^2}}$ and $e^{-K_s a} = e^{-\frac{pa}{c_d} \sqrt{k^2+s^2}}$ vanish for large, positive, real p while $e^{K_d a}$ and $e^{K_s a}$ approach infinity as p increases without limit.

Then, the factors $\frac{c_d^4}{p^4} F_g$ and $\frac{c_d^4}{p^4} F_u$ in the transforms and given in equations 100 can be written out as

$$\frac{c_d^4}{p^4} F_g = \frac{1}{4} \left\{ \begin{aligned} & \left[(k^2+2s^2)^2 - 4s^2 \sqrt{(1+s^2)(k^2+s^2)} \right] \left[e^{K_d a + K_s a} \quad -e^{-K_d a - K_s a} \right] \\ & + \left[(k^2+2s^2)^2 + 4s^2 \sqrt{(1+s^2)(k^2+s^2)} \right] \left[e^{-K_d a + K_s a} \quad -e^{K_d a - K_s a} \right] \end{aligned} \right\}$$

and

$$\frac{c_d^4}{p^4} F_u = \frac{1}{4} \left\{ \begin{aligned} & \left[(k^2+2s^2)^2 - 4s^2 \sqrt{(1+s^2)(k^2+s^2)} \right] \left[e^{K_d a + K_s a} \quad -e^{-K_d a - K_s a} \right] \\ & + \left[(k^2+2s^2)^2 + 4s^2 \sqrt{(1+s^2)(k^2+s^2)} \right] \left[e^{K_d a - K_s a} \quad -e^{-K_d a + K_s a} \right] \end{aligned} \right\} \quad (102)$$

Looking at both expressions in equations 102, one can see that for large, positive, real p the term made out of $e^{K_d a + K_s a}$ and its coefficients is larger than the remaining terms. More

precisely, there exists some \tilde{p} , independent of s , such that for all p greater than \tilde{p} the above mentioned term is greater than all of the remaining terms together. Then, we may apply the binomial

theorem in the form $(1-x)^{-1} = \sum_{n=0}^{\infty} x^n$ for $|x| < 1$ to obtain the result

desired. This expansion was suggested by Pekeris in a problem involving layered media (see reference 29, p. 131). It suffices only to consider p greater than \tilde{p} because the inverse of the Laplace transform is uniquely determined if the transform is known for all values of the transform parameter, p , greater than some fixed number, according to Lerch's theorem (31). Let

$$\begin{aligned}
 P &= e^{-2k_d a} = e^{-\frac{p}{c_d} 2a \sqrt{1+s^2}} \\
 \text{and} \\
 S &= e^{-2k_s a} = e^{-\frac{p}{c_d} 2a \sqrt{k^2+s^2}}
 \end{aligned}
 \tag{103}$$

the exponential factors relating to travel across the plate as P and S waves, respectively, and let

$$R(s) = \frac{(k^2+2s^2)^2 + 4s^2 \sqrt{(1+s^2)(k^2+s^2)}}{(k^2+2s^2)^2 - 4s^2 \sqrt{(1+s^2)(k^2+s^2)}}
 \tag{104}$$

a factor which will be identified as a reflection coefficient in the ray theory of wave fronts. Then, from equation 102

$$\frac{1}{\left(\frac{c_d}{p}\right)^{\frac{1}{4}} F_g} = \frac{\sum_{n=0}^{\infty} [SP + R(S-P)]^n}{\frac{1}{4} [(k^2 + 2s^2)^2 - 4s^2 \sqrt{(1+s^2)(k^2+s^2)}] e^{K_d a + K_s a}}$$

and

$$\frac{1}{\left(\frac{c_d}{p}\right)^{\frac{1}{4}} F_u} = \frac{\sum_{n=0}^{\infty} [SP + R(P-S)]^n}{\frac{1}{4} [(k^2 + 2s^2)^2 - 4s^2 \sqrt{(1+s^2)(k^2+s^2)}] e^{K_d a + K_s a}}$$

The transforms are written in a more useful form by substituting equations 105 into equations 101:

Plate, impact,

$$\bar{\varphi} = -\frac{Zc_d^2}{\pi p^3} \int_{-\infty}^{\infty} \frac{e^{\frac{iP}{c_d} sz}}{(1+s^2)} + \frac{Z\lambda c_d^2}{\pi \mu p^3} \int_{-\infty}^{\infty} \frac{(k^2 + 2s^2) [e^{-K_d(a-y)} + e^{-K_d(a+y)}]}{(1+s^2) [(k^2 + 2s^2)^2 - 4s^2 \sqrt{(1+s^2)(k^2+s^2)}]} ds$$

$$(1-S) \sum_{n=0}^{\infty} [SP + R(S-P)]^n e^{\frac{iP}{c_d} sz}$$

$$\bar{\psi} = \frac{2Z\lambda c_d^2}{\pi \mu p^3} \int_{-\infty}^{\infty} \frac{is [e^{-K_s(a-y)} - e^{-K_s(a+y)}]}{\sqrt{1+s^2} [(k^2 + 2s^2)^2 - 4s^2 \sqrt{(1+s^2)(k^2+s^2)}]} ds$$

$$(1-P) \sum_{n=0}^{\infty} [SP + R(S-P)]^n e^{\frac{iP}{c_d} sz}$$

Plate, pressure step.

Replace Z in equations 106i by -isZ. (106ii)

Plate, line force.

$$\bar{\varphi} = -\frac{Zc_d a}{2\pi p^2} \int_{-\infty}^{\infty} \frac{(k^2 + 2s^2)}{[(k^2 + 2s^2)^2 - 4s^2 \sqrt{(1+s^2)(k^2 + s^2)}]} \times \left\{ \frac{1}{2} [e^{-\kappa_d(a-y)} + e^{-\kappa_d(a+y)}] (1-S) \sum_{n=0}^{\infty} [SP + R(S-P)]^n + \frac{1}{2} [e^{-\kappa_d(a-y)} - e^{-\kappa_d(a+y)}] (1+S) \sum_{n=0}^{\infty} [SP + R(P-S)]^n \right\} e^{i\frac{P}{c_d} sz} ds$$

$$\bar{\psi} = -\frac{Zc_d a}{\pi p^2} \int_{-\infty}^{\infty} \frac{is \sqrt{1+s^2}}{[(k^2 + 2s^2)^2 - 4s^2 \sqrt{(1+s^2)(k^2 + s^2)}]} \times \left\{ \frac{1}{2} [e^{-\kappa_s(a-y)} - e^{\kappa_s(a+y)}] (1-P) \sum_{n=0}^{\infty} [SP + R(S-P)]^n + \frac{1}{2} [e^{-\kappa_s(a-y)} + e^{-\kappa_s(a+y)}] (1+P) \sum_{n=0}^{\infty} [SP + R(P-S)]^n \right\} e^{i\frac{P}{c_d} sz} ds \tag{106iii}$$

It may be anticipated that individual wave fronts will be found from single exponential functions. Looking at the transforms, equations 106, it is clear that one can separate out the exponential functions if the coefficient of $S^m P^n$ can be found for given m and n. The only difficulty is in working with the infinite sums. By the binomial theorem*

$$(a+b)^n = \sum_{m=0}^n \binom{n}{m} a^m b^{n-m} \text{ where } \binom{n}{m} = \binom{n}{n-m} = \frac{n!}{(n-m)! m!} .$$

$$\begin{aligned} \sum_{k=0}^{\infty} [SP+R(S-P)]^k &= \sum_{k=0}^{\infty} \sum_{l=0}^k \binom{k}{l} (SP)^{k-l} R^l (S-P)^l \\ &= \sum_{k=0}^{\infty} \sum_{l=0}^k \binom{k}{l} (SP)^{k-l} R^l \sum_{j=0}^l \binom{l}{j} S^{l-j} (-P)^j. \end{aligned}$$

Letting $m = k - j$, the sum becomes

$$\sum_{k=0}^{\infty} \sum_{l=0}^k \sum_{m=k-l}^k \binom{k}{l} \binom{l}{k-m} (-1)^{k-m} R^l S^m P^{2k-l-m}$$

The same combinations of l and m are covered if the limits are changed to

$$\sum_{k=0}^{\infty} \sum_{m=0}^k \sum_{l=k-m}^k \binom{k}{l} \binom{l}{k-m} (-1)^{k-m} R^l S^m P^{2k-l-m}$$

Then, letting $n = 2k - l - m$, the sum becomes

$$\sum_{k=0}^{\infty} \sum_{m=0}^k \sum_{n=k-m}^k \binom{k}{2k-m-n} \binom{2k-m-n}{k-m} (-1)^{k-m} S^m P^n R^{2k-m-n}$$

Again changing limits, but still covering the same combinations of k , m , and n , the final form is found as

$$\begin{aligned} &\sum_{k=0}^{\infty} [SP+R(S-P)]^k \\ &= \sum_{n, m=0}^{\infty} S^m P^n \sum_k \binom{k}{2k-m-n} \binom{2k-m-n}{k-m} (-1)^{k-m} R^{2k-m-n}, \quad (107) \end{aligned}$$

where the sum over k runs from the greater of m and n up to

$m+n$. The similar expansion of F_u gives the same series except for sign changes as can be seen from equations 105.

It is next possible to write the integrals of equations 106 for the transformed solutions as a sum of integrals. Each integral in the sum has an exponential which can be factored into three exponen-

tials, first, e^{ips/c_d} , second, either $e^{-\kappa_d(a \pm y)}$ or $e^{-\kappa_s(a \pm y)}$, and third $e^{-\frac{p}{c_d}(a \pm y) \sqrt{1+s^2}}$ or $e^{-\frac{p}{c_d}(a \pm y) \sqrt{k^2+s^2}}$.

and third $P^n S^m = e^{-\frac{p}{c_d} 2a(n \sqrt{1+s^2} + m \sqrt{k^2+s^2})}$ with n and m integers. For each pair of integers n and m a separate integral can be written. Calculation of wave fronts then boils down to studying transforms written in the form

$$\bar{\varphi} \text{ or } \bar{\psi} = \frac{1}{pN} \int_{-\infty}^{\infty} f(s) e^{-\frac{p}{c_d} [-i s a + \alpha \sqrt{1+s^2} + \beta \sqrt{k^2+s^2}]} ds, \quad (108)$$

where $f(s)$ is a known function and N is a known integer. For the dilatational potential

$$\alpha = (2n + 1)a \pm y \quad \text{and} \quad \beta = 2ma \quad (109a)$$

while for the shear potential

$$\alpha = 2na \quad \text{and} \quad \beta = (2m + 1)a \pm y. \quad (109b)$$

Let the exponent in equation 108 be $-p$ times the function $g(s)$,

where

$$g(s) = \frac{1}{c_d} \left[-i\alpha s + \alpha \sqrt{1+s^2} + \beta \sqrt{k^2+s^2} \right], \quad (110)$$

Since the factor $1/p$ in equation 108 is equivalent to a partial derivative with respect to time, the transform of the N^{th} derivative of φ or ψ is a sum of integrals of the form

$$\frac{\partial^N \varphi}{\partial t^N} \text{ or } \frac{\partial^N \psi}{\partial t^N} = \int_{-\infty}^{\infty} f(s) e^{-pg(s)} ds. \quad (111)$$

Each integral of the form of equation 111 will be seen to represent the disturbance following a single wave front. The functions $f(s)$ and $g(s)$ depend on whether the dilatational or shear potential is being studied, which plane strain problem is being considered, and the two integers, n and m . The functions, $f(s)$ are found from equations 106 by using equation 107. For the line force problem the two terms in each of equations 106iii should be compared upon change of sign of both S and P . It is clear that if $m+n$ is even only the terms with $a-y$ survive, and if $m+n$ is odd only the terms with $a+y$ survive. This will explain why only half of the wave fronts exist in the line force problem. Except for the first term in equations 106i, ii, for which $\alpha=\beta=0$, the functions $f(s)$ are as follows in terms of $R(s)$ given in equation 104:

Plate impact, (N=3)

For dilatational potential

$$f(s) = \frac{Z\lambda c_d^2(k^2+2s^2)[R_{m,n}(R) - R_{(m-1),n}(R)]}{\pi\mu(1+s^2)[(k^2+2s^2)^2 - 4s^2\sqrt{(1+s^2)(k^2+s^2)}} \quad (1121a)$$

For shear potential

$$f(s) = \frac{2Z\lambda c_d^2 is [R_{m,n}(R) - R_{m,(n-1)}(R)]}{\pi\mu\sqrt{1+s^2}[(k^2+2s^2)^2 - 4s^2\sqrt{(1+s^2)(k^2+s^2)}]}, \quad (1121b)$$

where

$$R_{m,n}(R) = \sum_{l=\text{greater of } m, n}^{m+n} \binom{l}{2l-m-n} \binom{2l-m-n}{l-m} (-1)^{l-m} R^{2l-m-n}$$

and

$$R_{-1,n}(R) = R_{m,-1}(R) = 0.$$

Plate, pressure step, (N=3)

$$\text{Replace } Z \text{ in equations 1121 by } -isZ. \quad (1121i)$$

Plate, line force, (N=2)

$$\text{Replace } Z\lambda/\mu \text{ in equations 1121 by } -\frac{a}{2c_d} Z(1+s^2)$$

$$\text{and take only the upper signs of } m+n \text{ is even,} \quad (1121ii)$$

the lower signs of $m+n$ is odd.

The first term in equations 106i, ii deserves special attention. That term can be integrated easily by contour integration. The results come from the pole at $s=i$ and give for the transform of φ

$$\bar{\varphi} = -\frac{Zc_d^2}{P} e^{-\frac{P}{c_d} z}$$

for both problems i and ii. This can be inverted easily, for instance, by means of tables of the Laplace transform. Then, differentiation in accordance with equations 86i, ii gives the displacements. The motion is only in the z direction with the strain in the z direction, ϵ_z , given by

$$\epsilon_z = \frac{\partial u_z}{\partial z} = -ZH\left(t - \frac{z}{c_d}\right) \quad (113)$$

Equation 113 represents the step found in both of the end load problems. It is the first wave formed by the load as it hits the edge of the plate. The significance of the step will be explained in conjunction with the ray theory.

C. EVALUATION OF THE INTEGRALS FOR THE WAVE FRONTS

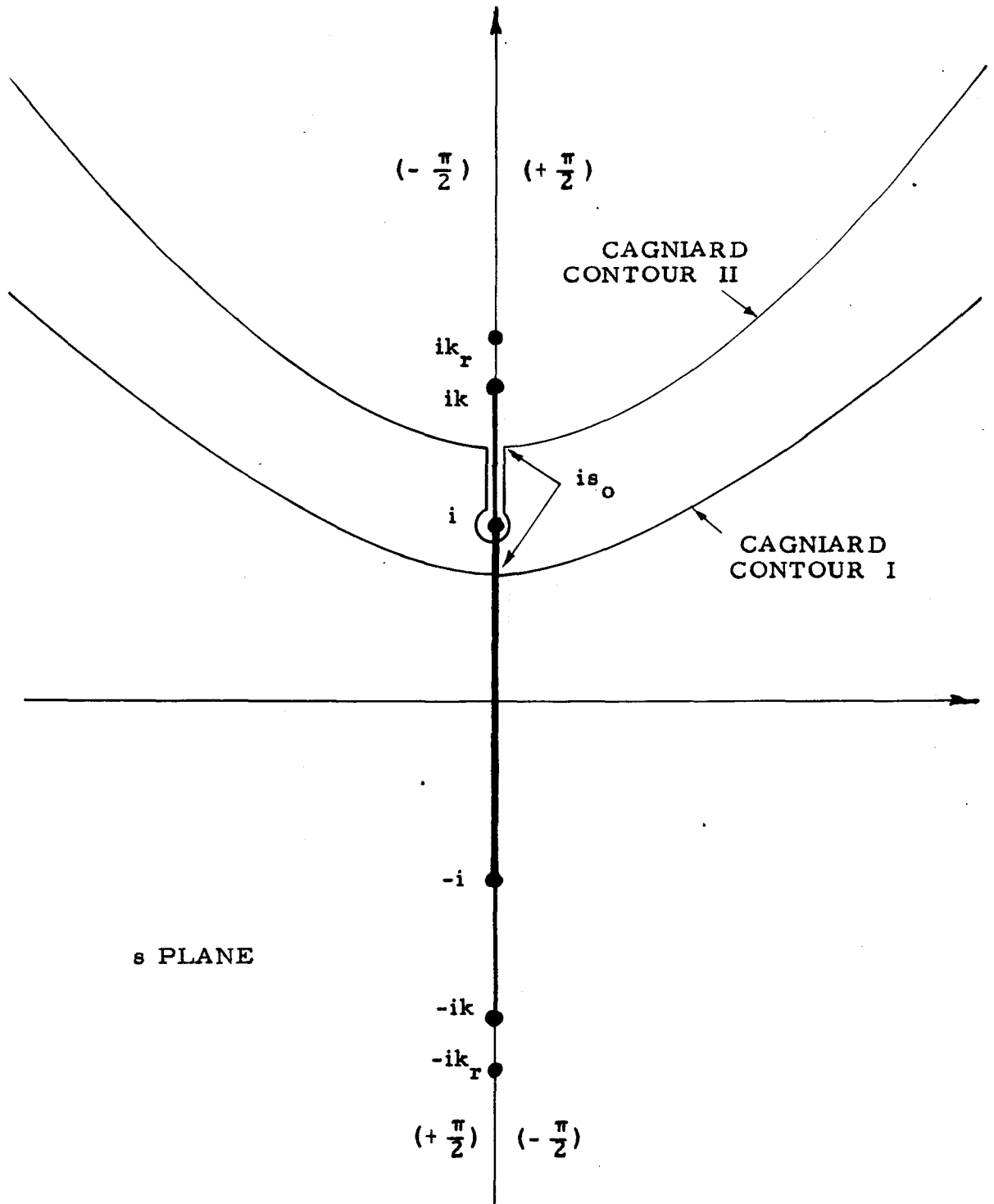
It is possible to find the amplitudes and times of arrival of the wave fronts associated with each integral of the form given in equation 111. To do this, the integrand must be continued into the complex plane of s and the contour of integration altered from the real axis. Either of two methods can be used, the saddle point method or Cagniard's method.

The only difficulty associated with the extension into the complex s plane is due to the radicals $\sqrt{1+s^2}$ and $\sqrt{k^2+s^2}$, which appear in $f(s)$ and $g(s)$. It is necessary and sufficient to make branch cuts running from the two roots of $1+s^2=0$, $\pm i$, and

from the two roots of $k^2 + s^2 = 0$, $\pm ik$, to infinity. This is done by using branch cuts running all along the imaginary axis except between $+i$ and $-i$, as is shown in figure 6. It will be recalled that previously $\sqrt{1+s^2}$ and $\sqrt{k^2+s^2}$ were both taken to be positive real numbers along the real s axis. Then, the values of $\sqrt{1+s^2}$ and $\sqrt{k^2+s^2}$ in the complex s plane are defined to be the analytic continuation off of the real axis and up to the branch cuts. The arguments of the radicals $\sqrt{1+s^2}$ and $\sqrt{k^2+s^2}$ along the branch cuts are given in parenthesis in figure 6

Great freedom is allowed in moving the contour of integration. The only poles are the poles of the functions $f(s)$ given in equations 112. The poles occur in some cases where $1+s^2 = 0$, which is also a branch point, and in all cases where $(k^2+s^2)^2 - 4s^2 \sqrt{(1+s^2)(k^2+s^2)} = 0$. Eliminating the radicals in this equation by squaring, one obtains the equation for the Rayleigh surface wave speed. (See the section below on Rayleigh waves.) Letting c_r be the speed of Rayleigh surface waves, the pole is at $s = ik_r \equiv ic_d/c_r$, which is along the branch cut since $k_r > k = c_d/c_s$. Thus, only the branch cuts interfere with moving the contour of integration. The ends of the contour may be moved freely because the exponential functions cause the integrand to vanish sufficiently rapidly in the first two quadrants as s goes to infinity.

The above considerations assure us that for $z > 0$ any contour in the s plane shown in figure 6 extending continuously from infinity in the second quadrant across the imaginary axis between



INVERSION CONTOURS

Figure 6

the branch points $\pm i$ and off to infinity again in the first quadrant is equivalent to the original contour along the real axis.

Cagniard's Method

Cagniard's method is to pick a contour such that the exponent of equation 111 is real and to let $-1/p$ times that exponent be a new, real variable of integration, t ; then,

$$t = g(s) \equiv \frac{1}{c_d} [-iss + a \sqrt{1+s^2} + \beta \sqrt{k^2+s^2}]. \quad (114)$$

Also,

$$ds = \frac{dt}{g'(s)} \equiv \frac{c_d dt}{-is + \frac{as}{\sqrt{1+s^2}} + \frac{\beta s}{\sqrt{k^2+s^2}}}$$

A glance at equation 15a defining the Laplace transform suggests that t will be identified with time.

It is not necessary here to solve explicitly for s as a function of t . The solution is possible by the quadratic formula only if a or β is zero. However, several features of the solution must be studied. As t goes to infinity, so does s . For t large and positive $s \approx \frac{c_d t}{-1E + a + \beta}$ in the first quadrant while in the second quadrant $s \approx \frac{c_d t}{-1E - a - \beta}$. The solutions for s as a function of t in the first and second quadrants, where the contour may be moved freely, exist only for t positive. While moving toward the imaginary axis from either end of the contour, t decreases continuously and is stationary where the two ends of the contour join at the imaginary axis and where

$$dt = g'(s) ds = 0. \quad (115)$$

This point is referred to in the saddle point method as the saddle point. It is located on the imaginary axis at a point $s = is_0$, where s_0 is the root of the real equation

$$-ig'(is_0) = -s + \frac{as_0}{\sqrt{1-s_0^2}} + \frac{\beta s_0}{\sqrt{k^2-s_0^2}} = 0. \quad (116)$$

Two cases must be distinguished. If the saddle point given by equation 116 is located between the branch points $s = \pm 1$, then the contour is closed at $s = is_0$ (Cagniard contour I, figure 6) and the value of $g(s)$ at the saddle point is the minimum value of t . From equation 114 and 116 that value is

$$\begin{aligned} \tau = g(is_0) &= \frac{1}{c_d} \left[s_0 z + a \sqrt{1-s_0^2} + \beta \sqrt{k^2-s_0^2} \right] \\ &= \frac{1}{c_d} \left[\frac{a}{\sqrt{1-s_0^2}} + \frac{k^2 \beta}{\sqrt{k^2-s_0^2}} \right] \end{aligned} \quad (117)$$

This τ will be seen to be the time of arrival of regular wave fronts. Equations 116 and 117 can be solved simultaneously to find the wave front locations and times of arrival. However, explicit solution by the quadratic formula is possible only if a or β is zero.

If the saddle point is located along the branch cut, then the contour is closed by extending it along the branch cut to close at $s = i$ (Cagniard contour II, figure 6). Then the minimum of t is the value of $g(s)$ at $s = i$;

$$\tau_H = g(t) = \frac{1}{c_d} [z + \beta \sqrt{k^2 - 1}], \quad (118)$$

where the subscript indicates that this is the time of arrival of head waves. The condition for Cagniard contour II is $s_0 > 1$. This only occurs when $\alpha = 0$, for if $\alpha > 0$, the term $\alpha s_0 / \sqrt{1 - s_0^2}$ in equation 116 ranges from zero to infinity with s_0 between zero and one; and it can be shown that that term can match the other two terms while s_0 remains between zero and one.

The integral of equation 111 can then be found by taking twice its real part and integrating only along the half of Cagniard's path in the first quadrant owing to the conjugate nature of the integrands and the two halves of the path. In the integral t goes from τ or τ_H to infinity and the transform is represented by an integral over real t with s expressed by equation 114 as a function of t , $s(t)$, in the first quadrant;

$$\frac{\partial N}{\partial t} \text{ or } \frac{\partial N_{\psi}}{\partial t} = 2\text{Re} \int_{\tau \text{ or } \tau_H}^{\infty} \frac{f[s(t)]}{g[s(t)]} e^{-Pt} dt. \quad (119)$$

When Cagniard contour I is applicable, τ is the lower limit; τ_H is used with Cagniard contour II. By the definition of the Laplace transform, equation 15a, and also because no two functions have the same Laplace transform,

$$\frac{\partial N}{\partial t} \text{ or } \frac{\partial N_{\psi}}{\partial t} = 2\text{Re} \frac{f[s(t)]}{g[s(t)]} H[t - (\tau \text{ or } \tau_H)]. \quad (120)$$

Thus, t is identified as time and τ or τ_H as the time of arrival

of the wave. This inversion is exact as applied here to plane strain problems. Integration N times over time is necessary to find the final solution for φ and ψ . Displacements and strains can be found similarly or by differentiation of the results for the potentials.

Regular Wave Fronts

The first term of the wave front expansion must be found by considering separately the cases where the saddle point is and is not on the branch cut. If $s_0 < 1$, the only wave front occurs at a time τ given by equation 117 and corresponds to the part of Cagniard contour I near the saddle point. Since $g'(is_0) = 0$, a Taylor series approximation of the Cagniard contour, equation 114, at the saddle point gives

$$t = g(is_0) + \frac{1}{2}(s-is_0)^2 g''(is_0) = \tau + \frac{1}{2}(s-is_0)^2 g''(is_0)$$

or

$$s-is_0 \approx \sqrt{\frac{2(t-\tau)}{g''(is_0)}} \quad (121)$$

Similarly, in the inversion by Cagniard's method, equation 120, the expression $g'(s)$ can be approximated by

$$g'(s) \approx (s-is_0)g''(is_0) \quad (122)$$

Using the last two equations in equation 120, the first term of the wave front expansion for regular waves is found to be the real

expression

$$\frac{\partial^N \varphi}{\partial t^N} \text{ or } \frac{\partial^N \psi}{\partial t^N} \approx f(is_0) \sqrt{\frac{2}{g^n(is_0)(t-\tau)}}$$

or

$$\varphi \text{ or } \psi \approx \frac{2^N f(is_0)}{1 \cdot 3 \cdot 5 \dots (2N-1)} \sqrt{\frac{2}{g^n(is_0)}} (t-\tau)^{\frac{2N-1}{2}} \quad (123)$$

which is zero for $t < \tau$. The coefficient of $(t-\tau)^{(2N-1)/2}$ is the wave front amplitude, which depends on position in a complicated way.

Head Waves and Two Sided Shear Waves

The shear disturbance found from Cagniard contour II has two wave fronts, the initial wave front, the head wave, corresponding to the branch point $s = i$, and a two sided shear wave corresponding to the saddle point. By the argument given following equation 118, $\alpha = 0$ and by equations 109 only shear waves can be involved and β may be replaced by $(2m+1)a+y$. The head wave arrives at a time given by equation 118;

$$\tau_H = \frac{1}{c_d} \{z + [(2m+1)a+y] \sqrt{k^2-1}\} \quad (124)$$

The location of the saddle point can be found explicitly by solving equation 116 to find

$$s_0 = \frac{kz}{\sqrt{z^2 + [(2m+1)a+y]^2}} \quad (125)$$

Then, the time of arrival for the two sided shear wave is given by

equation 117 as

$$\tau = \frac{k}{c_d} \sqrt{z^2 + [(2m+1)a+y]^2} = \frac{1}{c_s} \sqrt{z^2 + [(2m+1)a+y]^2} . \quad (126)$$

Consider the first arrival, the head wave. The singularity in $f(s)$ at $s = i$ is such that either $\sqrt{1+s^2} f(s)$ or $f(s)/\sqrt{1+s^2}$ remains finite and nonzero as s approaches i (see equations 112). Both cases must be considered. Near $s=i$ equation 114 for the Cagniard contour becomes

$$t \approx g(i) + (s-i)g'(i) = \tau_H - (s-i) \frac{1}{c_d} \left[z - \frac{(2m+1)a+y}{\sqrt{k^2-1}} \right] , \quad (127)$$

which gives

$$\sqrt{1+s^2} = \sqrt{(s+i)(s-i)} \approx i \sqrt{\frac{2c_d(t-\tau_H)}{(2m+1)a+y} \cdot \frac{1}{z - \frac{(2m+1)a+y}{\sqrt{k^2-1}}}} . \quad (128)$$

Notice that the denominator of the expression under the radical in equation 128 must be positive for there to be a head wave (recalling equation 125 and the condition $s_0 > 1$ for Cagniard contour II). Also, notice that $\sqrt{1+s^2}$ must be positive imaginary along the first quadrant side of the branch cut as shown on figure 6. Then, considering $\sqrt{1+s^2} f(s)$ finite and nonzero near $s=i$, the first term of the wave front expansion, found by using equation 128 to approximate equation 120 near $s=i$, is

$$\frac{\partial^N \psi}{\partial t^N} \approx 2 \left[\frac{\sqrt{1+s^2} f(s)}{g'(s)} \Big|_{s=i} \right] \frac{1}{I} \sqrt{\frac{(2m+1)a+y}{z - \frac{\sqrt{k^2+1}}{2c_d(t-\tau_H)}}$$

or

$$\psi \approx \frac{2^N}{1 \cdot 3 \cdot 5 \cdot \dots \cdot (2N-1)} \sqrt{\frac{2c_d}{(2m+1)a+y}} \left[\sqrt{1+s^2} f(s) \Big|_{s=i} \right] \times (t-\tau_H)^{(2N-1)/2} \quad (129)$$

And considering $f(s)/\sqrt{1+s^2}$ finite and nonzero near $s=i$, the result is

$$\frac{\partial^N \psi}{\partial t^N} \approx 2 \left[\frac{f(s)}{\sqrt{1+s^2} g'(s)} \Big|_{s=i} \right] \sqrt{\frac{2c_d(t-\tau_H)}{z - \frac{\sqrt{k^2-1}}{(2m+1)a+y}}}$$

or

$$\psi \approx \frac{2^N}{3 \cdot 5 \cdot \dots \cdot (2N+1)} \left[\frac{2c_d}{(2m+1)a+y} \right]^{3/2} \times \left[\frac{f(s)}{\sqrt{1+s^2}} \Big|_{s=i} \right] (t-\tau_H)^{(2N+1)/2} \quad (130)$$

The coefficient of $(t-\tau_H)^{(2N+1)/2}$ is real and is the amplitude of the head wave.

The wave front expansion for the two sided shear wave is found by expanding near the saddle point in almost the same way as was used to find the regular waves, but this time the branch cut

interferes. The time of arrival is given by equation 126. Near the saddle point

$$(t - \tau) \approx \frac{1}{2} (s - is_0)^2 g''(is_0) \quad (131)$$

and

$$g'(s) \approx (s - is_0) g''(is_0), \quad (132)$$

where

$$g''(is_0) = \frac{1}{c_d} \frac{k^2 [(2m+1)a+y]}{(k^2 - s_0^2)^{3/2}} .$$

Before the wave front arrives $t < \tau$ and from equation 131

$$s - is_0 \approx -i \sqrt{\frac{2(\tau-t)}{g''(is_0)}} \quad (133)$$

which must be negative imaginary as indicated. But, after the wave front arrives $t > \tau$ and

$$s - is_0 \approx \sqrt{\frac{2(t-\tau)}{g''(is_0)}} \quad (134)$$

Equations 132 through 134 are used to approximate equation 120.

For $t < \tau$

$$\frac{\partial^N \psi}{\partial t^N} \approx 2 \operatorname{Re} \frac{if(is_0)}{\sqrt{2(\tau-t)g''(is_0)}}$$

and

$$\psi \approx \frac{(-2)^N}{1 \cdot 3 \cdot 5 \cdots (2N-1)} \sqrt{\frac{2c_d(k^2 - s_0^2)^{3/2}}{k^2 [(2m+1)a+y]}} \operatorname{Re} [if(is_0)] (\tau-t)^{\frac{2N-1}{2}}, \quad (135)$$

where s_0 is given by equation 125. Similarly, for $t > \tau$

$$\psi \approx \frac{2^N}{1 \cdot 3 \cdot 5 \cdot \dots \cdot (2N-1)} \sqrt{\frac{2c_d(k^2 - s_0^2)^{3/2}}{k^2 [(2m+1)a+y]}} \operatorname{Re} [f(is_0)] (t-\tau)^{\frac{2N-1}{2}} \quad (136)$$

The nature of the two sided shear wave is then clear. Near the time of arrival of an ordinary wave front or a head wave, most contributions to the disturbance are essentially constant; but one term starts its contribution at the time of arrival. This behavior is seen in the general wave front expansion, equation 84. On the other hand, the two sided shear wave is found in a term which changes its behavior at the time of arrival. That one term gives a disturbance both before and after the arrival. One cannot always give in a simple manner a single number which is the amplitude of the two sided shear wave.

Rayleigh Waves

The Rayleigh wave is a motion which propagates along the free surface of an elastic medium with the speed c_r . The Rayleigh wave has no wave front, the discontinuity in the displacement being only at a single point on the surface. The Rayleigh wave is found from Cagniard's method by studying what happens when Cagniard's contour approaches the pole of $f(s)$ at $s = ic_d/c_r = ik_r$. The denominator of $f(s)$ as given in equations 112 can be shown to have that zero as follows. Letting $F(s)$ be that denominator, the equation for the root is

$$F(s) = (k^2 + 2s^2)^2 - 4s^2 \sqrt{(1+s^2)(k^2+s^2)} = 0. \quad (137)$$

Squaring to eliminate the radicals, equation 137 becomes

$$(k^2 + 2s^2)^4 = 16s^4(1+s^2)(k^2+s^2).$$

And then,

$$16(k^2-1)s^6 + k^2(24k^2-16)s^4 + 8k^6s^2 + k^8 = 0. \quad (138)$$

This is easily seen to be the equation for the Rayleigh surface wave speed (see reference 29, p. 32). The solution is $s = ik_r$. There are two extraneous roots of equation 138 which are not solutions of equation 137 because of the previous definition of the branches.

We wish to investigate the possibility that the Rayleigh pole will strongly influence the displacements in the plate. Since the pole is on the branch cut, the Cagniard contour can approach the pole only if α and β approach zero as can be seen from equation 114. Then t goes to z/c_r at the pole. According to equations 109 this means that m and n must be zero and y must approach $\underline{+} a$. It is convenient to replace $f(s)$ in equations 112 by

$$f(s) = \frac{f_0(s)}{F(s)}, \quad (139)$$

where $F(s)$ is given by equation 137. $f_0(s)$ is easily found from equations 112 by setting m and n equal to zero. Since α and β are small, equation 114 for the Cagniard contour can be approximated near the Rayleigh pole by

$$t = g(s) \approx g(ik_r) + (s - ik_r)g'(ik_r). \quad (140)$$

$F(s)$ and $f_0(s)$ are approximated near the Rayleigh pole by

$$F(s) \approx (s - ik_r)F'(ik_r) \text{ and } f_0(s) \approx f_0(ik_r). \quad (141)$$

Equations 140 and 141 are then substituted into the basic solution by Cagniard's method, equation 120, to show that

$$\frac{\partial N_\varphi}{\partial t N} \text{ or } \frac{\partial N_\psi}{\partial t N} \approx 2\text{Re} \frac{f_0(ik_r)}{F'(ik_r)[t - g(ik_r)]} \quad (142)$$

is the form of the Rayleigh wave.

Each of the functions on the right-hand side of equation 142 is known. For y approaching positive a we have from equations 139, 112, 109, and 114 for the impact problem

$$\left. \begin{aligned} &\text{for } \varphi, \\ &f_0(ik_r) = \frac{Z\lambda c_d^2}{\pi\mu} \frac{(2k_r^2 - k^2)}{(k_r^2 - 1)} \\ &g(ik_r) = \frac{z}{c_r} + i \frac{a-y}{c_d} \sqrt{k_r^2 - 1} . \\ &\text{for } \psi, \\ &f_0(ik_r) = \frac{2iZ\lambda c_d^2}{\pi\mu} \frac{k_r}{\sqrt{k_r^2 - 1}} \\ &g(ik_r) = \frac{z}{c_r} + i \frac{a-y}{c_d} \sqrt{k_r^2 - k^2} . \end{aligned} \right\} (143)$$

Notice from equation 137 that $F'(ik_r)$ is imaginary. Substituting equations 143 into equation 142 we have for the Rayleigh wave

$$\left. \begin{aligned} \frac{\partial^3 \phi}{\partial t^3} &= \frac{2Z\lambda c_d^2 (2k_r^2 - k^2)}{\pi\mu [iF'(ik_r)] (k_r^2 - 1)} \operatorname{Re} \frac{1}{t - \frac{x}{c_r} - i \frac{a-y}{c_d} \sqrt{k_r^2 - 1}} \\ \frac{\partial^3 \psi}{\partial t^3} &= - \frac{4Z\lambda c_d^2 k_r}{\pi\mu [iF'(ik_r)] k_r^2 - 1} \operatorname{Re} \frac{1}{t - \frac{x}{c_r} - i \frac{a-y}{c_d} \sqrt{k_r^2 - k^2}} \end{aligned} \right\} (144)$$

Each of the above expressions can be integrated once with respect to time, and then the displacements are derived by differentiating the potentials according to equations 86i, ii, iii. The results for the impact problem are

$$\left. \begin{aligned} \frac{\partial^2 u_x}{\partial t^2} &= \frac{2Z\lambda}{\pi\mu [iF'(ik_r)]} \left\{ \frac{k_r (2k_r^2 - k^2)}{\sqrt{k_r^2 - 1}} \frac{(a-y)}{[(t - \frac{x}{c_r})^2 + \frac{(a-y)^2}{c_d^2} (k_r^2 - 1)]} \right. \\ &\quad \left. - \frac{2k_r (k_r^2 - k^2) (a-y)}{\sqrt{k_r^2 - 1} [(t - \frac{x}{c_r})^2 + \frac{(a-y)^2}{c_d^2} (k_r^2 - k^2)]} \right\} \\ \frac{\partial^2 u_y}{\partial t^2} &= \frac{2Z\lambda c_d}{\pi\mu [iF'(ik_r)]} \left\{ - \frac{(2k_r^2 - k^2)}{\sqrt{k_r^2 - 1}} \frac{(t - \frac{x}{c_r})}{[(t - \frac{x}{c_r})^2 + \frac{(a-y)^2}{c_d^2} (k_r^2 - 1)]} \right. \\ &\quad \left. + \frac{2k_r^2}{\sqrt{k_r^2 - 1}} \frac{(t - \frac{x}{c_r})}{[(t - \frac{x}{c_r})^2 + \frac{(a-y)^2}{c_d^2} (k_r^2 - k^2)]} \right\} \end{aligned} \right\} (145)$$

From equations 112 it is clear that similar expressions result for the pressure step problem and the line force problem; s is merely

replaced by ik_r in the additional multiplicative factors given for those problems in equations 112ii, iii. But, for the line force problem equations 145 hold for the first time derivative rather than the second time derivative.

Equations 145 can be integrated once with respect to time without difficulty. The results for the velocities for the impact problem are as follows

$$\frac{\partial u_z}{\partial t} = \frac{2Z\lambda c_d}{\pi\mu[1F'(ik_r)]} \left\{ \frac{k_r(2k_r^2 - k^2)}{(k_r^2 - 1)} \tan^{-1} \left[\frac{c_d(t - \frac{z}{c_r})}{(a-y)\sqrt{k_r^2 - 1}} \right] - \frac{2k_r \sqrt{k_r^2 - k^2}}{\sqrt{k_r^2 - 1}} \tan^{-1} \left[\frac{c_d(t - \frac{z}{c_r})}{(a-y)\sqrt{k_r^2 - k^2}} \right] \right\} \quad (146a)$$

$$\frac{\partial u_y}{\partial t} = \frac{Z\lambda c_d}{\pi\mu[1F'(ik_r)]} \left\{ -\frac{(2k_r^2 - k^2)}{\sqrt{k_r^2 - 1}} \ln \left[\left(t - \frac{z}{c_r}\right)^2 + \frac{(a-y)^2}{c_d^2} (k_r^2 - 1) \right] + \frac{2k_r^2}{\sqrt{k_r^2 - 1}} \ln \left[\left(t - \frac{z}{c_r}\right)^2 + \frac{(a-y)^2}{c_d^2} (k_r^2 - k^2) \right] \right\} \quad (146b)$$

Equations 146 hold for the displacement for the line force problem, aside from a constant factor.

In both equations 145 and 146 the contribution from the dilatational potential, the first term, and the contribution from the shear potential, the second term, are very similar. At the surface equation 146a takes the form of a step in time and equation 146b goes to infinity as the natural logarithm of time. Inside the

plate the displacements are similar to those at the surface, but the discontinuities are smoothed over.

The Saddle Point Method

An alternative method of finding the wave fronts is the saddle point method used by Knopoff and Gilbert (13). This method gives only the wave fronts. In contrast, Cagniard's method gave an exact solution for plane strain in equation 120, which was approximated to find the wave fronts. The saddle point method is used to evaluate integrals involving a large parameter p in the form of equation 111. In the present case p is the Laplace transform parameter and it is well known from the Tauberian theorem that knowledge of the transform for large p is sufficient to determine the wave fronts.

In order to use the saddle point method, the contour of integration must pass through a point where $g(s)$ is stationary, called the saddle point, in a direction such that the imaginary part of $g(s)$ remains essentially constant near the saddle point. This only works without modification if the saddle point is not on a branch cut. The saddle point was identified in the study of Cagniard's technique as the point $s = is_0$, where s_0 is given by equation 116. The imaginary part of $g(s)$ is a constant, zero, along the imaginary axis and it follows that the imaginary part has zero second derivative in a direction parallel to the real axis of s (since the imaginary part satisfies Laplace's equation). Thus, for the saddle point

method the contour of integration must cross the imaginary axis parallel to the real axis. Notice that the Cagniard contour I in figure 6 is correct for this method, but only the part of the contour near the saddle point is fixed for the saddle point method. This is reasonable since the saddle point method only gives wave front information and Cagniard's method finds wave front information by studying the saddle point.

Provided the branch cut does not interfere, the general theory of the saddle point method (reference 26, p. 39) then gives for equation 111

$$\frac{\partial N}{\partial t} \frac{\partial \psi}{\partial N} \text{ or } \frac{\partial N}{\partial t} \frac{\partial \psi}{\partial N} \sqrt{\frac{2\pi}{pg''(is_0)}} f(is_0) e^{-pg(is_0)} \quad (147)$$

But the dependence on p in equation 147 is so simple that the transform can be inverted immediately to give equation 123, which was also found by Cagniard's method.

If the saddle point lies on a branch cut, the saddle point method must be modified as Knopoff and Gilbert did (13). Again, Cagniard's contour II in figure 6 is used. It is sufficient to take only the half of Cagniard's contour in the first quadrant and to take twice the real part of the results. As in Cagniard's method, the head waves are found by an expansion around the point $s=i$ which depends on $f(s)\sqrt{1+s^2}$ or $f(s)/\sqrt{1+s^2}$ being finite and non-zero at $s=i$. Also, the expansion near the saddle point again gives the two sided shear wave, the part of the Cagniard contour

on the imaginary axis giving the disturbance before the wave arrival, the part of the contour extending into the first quadrant giving the disturbance after the wave arrival.

The integrand of equation 111 is expanded at the point $s=i$ to find the head wave. Introducing a small, real variable of integration, η , such that $s-i = i\eta$, we have the approximations

$$g(s) \approx g(i) + i\eta g'(i) = \tau_H + i\eta g'(i), \text{ and } \sqrt{1+s^2} \approx i \sqrt{2\eta} \quad (148)$$

For very large p the main contribution to the integral in equation 111 comes in the neighborhood of $\eta = 0$. Hence, equations 148 may be used and the integration may be extended to $\eta = \infty$. With $f(s) \sqrt{1+s^2}$ finite and nonzero at $s = i$, this gives the approximation to equation 111,

$$\frac{\partial N_\psi}{\partial t^N} \approx 2\text{Re} [f(s) \sqrt{1+s^2}] \Big|_{s=i} \frac{e^{-p\tau_H}}{\sqrt{2}} \int_0^\infty \frac{e^{-ig'(i)p\eta}}{\sqrt{\eta}} d\eta.$$

The exponent is real and integration gives the result

$$\frac{\partial N_\psi}{\partial t^N} \approx \sqrt{\frac{2\pi}{ipg'(i)}} \text{Re} [f(s) \sqrt{1+s^2}] \Big|_{s=i} e^{-p\tau_H}. \quad (149)$$

Inversion of the Laplace transform in equation 149 gives the first term of the wave front expansion for the head wave given by Cagniard's method in equation 129. With $f(s)/\sqrt{1+s^2}$ finite and nonzero at $s=i$, which is the other possibility, the approximation to equation 111 is

$$\frac{\partial \overline{N}}{\partial t} \psi = -2 \operatorname{Re} \left[\frac{f(s)}{\sqrt{1+s^2}} \right]_{s=i} \sqrt{2} e^{-P\tau H} \int_0^{\infty} \sqrt{\eta} e^{-ig'(l)P\eta} d\eta.$$

Integrating

$$\frac{\partial \overline{N}}{\partial t} \psi = -\frac{1}{2\pi} \left[\frac{2\pi}{ig'(l)p} \right]^{3/2} \operatorname{Re} \left[\frac{f(s)}{\sqrt{1+s^2}} \right]_{s=i} e^{-P\tau H}. \quad (150)$$

The inverse is precisely equation 130, which was found by Cagniard's method.

From the saddle point, $s = is_0$, when it is on the branch cut is found the two sided shear wave. The function $f(s)$ is approximated by $f(is_0)$. For $g(s)$ we write the Taylor expansion

$$g(s) \approx \tau + \frac{(s-is_0)^2}{2} g''(is_0). \quad (151)$$

The integration in equation 141 away from the saddle point out into the first quadrant along the Cagniard contour II is approximated by using equation 151 as

$$\frac{\partial \overline{N}}{\partial t} \psi = \operatorname{Re} f(is_0) e^{-P\tau} \int e^{-P \frac{(s-is_0)^2}{2}} g''(is_0) ds.$$

This integral is identical to the integral which must be evaluated in deriving the results (equation 147) of the saddle point method when the saddle point is not on the branch cut. Carrying out the integral and inverting, the results of Cagniard's method, equation 136, are duplicated.

The integration near the saddle point and along the imaginary

axis is carried out by replacing $s-is_0$ by $-i\eta$ with η small, real, and positive. Then, equation 111 is approximated by

$$\overline{\frac{\partial N_\psi}{\partial t N}} \approx 2\text{Re} \int_0^\infty f(is_0) e^{-p\tau} e^{p \frac{g''(is_0)}{2} \eta^2} d\eta. \quad (152)$$

This integral only converges for p large and negative. Previously p had been restricted to positive values in order to expand the denominator of the double transforms. The use of negative p here for plane strain will be justified only by observing that the results will agree with those of Cagniard's method. Comparison to Cagniard's method is not rigorous for problem vi (point force) because, as will be seen, Cagniard's method follows the use of the asymptotic representations of the Bessel functions for large p (large argument). Knopoff and Gilbert (13) in a similar manner used negative p after expanding for positive p the denominator of the double transform for their plate problem. They made use of the Tauberian theorems in their work and developed new Tauberian theorems for negative p .

Evaluating the integral in equation 152 with p a negative number gives

$$\overline{\frac{\partial N_\psi}{\partial t N}} \approx \text{Re} \int_0^\infty f(is_0) e^{-p\tau} \frac{\sqrt{2\pi}}{\sqrt{-pg''(is_0)}} \quad (153)$$

This suggests identification with the Laplace integral

$$\frac{e^{-p\tau}}{\sqrt{(-p)}} = \int_0^{\infty} \frac{1}{\sqrt{\pi t}} e^{-(-p)(t-\tau)} dt$$

which, with a change of variables, can be written

$$\frac{e^{-p\tau}}{\sqrt{(-p)}} = \frac{1}{\pi} \int_{-\infty}^{\tau} \frac{e^{-pt}}{\sqrt{\tau-t}} dt.$$

Looking only at the part of the integration near $t=\tau$, it is clear that a disturbance before time τ of the form

$$1/\sqrt{\tau-t}$$

is contained in the transform of equation 153. Thus, one may write the disturbance before time τ as

$$\frac{\partial^N \psi}{\partial t^N} = \sqrt{\frac{2}{g(is_0)}} \frac{\text{Re}[if(is_0)]}{\sqrt{\tau-t}},$$

which is identical to the results found by Cagniard's method in equation 135.

D. MODIFICATIONS FOR CYLINDRICAL SYMMETRY

The results of the work on plane strain must be modified slightly when a Cartesian coordinate is replaced by a radial coordinate. The Bessel functions which result in cylindrically symmetrical problems must be approximated by their asymptotic forms, exponential functions. Then, the analysis is carried out using the exponential functions as for plane strain. The asymptotic forms of the Bessel functions will be good only for large p , but

this is adequate for studying wave fronts. Two cases are analyzed here. First, we treat the problem vi of the point force on a plate, where the radial coordinate is the direction of propagation, and second the problems iv and v of the rod where the radial coordinate is transverse to the direction of propagation.

The Point Force

For the problem of the point force on the plate the double transforms are the same as for the line force, but the inversion integrals, equations 96b, are different from the inversion integral for plane strain, equation 16b. In place of the exponential, $e^{ikz} = e^{is(p/cd)z}$, is a Hankel function, $H_n^{(1)}(kz)$. But, the Hankel function may be replaced by its asymptotic representation,

$$H_n^{(1)}(kz) \approx \sqrt{\frac{2}{\pi kz}} e^{i(kz - n\frac{\pi}{2} - \frac{\pi}{4})}, \quad (154)$$

and only the radical differentiates the point force and line force problems. The detailed analysis follows.

Applying the inversion integrals, equations 16b and 96b, to the double transforms, equations 99iii, vi, there are only two differences between the line and point force problems:

1. e^{ikz} in equation 16b of the line force problem is replaced by $\pi ka J_0(kz)$ for φ and by $i\pi ka J_1(kz)$ for ψ . We will indicate these two replacements by $i^n \pi ka J_n(kz)$, where $n = 0$ for φ , $n = 1$ for ψ .
2. For the point force problem the integration is only over

positive κ .

These differences do not interfere with expanding the double transforms to write individual integrals for each wave front in the form given in equation 111. The two changes carry through to the individual integrals. Now, we substitute the Hankel function $H_n^{(1)}(\kappa z) = J_n(\kappa z) + iN_n(\kappa z)$ for $J_n(\kappa z)$. The Neumann function, $N_n(\kappa z)$, adds only an imaginary part to the integral, so it is necessary to take the real part of the resulting integral. Since the Hankel function behaves like the exponential function for large argument, it is still possible to move the contour of integration (along the real axis from zero to infinity) off of the real axis onto the part of the Cagniard contour defined before in the first quadrant. The only error will be that of a line integral along the imaginary axis between the origin and the point where the Cagniard contour begins. But, such an integral is imaginary as ds is imaginary and the integrand [the double transform times $i^n H_n^{(1)}(\kappa z)$] is real along that path; and when the real part of the integral is taken, the error will be eliminated.

The asymptotic form in equation 154 may be used because $\kappa z = \frac{p}{c_d} sz$ is large along the Cagniard contour. Then, we combine the replacement given in difference number 1 above with equation 154 and multiply by $1/2$ to account for difference number 2. The result, letting $\kappa = sp/c_d$, is a factor which accounts approximately for cylindrical symmetry.

$$a \sqrt{\frac{\pi}{2} \frac{sp}{c_d^2}} e^{-i \frac{\pi}{4}} = a \sqrt{\frac{\pi}{2} \frac{p}{c_d^2} \frac{s}{l}}$$

This factor can be incorporated in $f(s)/p^N$ in equation 108. This approximation for large p is acceptable because only wave front information is desired. To find the wave front amplitudes of regular waves and the two sided shear waves following the head waves, the function $f(s)$ must be evaluated at the saddle point, $s = is_0$. Then, the additional factor introduced by cylindrical symmetry is

$$a \sqrt{\frac{\pi s_0 p}{2zc_d}} \quad (156)$$

For the head waves $f(s)$ is evaluated at the branch point, $s = i$. Then, the additional factor is

$$a \sqrt{\frac{\pi p}{2zc_d}} \quad (157)$$

The factor p changes the time dependence of the first term of the wave front expansion. A typical term for the line load which was proportional to $(t-\tau)^{N+\frac{1}{2}}$ becomes instead proportional to $(t-\tau)^N$. The geometrical factors in equations 156 and 157 will be interpreted in section V. It should be recalled that Z was defined differently for the line and point force. Z is the magnitude of the line force per unit length times $1/\mu a$ or it is the magnitude of the point force times $1/\pi \mu a^2$.

The Circular Rod

The double transforms for the rod, equations 99iv, v, are very similar to the double transforms for the plate, equations 99i, ii. There are two differences. First, F , given in equation 98a, has one more term than F_g , equation 98b. But, for large p this extra term in F is negligible compared to the other terms. Second, the hyperbolic functions $\sinh x$ and $\cosh x$, where $x = \kappa_d a$ or $\kappa_g a$ are replaced for the rod by $I_0(x)$ or $I_1(x)$. For large p (large x) we have the asymptotic representations,

$$I_0(x) \approx I_1(x) \approx \frac{e^x}{\sqrt{2\pi x}} \quad \text{and} \quad \sinh x \approx \cosh x \approx \frac{e^x}{2}. \quad (158)$$

Substituting these asymptotic forms into equations 99i, ii and 99iv, v, it is clear that the double transforms for the rod have an additional factor

$$\sqrt{a/y} \quad (159)$$

for large p . This factor strengthens the wave fronts near the axis of the circular rod. Equation 159 does not apply to the step, equation 113, which is the same in rod and plate.

Because the \sinh and \cosh functions were replaced by positive exponentials, the above argument does not apply to all wave fronts. Examination of the expansion procedure given prior to equations 112 shows that only the unreflected waves are kept when the asymptotic forms, equations 158, are used. Waves with n or $m > 0$ have more rapidly decaying exponential functions as shown in equation 108.

The double transforms of the reflected waves are asymptotically for large p negligible with respect to the unreflected waves. Apparently there is no way of determining the reflected wave fronts in the rod from the double transforms.

Ray theory can be used to show that the factor $\sqrt{a/y}$ relates the amplitude of all wave fronts in the bar to the corresponding ones in plane strain. It was shown above that the amplitudes of the unreflected wave fronts are related by $\sqrt{a/y}$. By ray theory all other fronts are derived from those wave fronts by reflection, a process which is the same in both problems. The only difference comes because the rays in the bar must be strengthened by the factor $\sqrt{a/y}$ for energy to be conserved as the rays approach the centerline.

E. RAY THEORY

Ray theory can be formulated by substituting an expansion of the form of equation 84 for φ or ψ into the governing wave equations 87. The conditions are then that the $\tau_n(y, z)$ must satisfy the Eiconal equation governing the geometry of rays and wave fronts and that the amplitudes of the wave fronts must vary in the directions of the rays in a certain prescribed manner.* The interpretation is that the energy, which is proportional to the square

* The governing partial differential equations are given by Karal and Keller (14) and Babich and Alekseev (15).

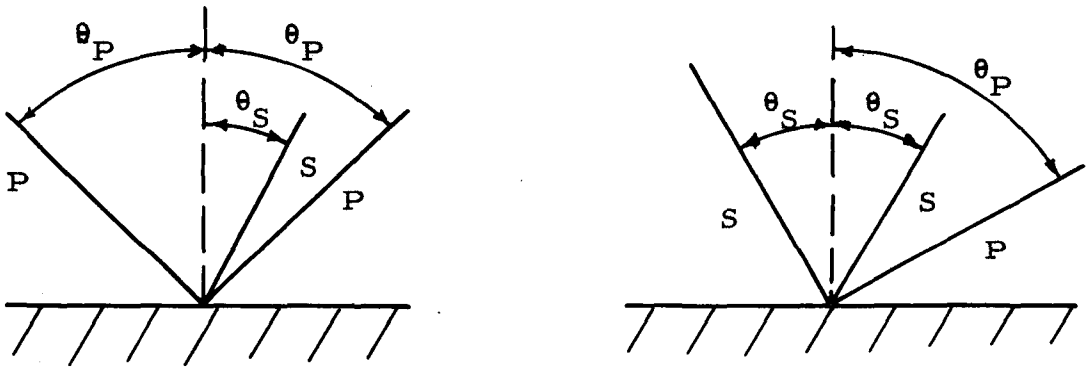
of the amplitude at a point on a wave front, must have followed the ray to that point from the source. The total energy which is transmitted between two adjacent rays in two dimensions depends on the source and is a constant as the rays vary in their separation.

When a ray hits a boundary, two rays are created which come off at angles determined by Snell's law. The reflection of rays is shown in figure 7. A dilatational (P) wave incident at an angle of incidence θ_P produces a P wave with angle of reflection θ_P and a shear (S) wave with angle of reflection θ_S in accordance with Snell's law

$$\frac{\sin \theta_P}{\sin \theta_S} = k. \quad (160)$$

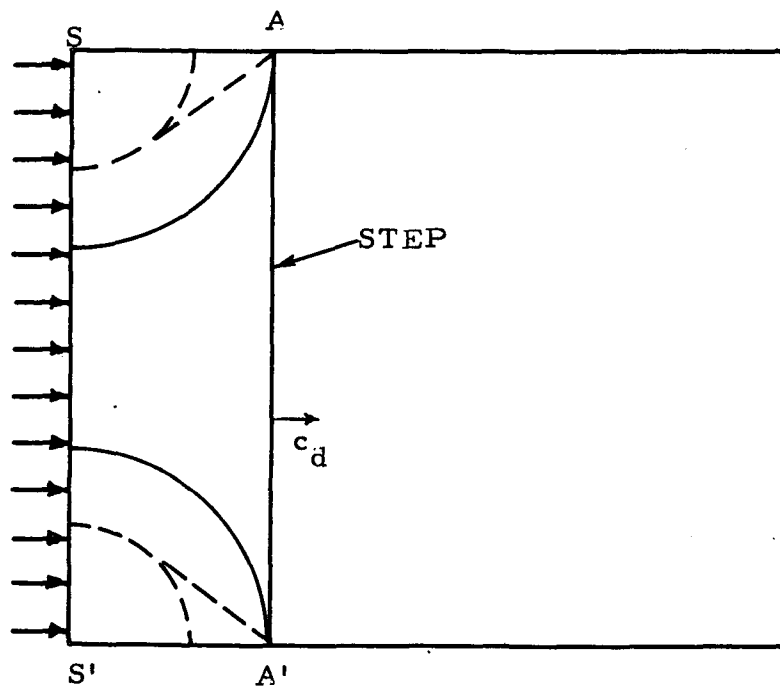
Similarly, an S wave incident at angle of incidence θ_S produces S and P waves with angles of reflection θ_S and θ_P respectively. Again, equation 160 holds. The amplitudes of the reflected rays are given linearly in terms of the amplitudes of the incident rays.

In the problems dealt with here there are only two sources of S and P rays. These are at $z = 0$ and $y = +a$. In the line force and point force problems it is obvious that the only source of rays is at $z = 0$ and $y = +a$, where the load is. The pressure step and longitudinal impact problems are shown in figure 8 for a time immediately after application of the load. The direct result of the application of the load is the step which is given in equation 113 and moves at the dilatational velocity. Since the dilatational



REFLECTION OF RAYS

Figure 7



SOURCES OF RAYS

Figure 8

velocity is the maximum velocity of any disturbance, the step moves ahead of all other waves. Because the step itself does not satisfy the boundary conditions at $y = \pm a$, a system of wave fronts starts at the two points S and S' . All rays leave those two points and reflect off of the free surfaces, $y = \pm a$, to produce the many wave fronts. Notice that the pattern of waves formed at S and S' is the same as that shown in figure 4.

Because of the simple geometry of the plate (or rod), in which rays reflect between parallel surfaces, any ray can be associated with a single angle θ_P . For P type rays this is the angle of reflection of that ray from the surface at which it was created and also the angle of incidence of that ray at the surface at which it will end. For S type rays θ_P is the angle of incidence of the P wave which created the S wave and it is the angle of reflection of the P wave created by the S wave. The formulas of ray theory can be identified with formulas found from the expansion of the double transforms by using the relationship

$$s_0 = \sin \theta_P \tag{161}$$

Only real rays will be considered here and hence $s_0 < 1$. (Grazing incidence, for which $s_0 = 1$, will not be considered here.) Formulas from ray theory are written here in terms of s_0 . The amplitudes in the neighborhood of the source depend primarily on angle (s_0). Reflection reduces the amplitudes by a factor depending only on angle. Only the formula which gives the weakening of the

rays as they diverge requires other variables.

Ewing, Jardetsky, and Press give the reflection coefficients for a free surface (reference 29, pp. 24-28). Their results for plane harmonic waves reflecting off of plane surfaces are independent of frequency and therefore apply here. The results are written differently for waves incident on the surface $y = +a$ than the surface $y = -a$ because there is a sign convention involved in the definition of the shear potential. If P_{inc} and S_{inc} are the amplitudes of the incident waves and P_{ref} and S_{ref} are the amplitudes of the reflected waves, the conditions at a free surface are that

$$\left. \begin{aligned} P_{ref} &= -R P_{inc} \mp R_{sp} S_{inc} \\ \text{and} \\ S_{ref} &= \mp R_{ps} P_{inc} - R S_{inc} \end{aligned} \right\} (162)$$

The upper signs apply for $y = +a$ and the lower signs for $y = -a$.

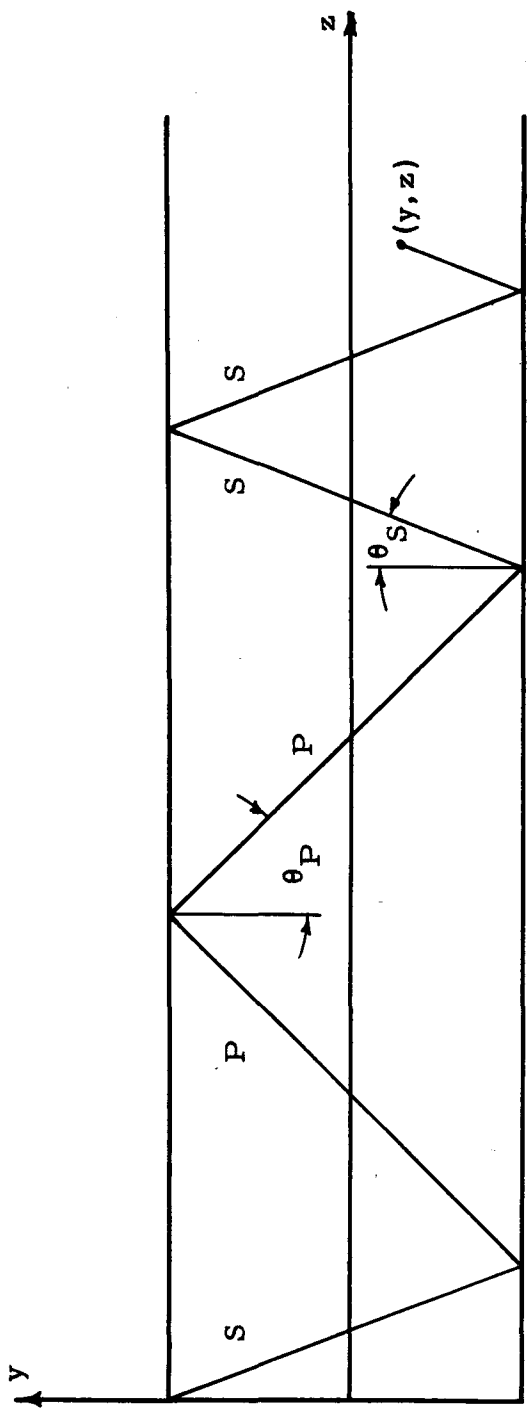
The reflection coefficients as functions of angle are

$$\left. \begin{aligned} R &= \frac{(k^2 - 2s_0^2)^2 - 4s_0^2 \sqrt{(1-s_0^2)(k^2 - s_0^2)}}{(k^2 - 2s_0^2)^2 + 4s_0^2 \sqrt{(1-s_0^2)(k^2 - s_0^2)}} \\ R_{sp} &= \frac{4s_0 \sqrt{k^2 - s_0^2} (k^2 - 2s_0^2)}{(k^2 - 2s_0^2)^2 + 4s_0^2 \sqrt{(1-s_0^2)(k^2 - s_0^2)}} \\ R_{ps} &= \frac{4s_0 \sqrt{1-s_0^2} (k^2 - 2s_0^2)}{(k^2 - 2s_0^2)^2 + 4s_0^2 \sqrt{(1-s_0^2)(k^2 - s_0^2)}} \end{aligned} \right\} (163)$$

Geometry of the Rays

Consider a ray which starts at $y = a$ and $z = 0$ and then zig zags down the plate as in figure 9, changing from P to S and back again in any order, and finally arrives at a point (y, z) . Let α be the component in the y direction of the distance travelled as a P wave. Each time the ray traverses the plate as a P wave, it contributes $2a$ to α . If the wave arrives at (y, z) as a P wave, α must also include the contribution $a-y$ or $a+y$. Similarly, let β be the component in the y direction of the distance travelled as an S wave. The distances travelled in the transverse direction, α and β , can be expressed in terms of the y coordinate of the end point of the ray (the observation point) and the number of whole traversals as a P wave and as an S wave, n and m , respectively. The contributions from total traversals are $2na$ and $2ma$, respectively. If the last segment of the ray is of the P type, then one must add to α either $a-y$ if the last segment is off of the top boundary or $a+y$ if the last segment is off of the bottom boundary. Thus, for P rays and P wave fronts α and β are given by equations 109a while for S rays and S wave fronts α and β are given by equations 109b.

With equations 160 and 161 in mind the geometry of the rays can be discussed as follows. The total distance travelled as a P wave is



REFLECTING RAY

Figure 9

$$\frac{a}{\cos \theta_P} = \frac{a}{\sqrt{1 - s_0^2}},$$

and the distance travelled as an S wave is

$$\frac{\beta}{\cos \theta_S} = \frac{\beta}{\sqrt{1 - \sin^2 \theta_S}} = \frac{k\beta}{\sqrt{k^2 - s_0^2}}.$$

Then, the total distance travelled in the z direction is

$$z = a \tan \theta_P + \beta \tan \theta_S = \frac{as_0}{\sqrt{1 - s_0^2}} + \frac{\beta s_0}{\sqrt{k^2 - s_0^2}} \quad (164)$$

and the total time of travel, which is the time of arrival of the wave front, is

$$\tau = \frac{1}{c_d} \frac{a}{\sqrt{1 - s_0^2}} + \frac{1}{c_s} \frac{k\beta}{\sqrt{k^2 - s_0^2}} = \frac{1}{c_d} \left[\frac{a}{\sqrt{1 - s_0^2}} + \frac{k^2 \beta}{\sqrt{k^2 - s_0^2}} \right]. \quad (165)$$

Equations 164 and 165 are identical with equations 116 and 117. The locations of the wave fronts can be calculated by considering τ a constant and solving equation 165 for s_0 and then substituting into equation 164 to find z as a function of y for that τ . That gives a picture of the wave fronts at a given time. One can also consider z and y as given and solve for the times of arrival, τ , associated with different values of m and n .

Divergence Factor

Consider two adjacent rays parameterized by s_0 and $s_0 + \Delta s_0$. The energy propagating between the rays must depend

only on s_0 . The energy is proportional to the square of the amplitude of the wave front multiplied by the area between the rays.

The area in plane strain is given by $\sqrt{(\Delta y)^2 + (\Delta z)^2}$, where the variations are at constant τ . Thus, the amplitude, A , for given s_0 must vary such that

$$A^2 \sqrt{(\Delta z)^2 + (\Delta y)^2}$$

is a constant.

We wish to find relationships between the differentials Δs_0 , Δy , and Δz along a wave front. We consider, for example, the shear wave fronts, for which $\Delta \beta = + \Delta y$. Then, we differentiate equations 164 and 165 to find, respectively

$$\left[\frac{a}{(1 - s_0^2)^{3/2}} + \frac{k^2 \beta}{(k^2 - s_0^2)^{3/2}} \right] \Delta s_0 + \frac{s_0}{\sqrt{k^2 - s_0^2}} \Delta y = \Delta z,$$

$$\left[\frac{a s_0}{(1 - s_0^2)^{3/2}} + \frac{k^2 \beta s_0}{(k^2 - s_0^2)^{3/2}} \right] \Delta s_0 + \frac{k^2}{\sqrt{k^2 - s_0^2}} \Delta y = 0.$$

Solving these two equations and substituting the correct expression from equation 110 for $g''(is_0)$,

$$g''(is_0) = \frac{1}{c_d} \left[\frac{a}{(1 - s_0^2)^{3/2}} + \frac{k^2 \beta}{(k^2 - s_0^2)^{3/2}} \right], \quad (166)$$

we have along a shear wave front

$$\Delta y = \mp c_d s_0 \frac{\sqrt{k^2 - s_0^2}}{k^2} g''(is_0) \Delta s_0$$

$$\Delta z = \frac{c_d}{k^2} (k^2 - s_0^2) g''(is_0) \Delta s_0.$$

Then, between two rays

$$A^2 \sqrt{(\Delta y)^2 + (\Delta z)^2} = A^2 \frac{c_d}{k^2} \sqrt{(k^2 - s_0^2)s_0^2 + (k^2 - s_0^2)^2} g''(is_0) \Delta s_0$$

must be a constant. Therefore, the shear wave front amplitude must be expressed as a function of s_0 alone times the simple divergence factor;

$$A = \frac{f_S(s_0)}{\sqrt{g''(is_0)}} = \frac{f_S(s_0)}{\sqrt{\frac{1}{c_d} \left[\frac{a}{(1-s_0^2)^{3/2}} + \frac{k^2 \beta}{(k^2 - s_0^2)^{3/2}} \right]}} \quad (167)$$

The function $f_S(s_0)$ will depend on the source of the rays and on the amount the ray has been diminished by multiple reflections. The amplitude along dilatational fronts has the same divergence factor. Equation 123, found for the double transform for regular wave fronts, agrees with equation 167.

The Source

The problem of finding the strength of the rays at the sources $y = \pm a$ and $z = 0$ is a canonical problem of ray theory. The problem is solved here by extracting from the double transform solution for the plate the part which includes only the rays going out from one or the other source. That part will be the complete solution to a simpler problem, one where the plate becomes a half-space or quarter-space as one surface of the plate moves to infinity.

The wave front expansion for regular waves found by

Cagniard's method was given in equation 123. The functions which must be evaluated at the saddle point are found in equations 112. The sums involving R in equations 112 are replaced by unity (i. e., n and m are taken as zero) to obtain the correct expressions for the rays leaving the source. The time dependence in equation 123 is left out in writing the wave front amplitudes. Here, the divergence factor, $1/\sqrt{g''(is_0)}$, is also left out to leave functions of s_0 only. Those functions, the source amplitude functions, will be called S_0 for shear waves and P_0 for dilatational waves. For $z = 0$ and $y = \pm a$ they are

$$\left. \begin{aligned} S_0 &= \mp \frac{16\sqrt{2} Z \lambda c_d^2 s_0^2}{15\pi\mu \sqrt{1-s_0^2} [(k^2 - 2s_0^2)^2 + 4s_0^2 \sqrt{(1-s_0^2)(k^2 - s_0^2)}]} \\ P_0 &= \frac{8\sqrt{2} Z \lambda c_d^2 (k^2 - 2s_0^2)}{15\pi\mu(1-s_0^2) [(k^2 - 2s_0^2)^2 + 4s_0^2 \sqrt{(1-s_0^2)(k^2 - s_0^2)}]} \end{aligned} \right\} (168)$$

for the impact problem. For the pressure step problem multiply the above functions by s_0 , and for the line force multiply by

$$-\frac{5}{4} \frac{a}{c_d} \frac{\mu}{\lambda} (1 - s_0^2)$$

and take the upper sign only since only $y = +a, z = 0$ is a source.

The difference in dimensions for the line source problem is accounted for by the difference in time dependence of the wave fronts.

If one could find S_0 and P_0 for problems with nonmixed end boundary conditions, then one could find all of the wave fronts

by the ray method. However, even the canonical source problems remain unsolved for nonmixed boundary conditions.

Multiply Reflected Rays

Wave fronts and rays arising upon reflection of the source rays from the surfaces can be calculated by using the reflection conditions given in equations 162. Consider the wave front which arises from rays which have traversed the plate n times as P rays and m times as S rays. There are several different paths for rays, all of which cross the plate n times as P rays and m times as S rays. Each path contributes a different amount to the amplitude of the final wave front. The problem is to add up all of the contributions. For simplification consider only rays arising from the upper source. Because of the symmetry in the plate, that is sufficient.

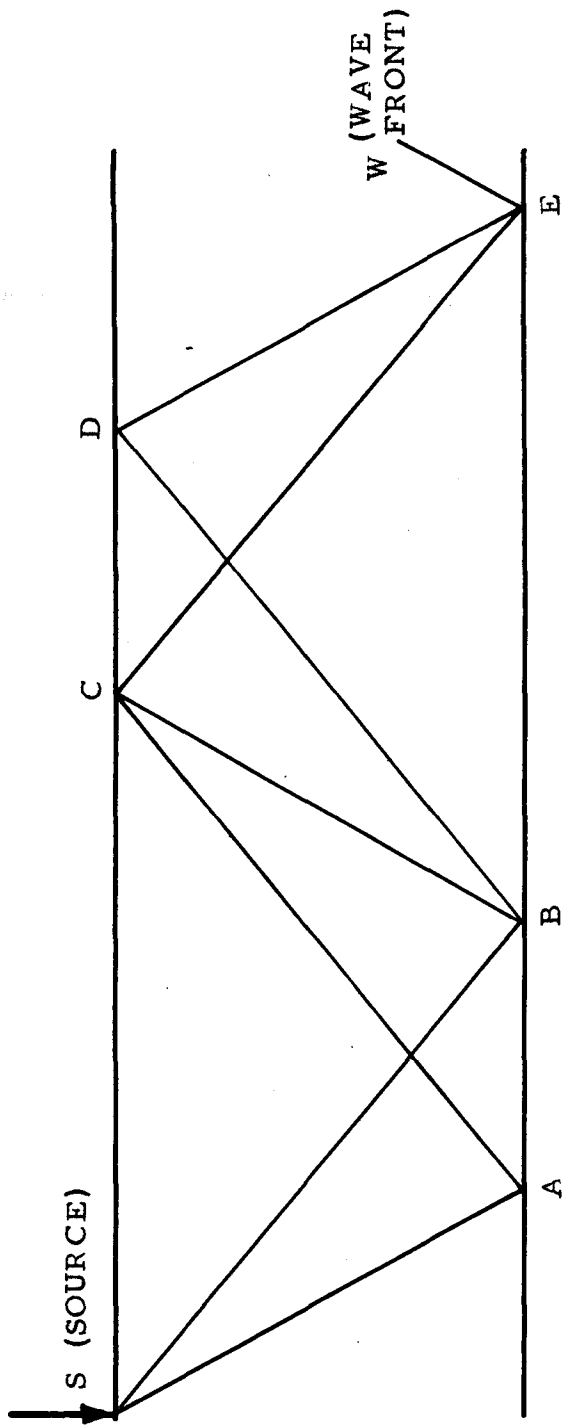
A precise statement of the problem is the following. Let P represent a P wave traversal and S an S wave traversal. Then, we wish to know every permutation of n P 's and m S 's. For instance, if $n = 2$ and $m = 1$, the three permutations represent three ways of creating the S ray EW shown in figure 10:

PPS represents path SBDEW

PSP represents path SBCEW

SPP represents path SACEW.

Next, add to each of the permutations of $n + m$ letters the letter S if shear amplitudes are being calculated, or the letter P if dilatational wave amplitudes are being calculated. For each per-



FAMILY OF RAYS

Figure 10

mutation one finds a contribution to the amplitude by multiplying a series of factors. The first factor is P_o if the first letter is P, S_o if the first letter is S. The second factor is $-R$ multiplied as many times as an S is followed by an S plus the number of times a P is followed by a P. The third factor is found by multiplying by $\mp R_{sp}$ each time S is followed by P. The upper sign is used when the S is in an even numbered position, the lower sign when S is in an odd numbered position.* The fourth factor is found by multiplying by $\pm R_{ps}$ each time a P is followed by an S, taking the upper sign when P is in an even numbered position. For instance, PSPSS becomes PSPSSS for a shear front and contributes $P (-R)^2 (-R_{sp}) (-R_{ps})^2$ to the amplitude. The following identities, which come from the defining equations, equations 163 and 168, will be useful

$$\left. \begin{aligned} R_{sp} R_{ps} &= 1 - R^2 \\ S_o R_{sp} &= -P_o (1 - R) \\ P_o R_{ps} &= -S_o (1 + R) \end{aligned} \right\} (169)$$

Equations 169 hold with the sign of S_o in equation 168 taken appropriately for the upper source. It is expected that only R need be involved in the results in any complicated way as the expansion of the double transform produced polynomials depending only on n, m, and R, but not on R_{sp} or R_{ps} .

Consider shear waves. In any permutation let l be the

* Multiplication by the divergence factor then gives the correct wave front amplitudes.

number of times an S is followed by a P. Now consider first only those permutations starting with S. If S is followed by P l times, then P is followed by S l times also. Then, the amplitude is found by taking as factors S_o and then $(-R)^{n+m-2l}$ and then $\frac{+}{-} R_{sp}$ and $\frac{+}{-} R_{ps}$ l times each. Only the sign of the result remains to be determined. Consider in pairs the occurrence of SP in the permutation and the next to follow PS. If between the two S's there are k P's, then one must take the factor $(R_{sp} R_{ps})(-1)^{k-1}$. One then must take $(-1)^{k-1}$ a total of l times. The sum of the k 's is n and $(-1)^{-1}$ occurs l times, so the amplitude contribution is

$$S_o (-R)^{n+m-2l} (R_{sp} R_{ps})^l (-1)^{n-l} = S_o (-1)^{m+l} (R)^{n+m-2l} (1-R^2)^l,$$

where equation 169 has been used.

Next, it is necessary to count the number of permutations with S followed by P l times. Any but the last of the $m+1$ S's may be followed by a P and l of them are. There are $\binom{m}{l}$ ways of choosing which S's are to be followed by P's. The last of the P's must be followed by an S. Then, provided $l \geq 1$ and $n \geq 1$, there are $\binom{n-1}{l-1}$ ways of choosing among the remaining P's which will be followed by S's. Those two choices completely determine a permutation. Clearly l may be as small as one and may range up to either n or m as a maximum, whichever is smaller. Then, one may sum over all values of l to find the total contribution to the amplitude of an S wave due to rays starting as S waves. It is

$$S_0 \sum_{l=1}^{\text{lesser of } m, n} \binom{m}{l} \binom{n-1}{l-1} (-1)^{m+l} R^{n+m-2l} (1-R^2)^l \quad (m \geq 1, n \geq 1). \quad (170)$$

Next, consider all permutations starting with P which create shear waves. Again, l is the number of times an S is followed by a P. The number of times a P is followed by an S is $l + 1$. The amplitude is found by taking the factor P_0 and then the factor $-R$ a total of $n + m - 2l - 1$ times, once for each time an S is followed by an S or a P is followed by a P, and then by taking the factors $\underline{+}R_{sp}$ and $\underline{+}R_{ps}$ the correct number of times. The factor $\underline{+}R_{sp}$ will occur l times and $\underline{+}R_{ps}$ will occur $l + 1$ times. Again, consider in pairs the occurrence of SP in the permutation and the next to follow PS. Between any two S's let there be k P's and then a factor $(R_{sp}R_{ps})(-1)^{k-1}$ is introduced. This happens l times. In addition, let there be j P's before the first S. This introduces a factor $R_{ps}(-1)^j$. The total of the k 's plus j is n and the factor $(-1)^{-1}$ occurs l times. Hence, the contribution to the amplitude is, using equations 169,

$$P_0 (-R)^{n+m-2l-1} R_{ps} (R_{sp}R_{ps})^l (-1)^{n-l} = S_0 (-1)^{m+l} (1+R)(1-R^2)^l R^{n+m-2l-1}$$

Next, the number of permutations for each value of l must be counted. Any but the last of the $m+1$ S's may be followed by one of l P's. The S's to be followed by P's may be chosen in $\binom{m}{l}$ ways. The last P must be followed by an S. The remaining $n-1$ P's may be followed by l S's in $\binom{n-1}{l}$ different

ways. These two choices completely determine the permutations. The number l may range from zero up to either m or $n-1$, whichever is smaller. Then, rays starting as P rays contribute to an S wave front a total amplitude

$$\sum_{l=0}^{\text{lesser of } m, n-1} S_o (-1)^{m+l} \binom{n-1}{l} \binom{m}{l} (1+R)(1-R^2)^l R^{n+m-2l-1}. \quad (171)$$

($m \geq 1, n \geq 1$)

The special cases $n = 0$ or $m = 0$ are easy to calculate.

The amplitudes of the S waves are

$$\left. \begin{aligned} S_o (-R)^m &= S_o (-1)^m R^m && (n=0) \\ P_o (-R)^{n-1} (-1)^n R_{ps} &= S_o (1+R) R^{n-1}. && (m=0, n \geq 1) \end{aligned} \right\} (172)$$

The total amplitude of any shear wave front exclusive of the divergence factor is then taken from equations 170, 171, and 172 as

$$\left. \begin{aligned} S_o \left\{ \sum_{l=1}^{\text{lesser of } m, n} \binom{m}{l} \binom{n-1}{l-1} (-1)^{m+l} (1-R^2)^l R^{n+m-2l} \right. \\ + \left. \sum_{l=0}^{\text{lesser of } m, n-1} \binom{n-1}{l} \binom{m}{l} (-1)^{m+l} (1+R)(1-R^2)^l R^{n+m-2l-1} \right\} \\ (m \geq 1, n \geq 1) \\ S_o (-1)^m R^m &&& (n=0) \\ S_o (1+R) R^{n-1} &&& (m=0, n \geq 1) \end{aligned} \right\} (173)$$

Dilatational wave fronts can be found in a similar manner. In the derivation above P and S , P_o and S_o , and n and m interchange their roles, but R_{ps} and R_{sp} are interchanged with a reversal in sign. The identity relating S_o and P_o takes a different form. One may then write the total amplitudes of the dilatational fronts exclusive of the divergence factor as

$$\left. \begin{aligned}
 P_o & \left\{ \begin{aligned}
 & \sum_{l=1}^{\text{lesser of } m, n} \binom{n}{l} \binom{m-1}{l-1} (-1)^{n+l} (1-R^2)^l R^{n+m-2l} \\
 & - \sum_{l=0}^{\text{lesser of } n, m-1} \binom{m-1}{l} \binom{n}{l} (-1)^{n+l} (1-R)(1-R^2)^l R^{n+m-2l-1}
 \end{aligned} \right\} \\
 & P_o (-1)^n R^n \qquad \qquad \qquad (m = 0) \\
 & - P_o (1 - R) R^{m-1} \qquad \qquad \qquad (n = 0, m \geq 1) .
 \end{aligned} \right\} (174)$$

If the transform methods are to give the same wave front amplitudes as the ray method, then the formulas above should agree with equations 112 when the functions $f(s)$ in equations 112 are evaluated at the saddle point. First, notice that $R(is_o)$ in equation 104 is the same as the reflection coefficient R defined in equation 163. It has been verified that the formulas in equations 173 and 174 agree with equations 112 for the special cases $m = 0, 1, 2$ (n arbitrary) and $n = 0, 1, 2$ (m arbitrary). Though the formulas found by the two methods take different forms, there is no reason to believe that they are not in complete agreement for all n and m .

V. RESULTS FROM WAVE FRONT THEORY

A. WAVE FRONT LOCATIONS

Solution of equations 116 and 117 (or 164 and 165) to find the many wave fronts created by reflection was carried out numerically. The wave front locations were found for a Poisson's ratio of 0.3 ($k^2 = 3.5$) for two times: first a time $t = 8a/c_d$, when the leading wave front would have travelled a distance of four thicknesses, and second a time $t = 16a/c_d$. The results are presented to geometrical scale in figures 11 and 12. Only the wave fronts of the line force problem are shown; twice as many wave fronts are created by end loads, the additional wave fronts being necessary for symmetry about the center of the plate. Dilatational wave fronts are shown as solid lines, shear fronts as dashed lines. Figure 12 is broken into two parts for convenience. The integers n and m of equations 109 are shown on the wave fronts.

The wave fronts in figures 11 and 12 should be compared to those shown in figure 4. The points A, B, D, and E on the three figures are the same. In figures 11 and 12 the leading circular dilatational wave front, AB, can be seen to reflect off to create a dilatational wave front and a shear wave front. Then, each of these fronts reflects off to create two more, and so forth. Similarly, the leading circular shear front, which starts out from the source, reflects to create two new wave fronts, which in turn reflect off of the boundaries. The two sided shear wave front, KD in figures 11 and 12, has too great an angle of incidence to

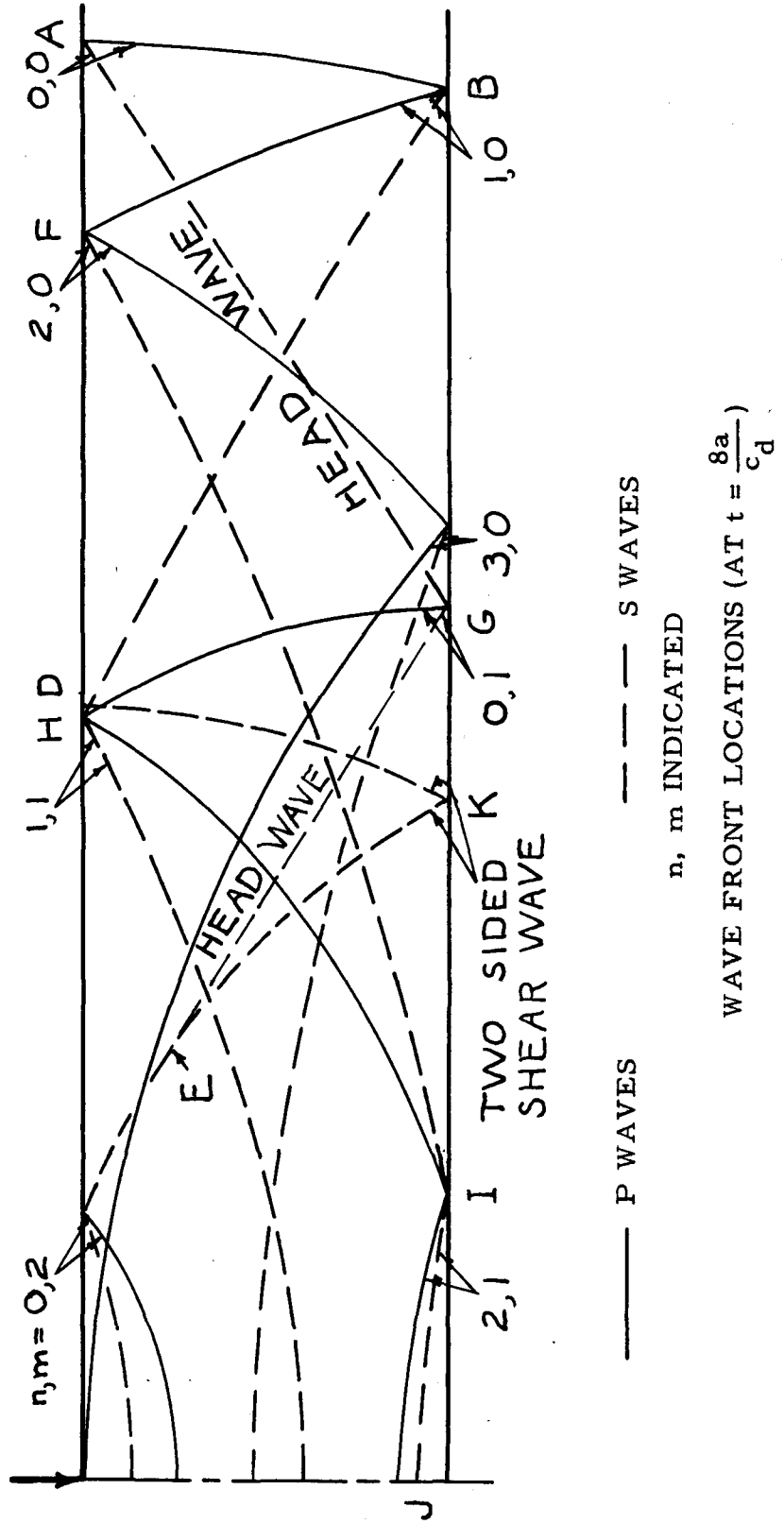


Figure 11

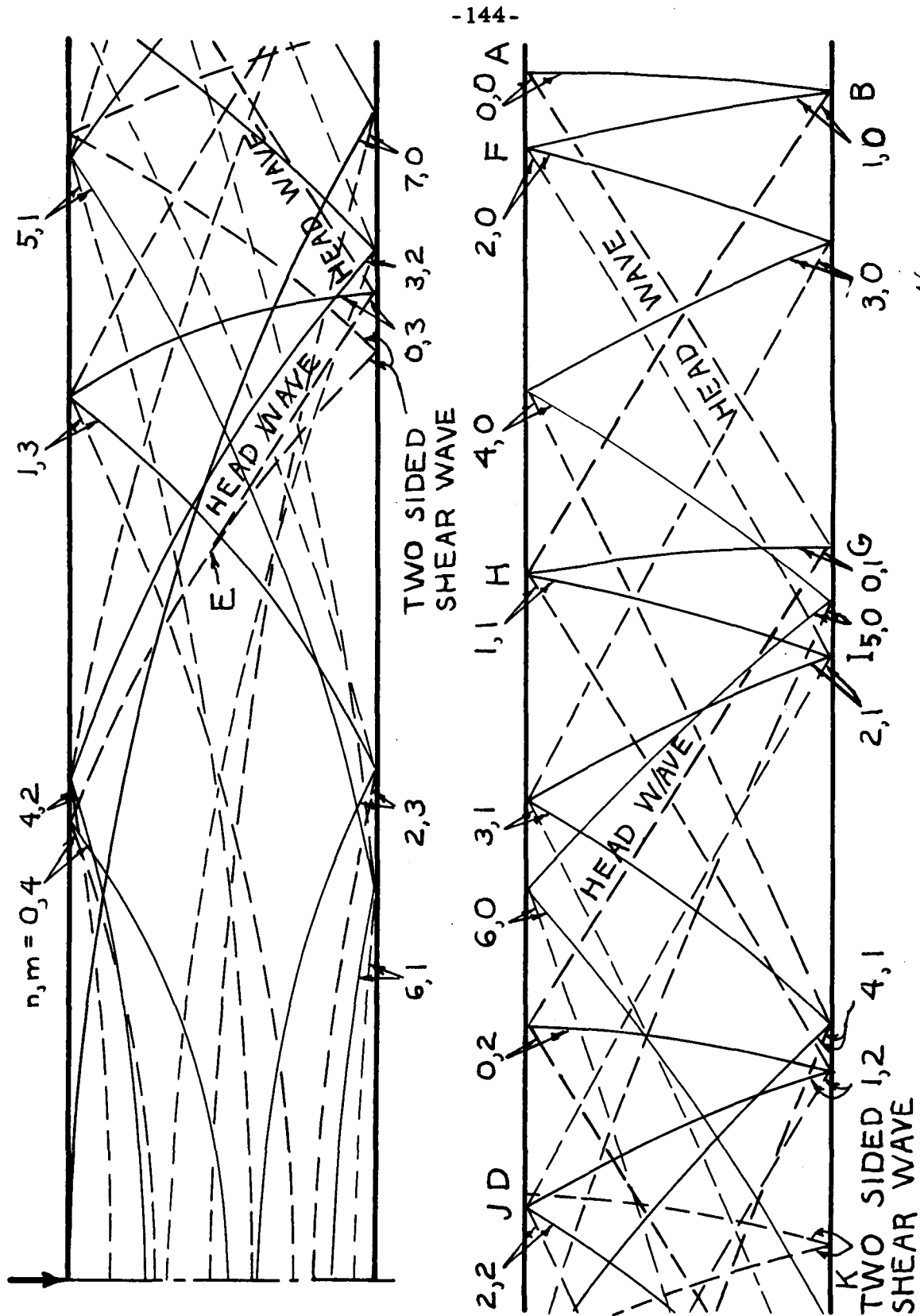


Figure 12 WAVE FRONT LOCATIONS (AT $t = \frac{16a}{c_d}$)

create a dilatational wave front. It reflects to form another two sided shear wave. The head wave, AG, reflects to create a continuation of itself and also to create a dilatational wave front at grazing incidence. The continuation of the head wave is tangent at E to the two sided shear wave and a regular shear wave front which comes directly from the leading circular shear front by reflection.

Each wave front can be labeled by its type, P or S, and by the two numbers n and m as shown in figures 11 and 12. One can follow back from the very first wave fronts along n P wave fronts and m S wave fronts in some order, but always following as one wave is created by another, and finally one arrives at a P or S wave which would be identified by the numbers n and m . Notice for instance the S wave front marked IJ in the figures, for which $n = 2$ and $m = 1$. It is created as two wave fronts come together. One, the P wave front HI, was created when a head wave, AG, was followed by a P wave front, GH, and at the same time when the first P wave front, AB, was followed by an S wave front, BH. The second, an S wave front, FI, was created when the first P wave front, AB, reflected to form another P wave front, BF, which in turn created the S wave front, FI. By these three paths energy could travel along rays to the S wave front IJ. This special circumstance, that different rays merge, occurs only because the parallel faces of the plate form a simple geometry.

The form of the wave fronts near the end of the plate can be investigated theoretically by imposing small s_0 on equations 116

and 117. The approximate equations for the wave fronts are then

$$\tau \approx \frac{1}{c_d} \left[\alpha \left(1 + \frac{s_o^2}{2} \right) + k\beta \left(1 + \frac{s_o^2}{2k^2} \right) \right]$$

$$\text{and } z \approx \left(\alpha + \frac{\beta}{k} \right) s_o,$$

which together give

$$z^2 \approx 2 \left(\alpha + \frac{\beta}{k} \right) (c_d \tau - \alpha - k\beta).$$

Along a wave front either α or β is constant while the other varies as y . In either case z is given as a quadratic function of y and the wave front must cross the line $z = 0$ parallel to the free surfaces and with some finite curvature.

To study wave front arrivals as they occur in time at the surface, it is convenient to group them. Looking particularly at figure 12, it is clear that the initial wave front will be followed closely by a series of wave fronts created as the P wave fronts reflect back and forth. Each member of this series of wave fronts is found by actual calculation (as shown below) to be weaker than the preceding member. After a longer delay a wave front arrives which is created by the head wave travelling once across the plate. This wave front is followed closely by successively weaker and weaker wave fronts. After another long delay a wave front arrives which is created when the head wave travels twice across the plate. That wave front is followed closely by successively weaker and

weaker wave fronts created by P wave reflections after the head wave. The process continues through several sets of wave fronts. An observer far from the source is able to distinguish the grouping better.

The head waves, which start each series of arrivals at the surface, have been observed experimentally because they are the strongest. Hughes, Pondrom, and Mims (32) were the first to observe the head waves arriving and gave the correct explanation. Meitzler (33) and Miklowitz and Nisewanger (19) observed the head waves under experimental conditions more similar to the theoretical conditions imposed in this thesis. They placed a rod at the end of the expansion chamber of a shock tube, which supplied a sudden step in pressure. The strain pattern as a function of time was displayed on an oscilloscope and photographed. The patterns show a large number of wiggles which were caused by the wave front arrivals. Certain of the wiggles are distinctly larger than the others. They were identified and attributed to the head waves by Meitzler, who was studying wave fronts. Miklowitz and Nisewanger were looking at the low frequency behavior and measured radial displacement as well as axial strain. However, their records also show the head waves at the expected times.

The experimental records of Meitzler and Miklowitz and Nisewanger were searched carefully with the hope of finding a larger number of the wave fronts predicted by the theory.

Choosing only the clearest records, it was possible to identify some of the wiggles with predicted wave fronts. This identification was not at all certain however. The records are not accurate to sufficiently high frequencies to bring out the wave fronts clearly. The wiggles are so wide that they tend to merge into each other. And so, it is not possible to distinguish which part of each wiggle really represents the beginning of a wave front. Only the head waves could be identified beyond any reasonable doubt. The other wave fronts and the Rayleigh waves require more sensitive instrumentation for positive identification.

B. WAVE FRONT AMPLITUDES

Time Dependence

Before discussing the amplitudes of the wave fronts it is necessary to examine their time dependences. The potentials were studied in section IV. The displacements are found by differentiating the potentials once with respect to space coordinates and the strains are found by differentiating the potentials twice with respect to space coordinates. Looking back at equation 108, it is clear that each differentiation brings out a factor of p . Then, a time dependence of $(t-\tau)^h$ in the potential becomes $(t-\tau)^{h-1}$ in the displacements and $(t-\tau)^{h-2}$ in the strains. The strains have severer changes at the wave fronts than the displacements.

The time dependences at the wave fronts of the potentials in plane strain are given in equations 123, 129, 130, 135, and 136 in terms of the integer N , which is given in equations 112

as three for the two end load problems and two for the line force problem. In the rod the wave fronts have the same time dependences as the fronts in the equivalent plane strain problem. The wave fronts caused by propagation from a point force are more severe because of the \sqrt{p} in equation 157; one-half must be subtracted from the exponent of $(t - \tau)$ which is found for the line force problem. Then, the time dependences of the strain at the wave fronts are as follows.

First arrival at $\tau = z/c_d$:

end load only, $H(t - \tau)$.

Regular waves:

end load, $(t - \tau)^{1/2}$; line force, $(t - \tau)^{-1/2}$; point force, $\delta(t - \tau)$.

Head waves:

end load, $(t - \tau)^{1/2}$; line force, $(t - \tau)^{1/2}$; point force, $H(t - \tau)$.

Two sided shear waves, for $t > \tau$:

end load, $(t - \tau)^{1/2}$; line force, $(t - \tau)^{-1/2}$; point force, $\delta(t - \tau)$.

Two sided shear waves, for $t < \tau$:

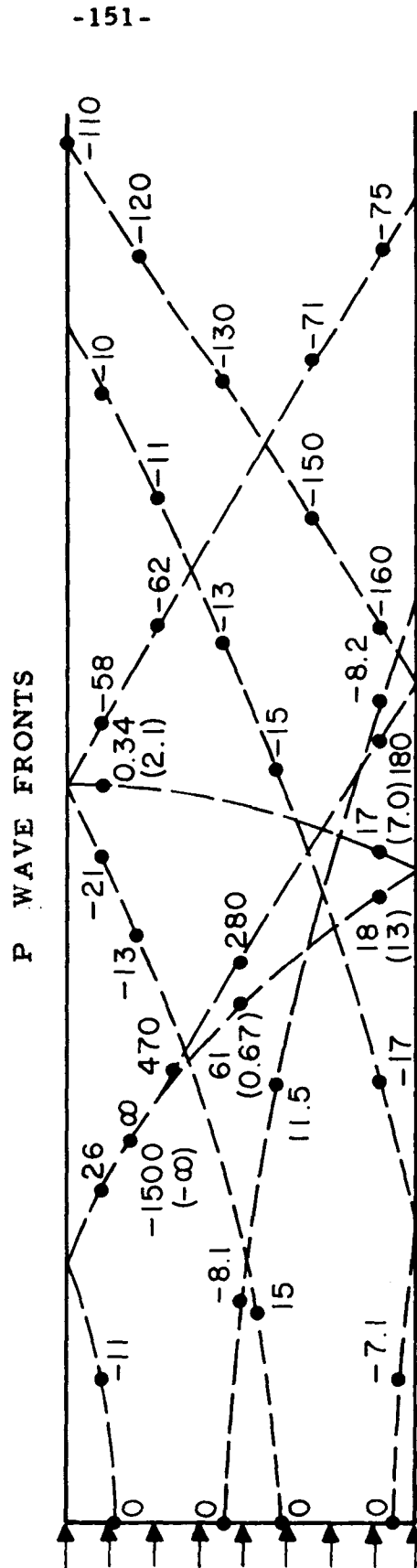
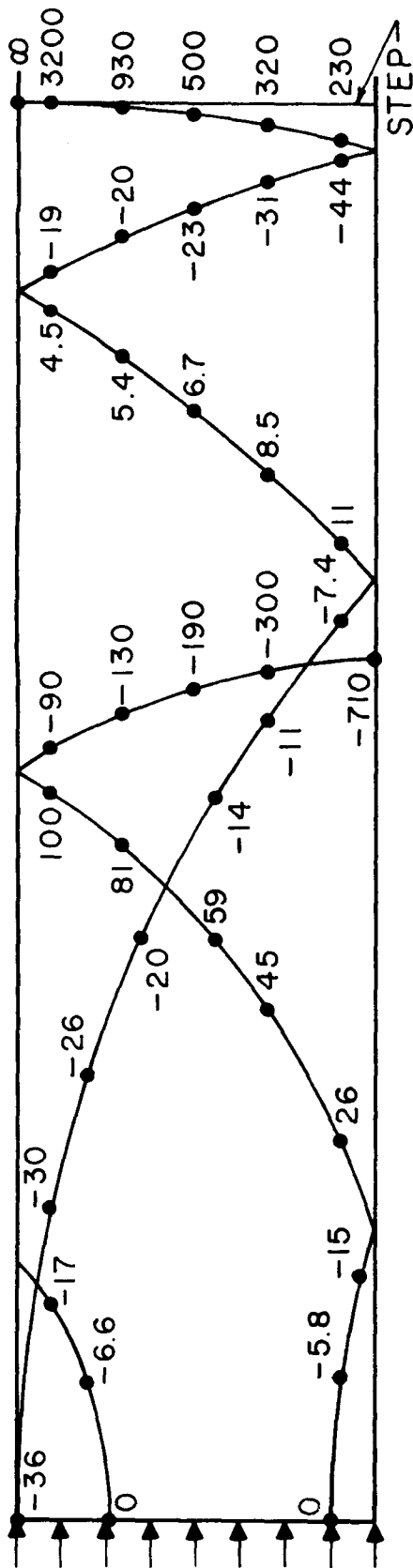
end load, $(\tau - t)^{1/2}$; line force, $(\tau - t)^{-1/2}$; point force, $\delta(\tau - t)$.

For the end load problems the time dependences are all the same except for the initial step which has the strongest time dependence. In the point force and line force problems the head waves are weaker than any of the other waves. The greater severity of the wave fronts under a line force or point force is not surprising in view of the fact that a finite force is applied to only an infinitesimal area.

Amplitudes

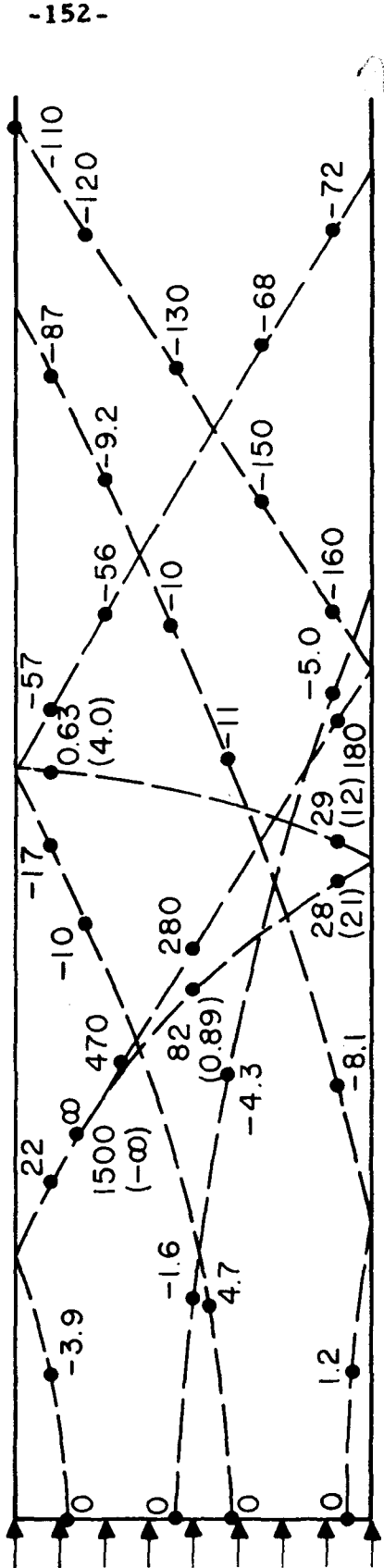
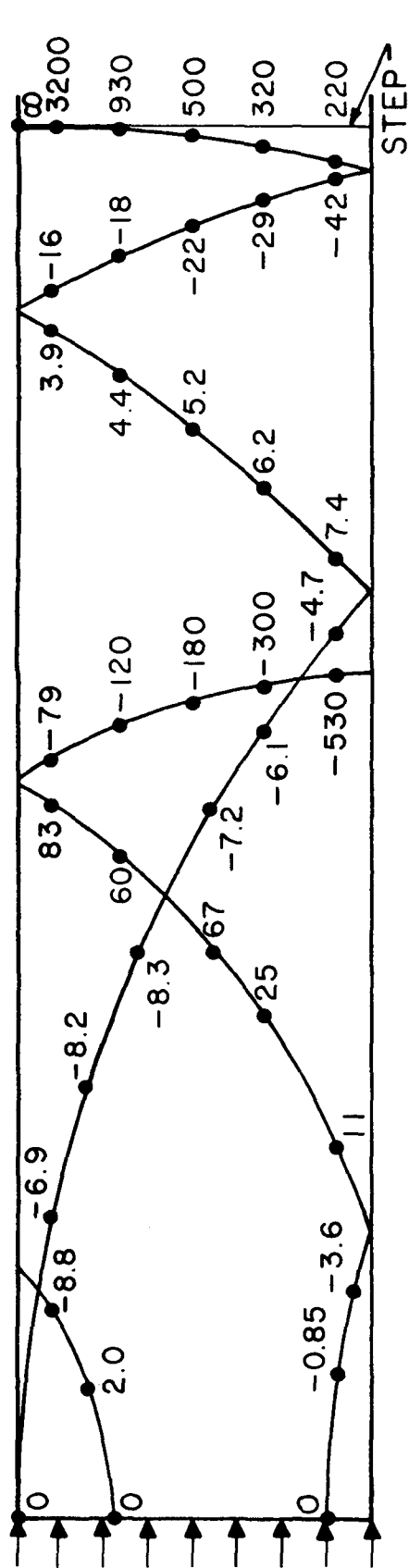
The wave front amplitudes were calculated for the three plane strain problems for Poisson's ratio equal to 0.3 for two different times, $t = 8a/c_d$ and $t = 16a/c_d$. The wave fronts are shown in figures 13 to 21 plotted to geometrical scale with the amplitudes in non-dimensional form written in along the wave fronts. Dilatational wave fronts are shown with solid lines and shear wave fronts are shown with dashed lines. The amplitudes of the two sided shear waves for $t < \tau$ are given in parenthesis. The amplitudes of the head wave for the line force are not shown as the time dependence of the head wave is weaker, and therefore the disturbance near the head wave is an order of magnitude smaller than the disturbance near other wave fronts. Only half of the wave fronts produced by the end loads are shown. The manner in which the various factors affect the wave front amplitudes can be studied in the several figures.

The effects of the source of rays and the divergence factor are studied most easily by looking at the circular wave fronts which have undergone no conversion from one type of wave front to the other type through reflection. Those are the P (S) wave fronts shown in figures 11 and 12 with $m = 0$ ($n = 0$). According to equations 162, along such wave fronts the two leading wave fronts are reduced in magnitude through successive reflections into wave fronts of the same type by the factor R which is never



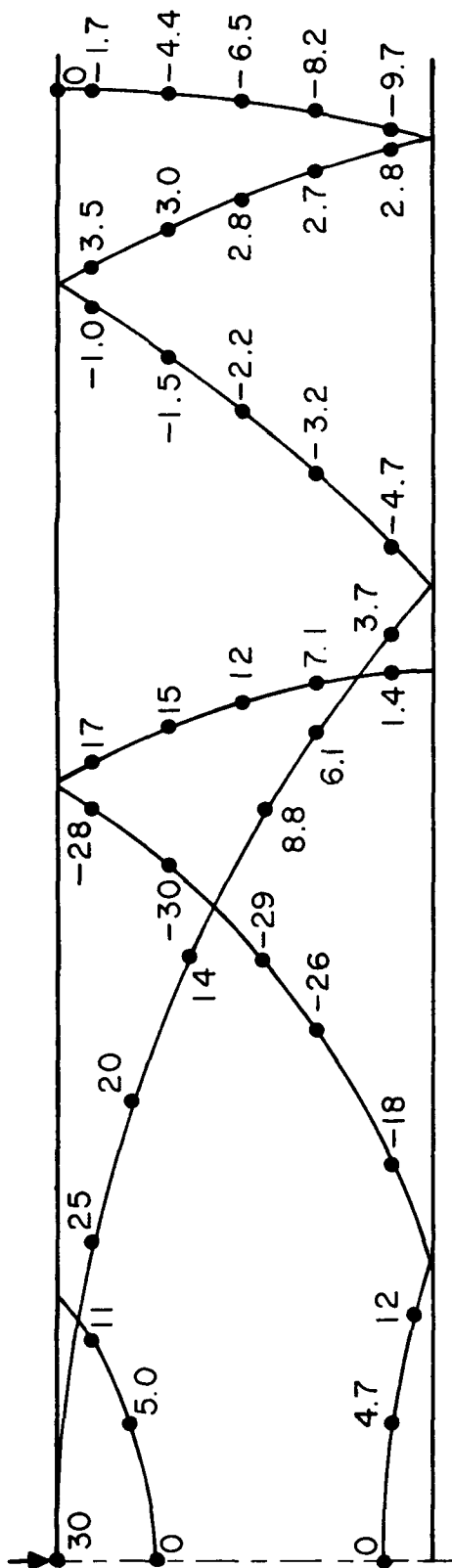
IMPACT PROBLEM AMPLITUDES TIMES $\frac{1000 \sqrt{\frac{a}{2}}}{Zc_d}$ (AT $t = \frac{8a}{c_d}$)

Figure 13

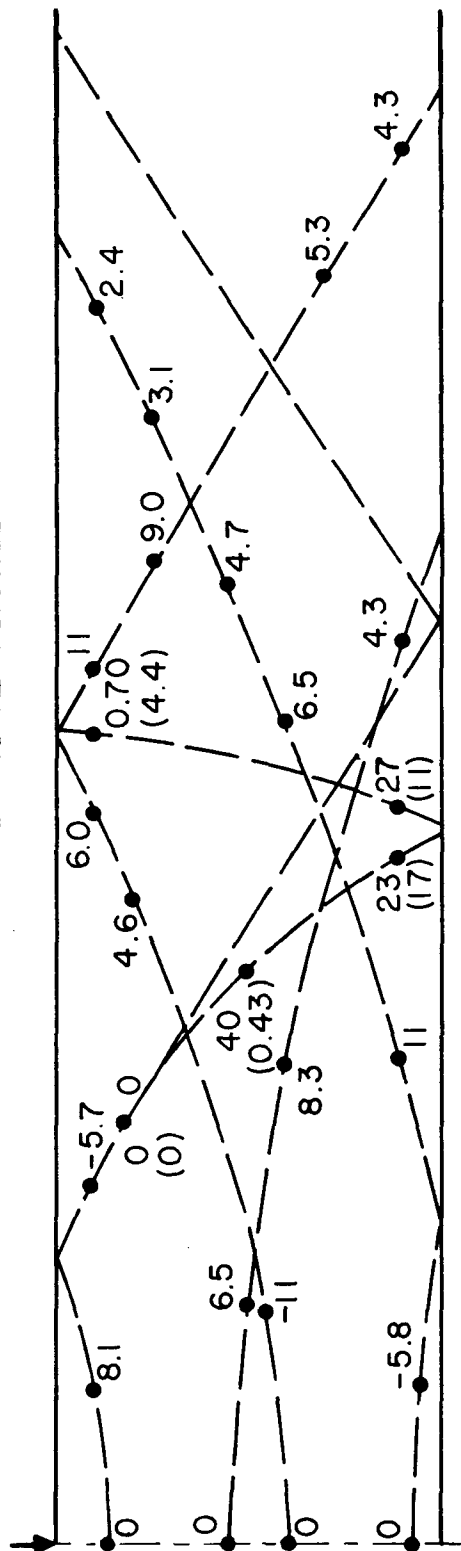


$$\frac{1000}{Zc_d} \sqrt{\frac{a}{2}} \sqrt{c_d} \quad (\text{AT } t = \frac{8a}{c_d})$$
 PRESSURE PROBLEM AMPLITUDES TIMES

Figure 14

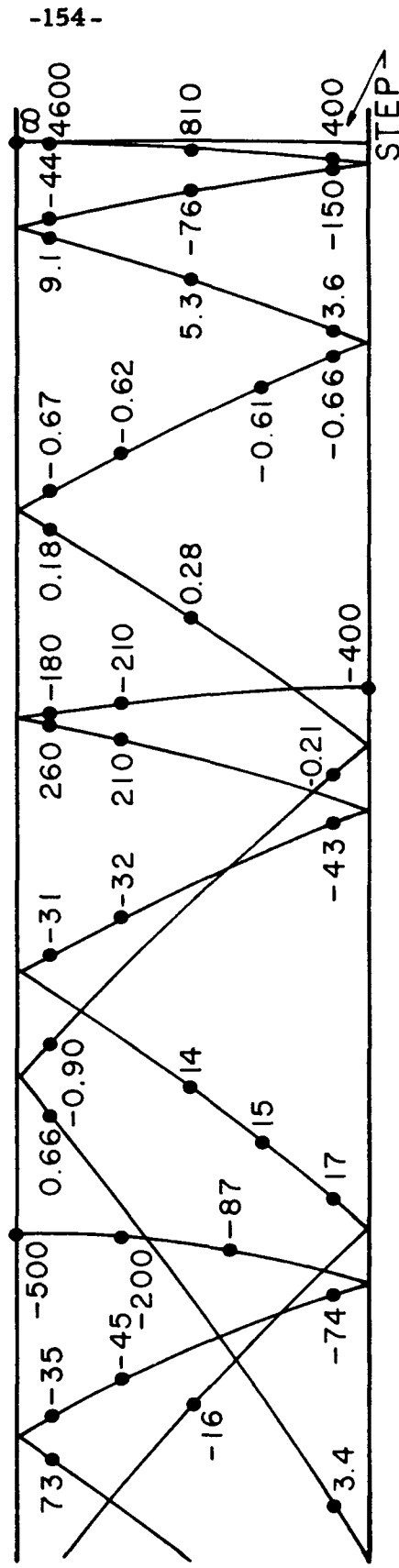
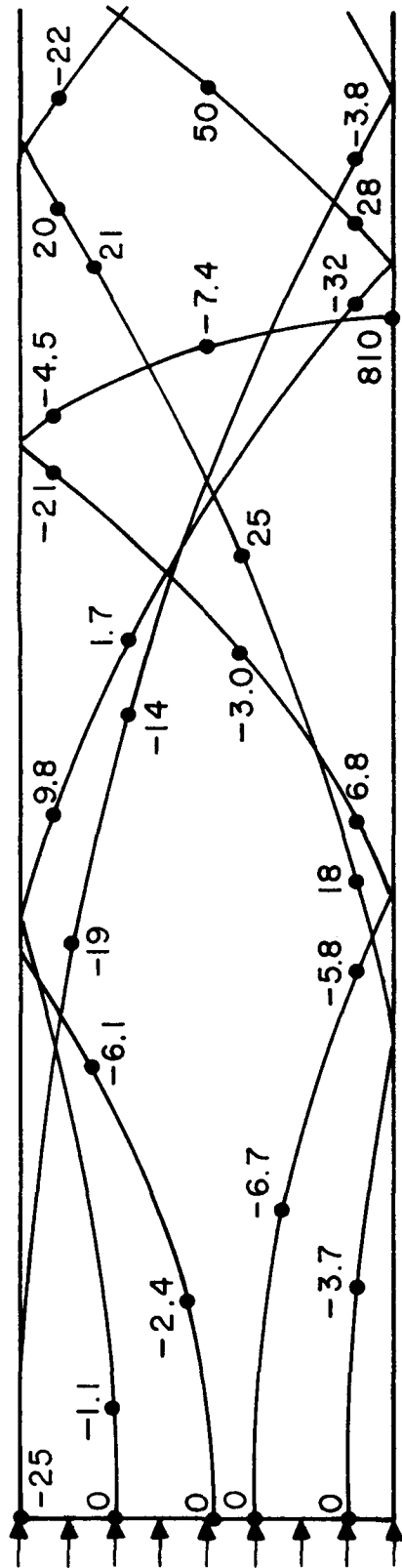


P WAVE FRONTS



LINE FORCE PROBLEM AMPLITUDE TIMES $\frac{1000}{Zc_d} \sqrt{\frac{c_d}{a}}$ (AT $t = \frac{8a}{c_d}$)

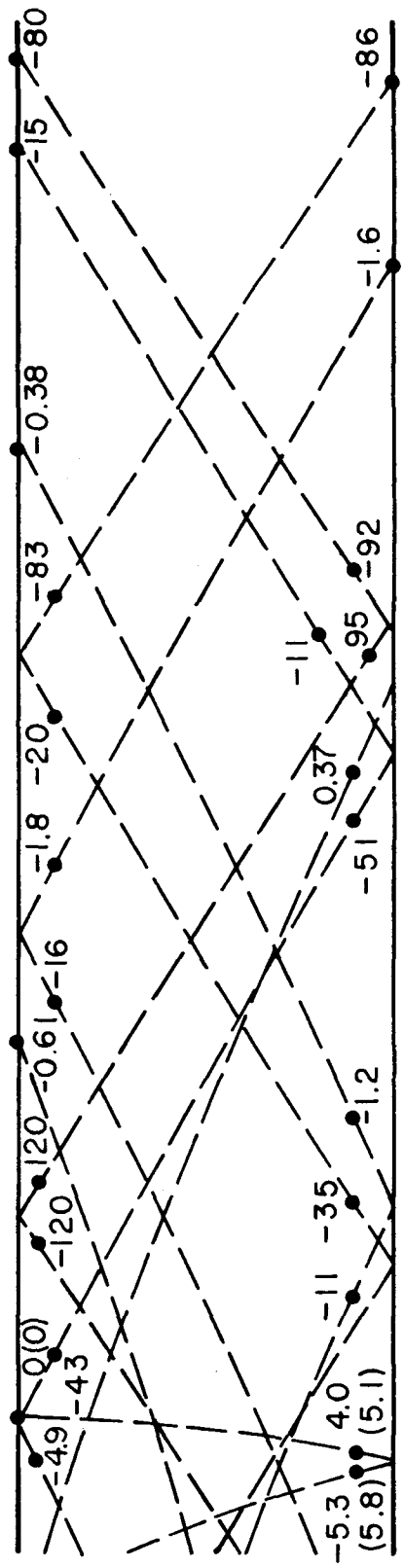
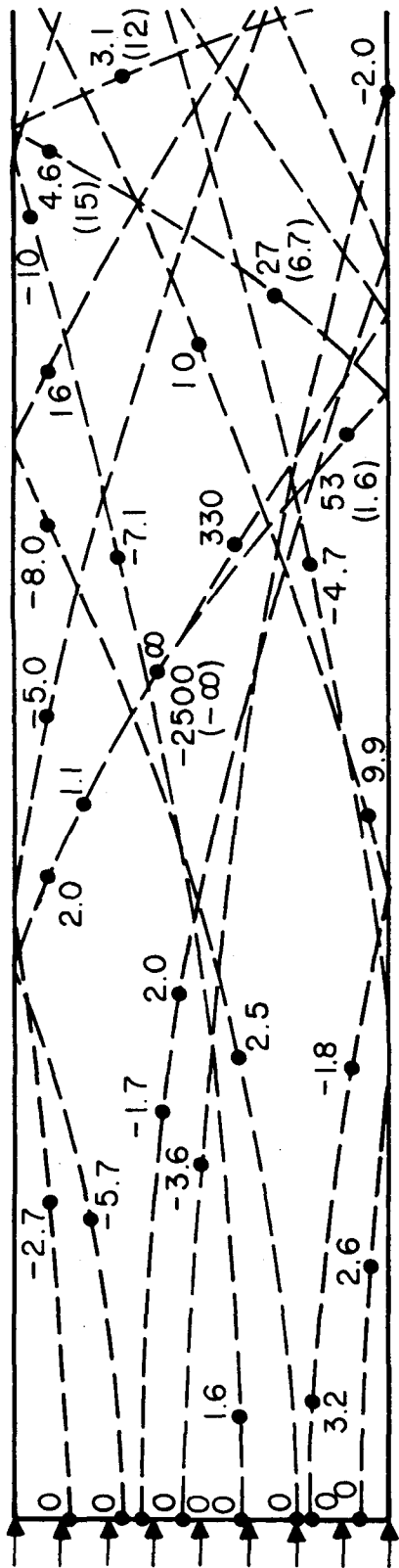
Figure 15



IMPACT PROBLEM P WAVE FRONT

AMPLITUDES TIMES $\frac{1000 \sqrt{a}}{2 \sqrt{c_d}} \quad (AT \ t = \frac{16a}{c_d})$

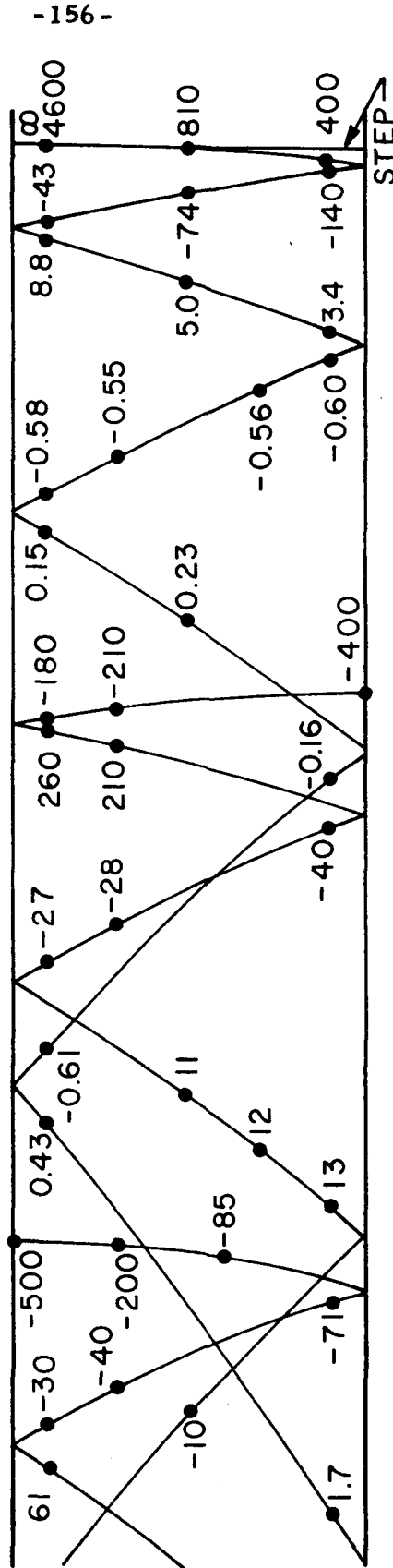
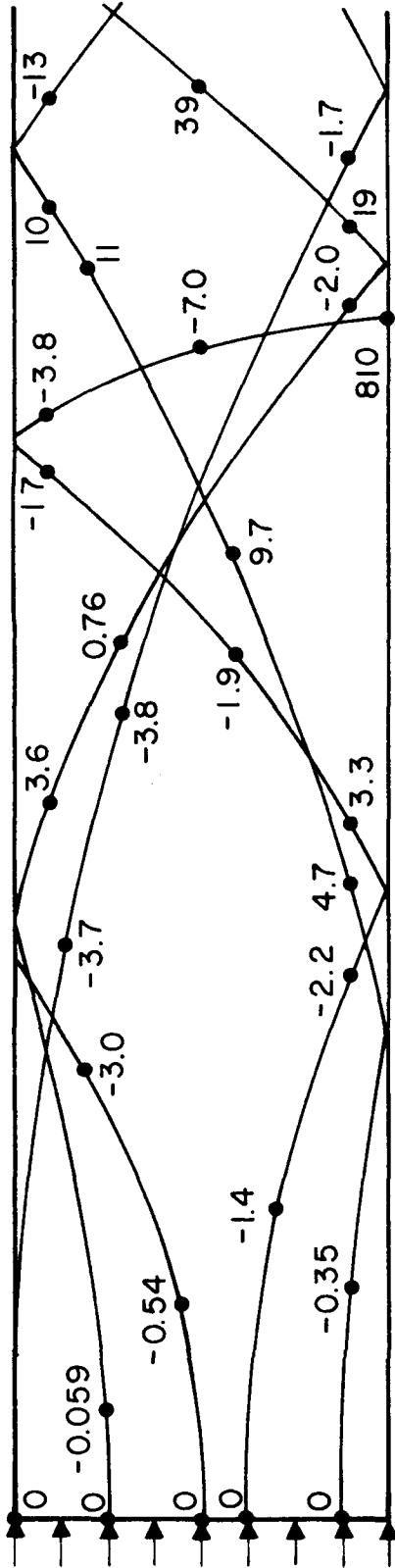
Figure 16



IMPACT PROBLEM S WAVE FRONT

$$\text{AMPLITUDES TIMES } \frac{1000}{z c_d^2} \sqrt{\frac{a}{c_d}} \text{ (AT } t = \frac{16a}{c_d} \text{)}$$

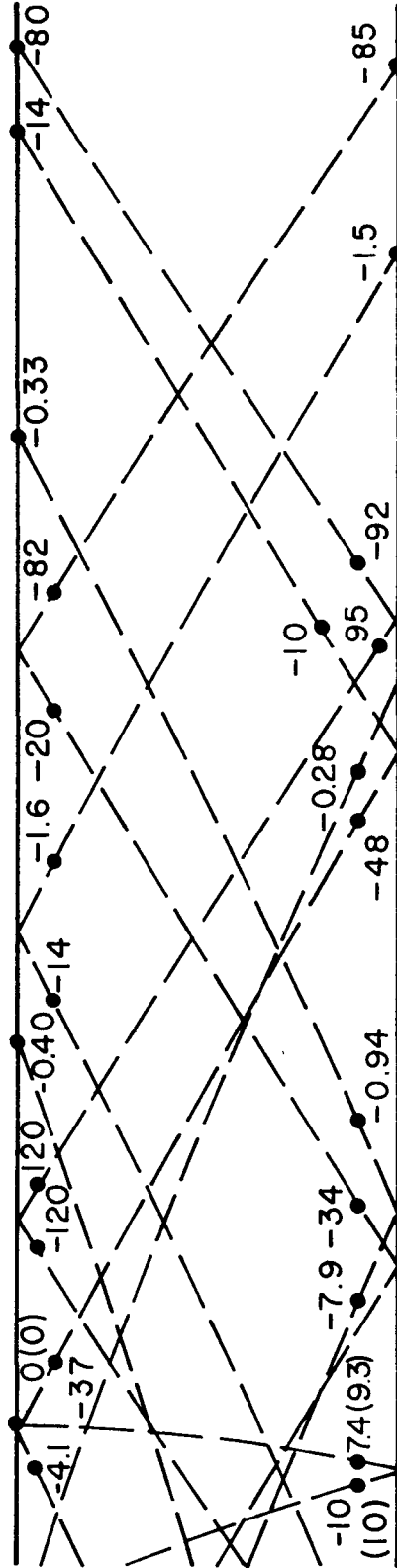
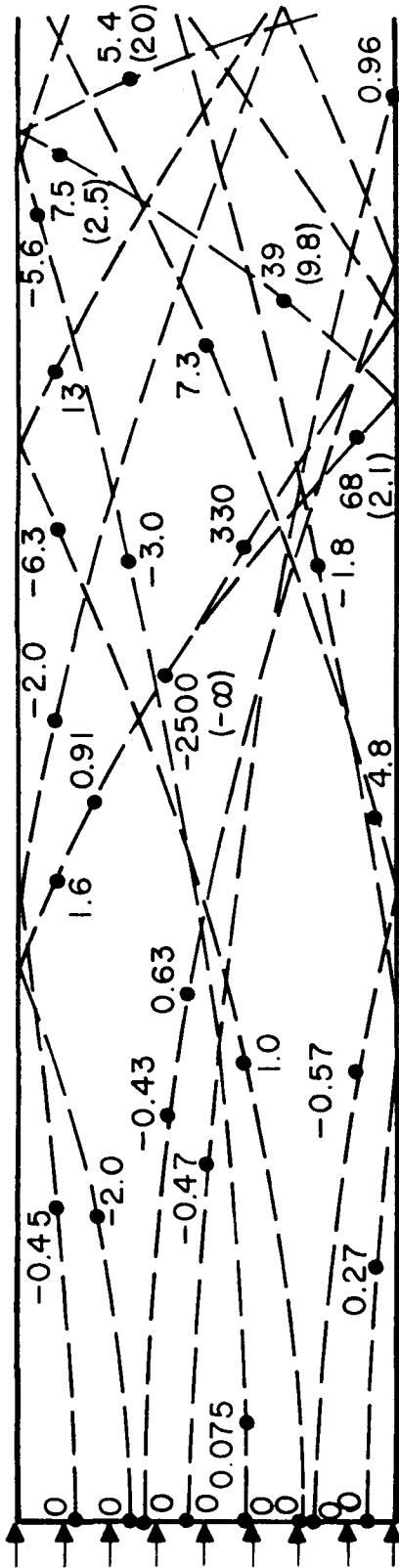
Figure 17



PRESSURE PROBLEM P WAVE FRONT

AMPLITUDES TIMES $\frac{1000}{Zc_d} \sqrt{\frac{a}{Z}} \sqrt{c_d}$ (AT $t = \frac{16a}{c_d}$)

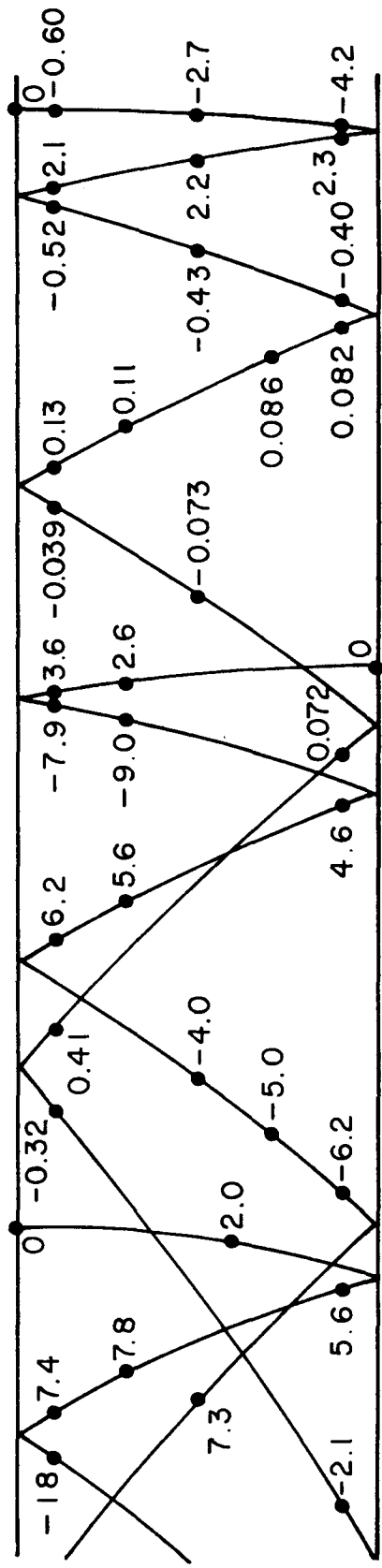
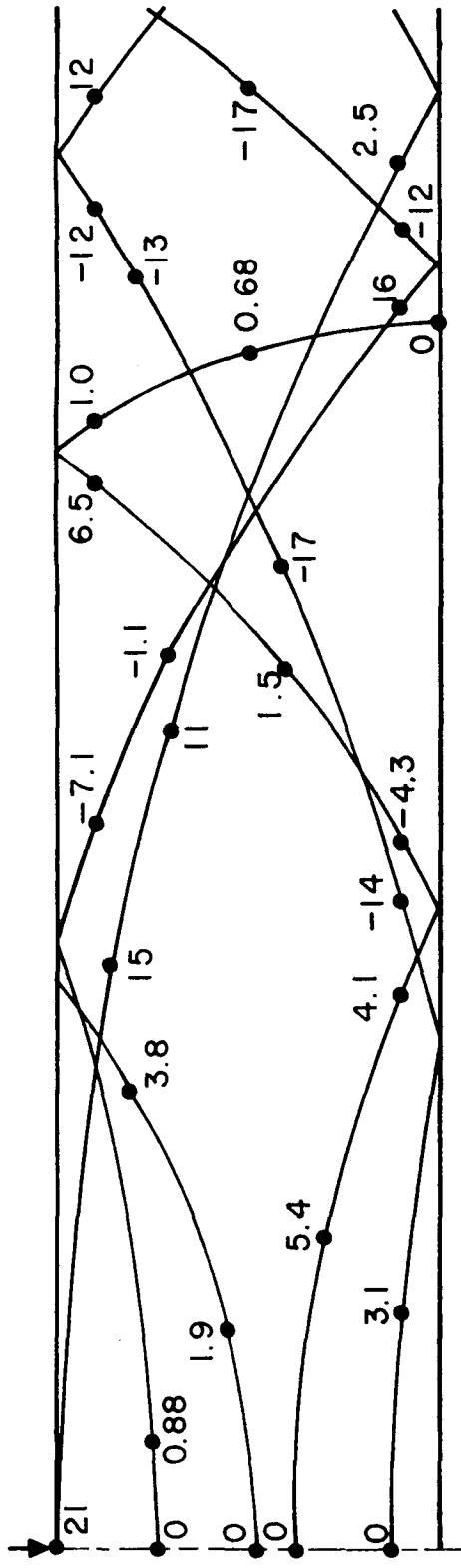
Figure 18



PRESSURE PROBLEM S WAVE FRONT

$$\text{AMPLITUDES TIMES } \frac{1000}{z c_d} \sqrt{\frac{a}{c_d}} \text{ (AT } t = \frac{16a}{c_d} \text{)}$$

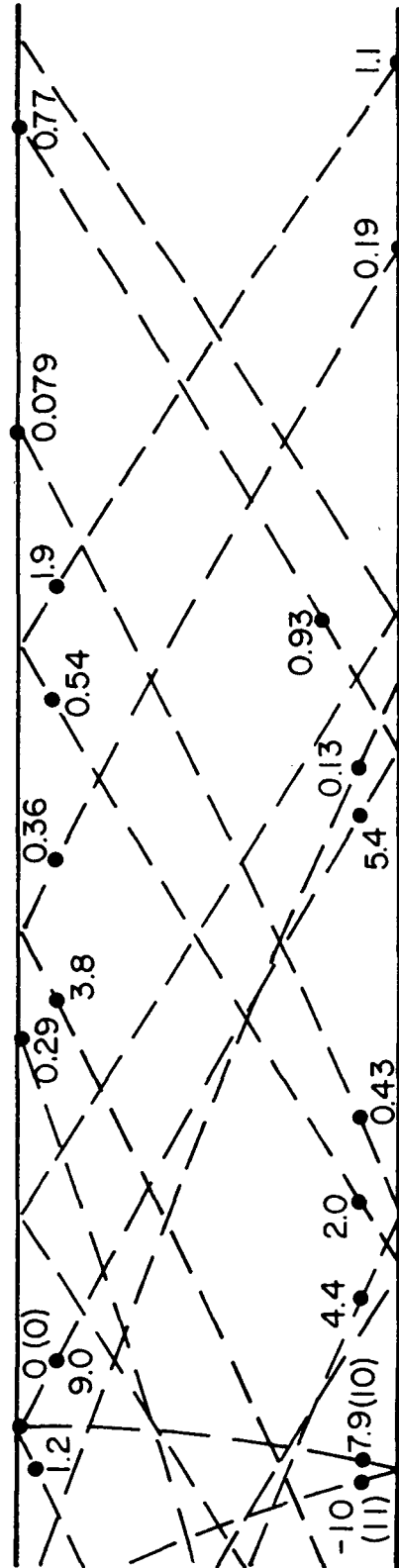
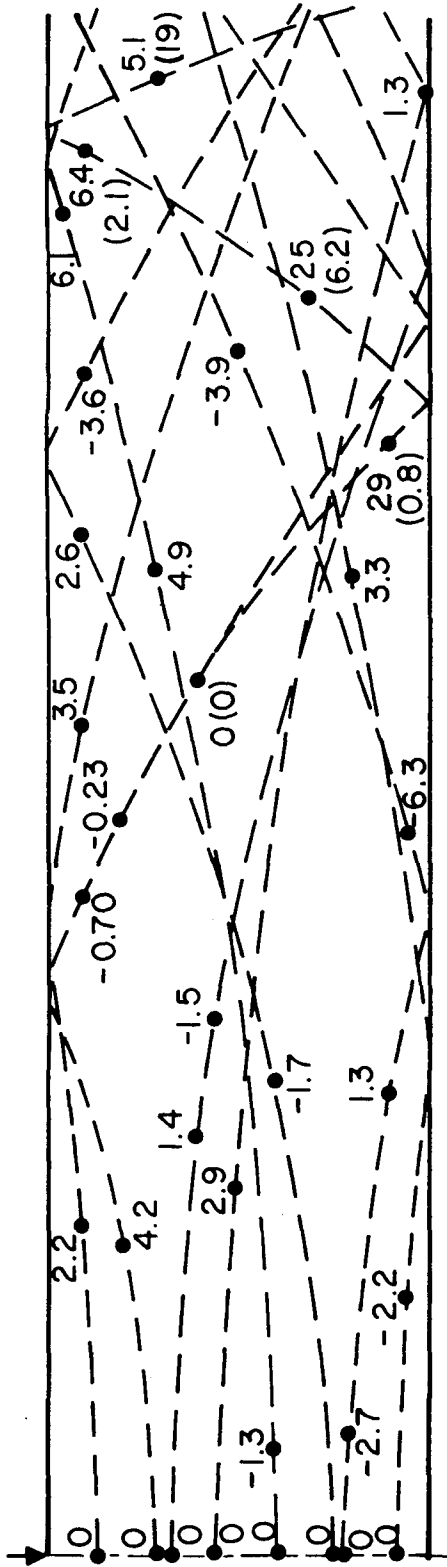
Figure 19



LINE FORCE PROBLEM P WAVE FRONT

AMPLITUDES TIMES $\frac{1000}{Z} \sqrt{\frac{c}{d}}$ (AT $t = \frac{16a}{c_d}$)

Figure 20



LINE FORCE PROBLEM S WAVE FRONT

AMPLITUDES TIMES $\frac{1000}{Zc_d} \sqrt{\frac{c_d}{a}} \quad (\text{AT } t = \frac{16a}{c_d})$

Figure 21

zero or infinite, and so the behavior of the reflected wave fronts is determined mostly by the source of rays and by the divergence factor. The effects of reflection on the amplitudes can be studied by looking at the wave fronts which arise after multiple reflections.

The variable s_0 ($s_0 = \sin \theta_P = k \sin \theta_S$), which appears in the equations, must be interpreted in light of ray theory. When s_0 is small, an S or P wave front is nearly parallel with the free surfaces. When s_0 is nearly one, a P wave front is nearly perpendicular to the free surfaces, and an S wave front is nearly at the angle of the head waves. Along the two sided shear wave s_0 varies between one and k as the wave front varies in slope between the slope of the head wave and the direction perpendicular to the free surfaces. In that case ($s_0 = \sin \theta_P > 1$) the saddle point is on the branch cut, a head wave arrives before the shear wave (which is two sided), and θ_P is not a real angle.

The Source

The source of waves affects the wave front amplitudes mainly through the source factors given in equations 168 and the following remarks. The divergence factor given in equation 167 also has a variation with angle which must be attributed to the source. The line force problem is the easiest to understand. The source function for P waves, P_0 , varies slowly with angle; but the divergence factor vanishes when s_0 approaches one. This is a natural result that the P waves are pushed out most strongly

directly under the load and most weakly to the side of the load ($s_0 = 1$). The source function for S waves, S_0 , vanishes at $s_0 = 0$ and at $s_0 = 1$. Directly under the load ($s_0 = 0$) the shear wave fronts must have zero amplitude by symmetry.

The end load problems are not so simple. The load itself causes a simple step to move down the plate. Then, that step cannot satisfy the boundary conditions on the free surfaces and so a complicated system of wave fronts of weaker time dependence is formed as shown in figure 8. As s_0 approaches zero, so do S_0 in both end load problems and P_0 in the pressure step problem. The boundary conditions at the end of the plate govern wave fronts moving along the end of the plate at grazing incidence ($s_0 = 0$). There, P waves must have zero amplitude in the pressure step problem for the displacement u_y to vanish and S waves have zero amplitude in the longitudinal impact problem in order that σ_{yz} be zero. The product of the source function S_0 and the divergence factor approaches zero as s_0 approaches one except if α is zero. That one exception, $\alpha = 0$ and s_0 going to one, corresponds to the point of tangency of the two sided shear wave and the head wave, point E in figures 4, 11, and 12. There the regular shear wave, two sided shear wave, and head wave all approach infinite amplitude. (Equations 129, 135, and 136 govern the head wave and two sided shear wave.) (The approach to infinity is too fast to show clearly in figures 13, 14, 17 and 19.) The product of the other source function, P_0 , and the divergence factor approaches

infinity as s_0 approaches one. But s_0 becomes one only where a P wave intersects the head wave at the free surfaces (A, G, etc. in figures 11 and 12). The amplitude remains finite due to the reflection coefficients going to zero except at the very point where the head wave starts, point A on figures 8, 11, and 12. There the dilatational wave front has infinite amplitude.

Reflection at Grazing Incidence

A critical examination of that one point A on figures 8, 11, and 12 is enlightening. The strain at the surface due to the dilatational potential can be calculated by considering the two integrals containing the dilatational wave fronts at point A. No wave fronts arrive before those two wave fronts. The first integral is for the unreflected P wave, for which $n = m = 0$; and the other integral is the first integral in equations 106i, ii for $\bar{\phi}$ and represents the step. We will consider the impact problem. The pressure step problem gives the same approximate result since the Cagniard contours appropriate to the region of point A are near the point $s = i$ in the s plane. Thus, the factor $-is$, which differentiates the impact and pressure step problems, is unity.

We wish to find the strain in the z direction due to the dilatational potential,

$$\bar{e}_z = \frac{\partial u_z}{\partial z} = \frac{\partial^2 \phi}{\partial z^2}. \quad (175)$$

First, we take the double transform of equation 175 according to scheme 2 of table 1. Equation 175 is multiplied by $e^{-pt} \cos \kappa z$ dt dz and integrated over t and z. The integration over z is carried out by parts using a boundary condition from equations 93i with the result

$$\bar{e}_z = -\kappa^2 \bar{\phi} - \frac{Z c_d}{p}. \quad (176)$$

Next, equations 106i and 176 are combined to form an integral for \bar{e}_z ;

$$\bar{e}_z = -\frac{Z}{\pi p} \int_{-\infty}^{\infty} \left\{ e^{i \frac{p}{c_d} sz} - \frac{s^2 e^{i \frac{p}{c_d} sz}}{1+s^2} + \frac{s^2 (k^2 - 2) (k^2 + 2s^2) e^{-\kappa_d (a-y) + i \frac{p}{c_d} sz}}{(1+s^2) [(k^2 + 2s^2)^2 - 4s^2 \sqrt{(1+s^2)(k^2 + s^2)}]} \right\} ds. \quad (177)$$

The first term in equation 177 comes directly from the second term on the right hand side of equation 176. The second term in equation 177 is the integral for the step from equation 106i multiplied by $-\kappa^2 = -\frac{p^2}{c_d^2} s^2$. The third term in equation 177 represents the unreflected dilatational wave front for which $n = m = 0$. It is found by taking the $f(s)$ for n and m equal to zero as given in

equations 112i and multiplying by $-L^2$. (Note that $k^2 - 2 = \lambda/\mu$.)

The analysis of equation 177 for the two wave fronts inside the plate has already been done. The first two terms together give the step in equation 113*. The third term is like equation 111 and the wave front is given by equation 123 as

$$e_z \approx 2 f(is_0) \sqrt{\frac{2}{g''(is_0)}} (t - \tau)^{1/2},$$

where

$$f(s) = - \frac{Z(k^2 - 2) s^2 (k^2 + 2s^2)}{\pi (1 + s^2) \left[(k^2 + 2s^2)^2 - 4s^2 \sqrt{(1 + s^2)(k^2 + s^2)} \right]},$$

$$g''(s) = \frac{a - y}{c_d (1 + s^2)^{3/2}},$$

from equation 117 with $\beta = 0$ and $\alpha = a - y$

$$\tau = \frac{1}{c_d} \left[\frac{(a - y)}{\sqrt{1 - s_0^2}} \right],$$

and from equation 116

*The residue of the sum of the first two terms taken at the pole $s = i$ and multiplied by $2\pi i$ is the Laplace transform of equation 113. The sum of the terms must be used because it is only the sum of the terms to which Jordan's lemma (reference 30, p. 137) applies and the total integral is given by the residue.

$$z = \frac{(a - y) s_0}{\sqrt{1 - s_0^2}} .$$

The above can be combined for $(a - y)/z$ small (then, $s_0 \approx 1$) and the step added with the result

$$e_z \approx -Z H \left(t - \frac{z}{c_d} \right) + \frac{2\sqrt{2}Z}{\pi} \left(\frac{z}{a - y} \right) \sqrt{\frac{c_d}{z} \left[t - \frac{1}{c_d} \sqrt{z^2 + (a - y)^2} \right]} . \quad (178)$$

Equation 178 holds approximately inside the plate near the surface and near to the point in question, point A.

At the surface we let y equal a in equation 177 and combine the three terms. The result is easily seen to have no pole at $s = i$ and can be handled like equation 111 with $g(s) = -isz/c_d$. (See equation 110.) According to equation 114 the Cagniard contour is given by

$$s = i \frac{tc_d}{z} .$$

The two arms of the Cagniard contour in figure 6 are collapsed onto the imaginary axis branch cut. The solution by Cagniard's method is then given by equation 120 as

$$\frac{\partial \epsilon_z}{\partial t} = \frac{2Z}{\pi} \operatorname{Re} \left\{ \frac{1}{1+s^2} \right.$$

$$\left. - \frac{(k^2 - 2)(is^2)(k^2 + 2s^2)}{(1+s^2) \left[(k^2 + 2s^2)^2 - 4s^2 \sqrt{(1+s^2)(k^2 + s^2)} \right]} \right\} \frac{c_d}{iz} H\left(t - \frac{z}{c_d}\right).$$

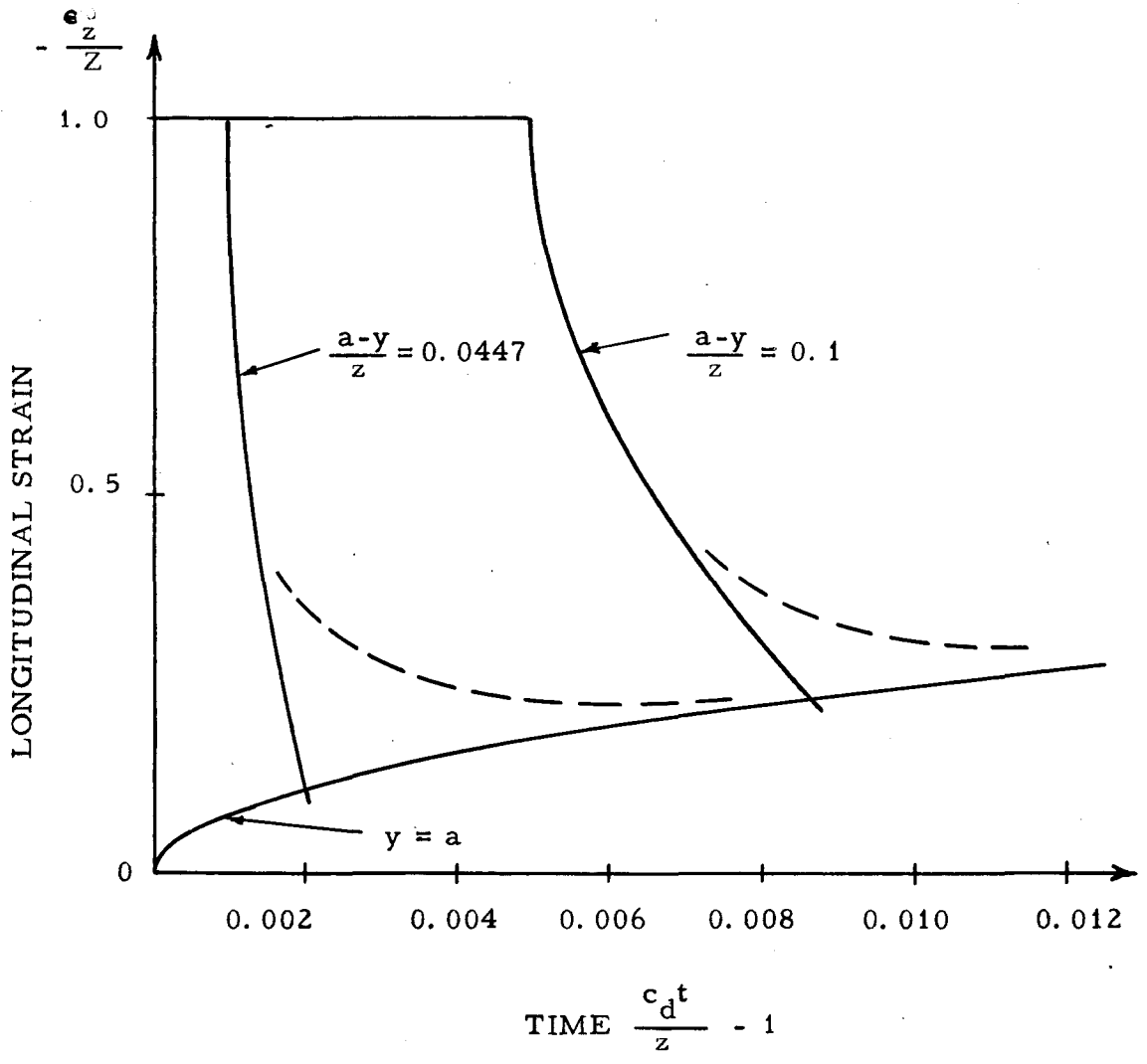
$$s = \frac{it c_d}{z} \quad (179)$$

Equation 179 is easily approximated near $t = z/c_d$ with the result for $y = a$

$$\epsilon_z \approx - \frac{8\sqrt{2}Z}{\pi} \frac{\sqrt{k^2 - 1}}{(k^2 - 2)} \sqrt{\frac{c_d}{z} \left(t - \frac{z}{c_d}\right)} \quad (180)$$

By a similar analysis using equation 112ib the contribution at the surface from the shear potential of the head wave is found to be the same thing multiplied by a constant.

Equations 178 and 180 are plotted in nondimensional form in figure 22 for $(a - y)/z$ equal to 0.0, 0.1, and 0.0447 and $k^2 = 3.5$. Essentially, figure 22 is a plot of longitudinal strain versus time for three stations with the same z coordinate and located at three different distances from the surface, one station being on the surface. The results of wave front theory, equations 178 and 180, are shown with solid lines. Notice that the strain on the surface behaves simply as the square root of time. Also, notice that the strain inside the plate takes a jump and then quickly reverses itself, starting back to zero as the square root of time. The



STRAIN FOLLOWING STEP NEAR SURFACE

Figure 22

nearer the station to the surface, the more quickly the reversal takes place. Because the strain due to the dilatational potential must vary continuously as y approaches a , it can be inferred that after the jump and subsequent reversal takes place the strain inside the plate behaves almost the same as the strain on the surface. This is indicated by the dashed line in figure 22.

Some light can be thrown on this strange behavior, in which the strain is influenced by a regular dilatational wave front and the step, by looking at two different limiting procedures. If $a - y$ is considered small but fixed and t approaches the arrival time for the circular wave, the step plus the wave front approximation for the circular wave front is found and equation 178 holds. But, if t is allowed to approach z/c_d while $(a - y)/c_d$ remains small in comparison to $(t - z/c_d)$, then the wave front form at the surface is found. The second limiting procedure is carried out by letting y go to a first and then the results are the same as those found for the surface in equation 180.

In this situation one is led to ask for what length of time the first term of the wave front expansion--that is, the first term of the inner expansion of equation 84--is a good approximation to the total strain. Here it is evident from figure 22 and equation 178 that as y approaches a the amplitude of the first term increases but the first term becomes valid for a lessening interval of time. (Note in figure 22 the more rapid fall of that term.) If one considers the whole wave front expansion in equation 84 as a Taylor

series times $(t - \tau)^{1/2}$, then one might ask what is the region of convergence, if any. It would appear that the Taylor series would converge to the correct solution over a smaller and smaller region of convergence as y approaches a .

The preceding discussion should shed some light on the grazing incidence problem. Goodier and Bishop (34) have studied this problem for harmonic waves. The problem is to determine the reflected waves when a dilatational wave is incident on a surface at a ninety degree angle of incidence. Figure 22 shows what actually happens in a certain transient problem. When there is an end load on a plate, a step wave travels down the plate at a ninety degree angle of incidence to the free surface. By ray theory the wave fronts created by the step have been considered as part of the canonical problem of the source. More generally speaking, however, grazing incidence is a refraction rather than a reflection problem or a source problem. In the case of harmonic waves that Goodier and Bishop considered, the same comments should apply since harmonic waves can be used to synthesize transient waves by means of the Fourier transform.

Head Waves

The head waves have a very simple dependence of amplitude on position. Looking at equations 129 and 130, one can see that the amplitude at a point on the wave front depends on one coordinate which is the distance in the z direction from the point of tangency of the head wave and the circular shear wave (E on

figures 4, 11, and 12). Going away from the point of tangency, the amplitude decreases monotonically from infinity. However, in the line force and point force problems the amplitude must be considered as negligible compared to the other wave fronts since the time dependence is weaker, as has been shown.

Effects of Divergence, Reflection, and Cylindrical Symmetry

The divergence factor given in equation 167 is the only factor making up the wave front amplitudes that cannot be written in terms of s_0 alone. The dependence on α and β at constant s_0 is such that the larger α and β , that is, the farther the wave front from the source, the weaker is the wave. This satisfies the intuitive notion that the amplitude of the wave front must decrease as the wave front spreads out.

The reflection coefficient R given in equations 163 varies smoothly with s_0 and takes on the value one when s_0 is zero or one. With $R = 1$ the polynomial functions of R in equations 112 which account for the multiple reflections are zero only for dilatational waves when m is not zero. When s_0 is nearly one, those are the dilatational waves which are created where the head wave reflects at the surface. Those dilatational waves are not zero because the product of the source factor (equations 112) and divergence factor (equation 167) becomes infinite as s_0 approaches one. The dilatational waves with s_0 zero must have zero amplitude because of the reflection factors except for the one wave front which is created through multiple reflections as a P wave front only. The

other dilatational wave fronts with s_0 zero have zero amplitude according to equations 162 because both R_{sp} and R_{ps} given in equations 163 are zero when s_0 is zero.

The point force problem differs from the line force problem through the correction factor $a\sqrt{\frac{ws_0p}{2zc_d}}$ given in equation 156 and through the difference in the definitions of Z . The p affects the time dependence as explained above. The distance z/s_0 is the distance from the observation point back to the line $z = 0$ measured along a line inclined at the angle of a P ray. For the circular dilatational wave front that is simply the distance to the point force measured along a ray. For all wave fronts z/s_0 is a measure of the distance from the point force. For the head waves the factor $a\sqrt{\frac{wp}{2zc_d}}$ given in equation 157 indicates a lessening of amplitude compared to the line force problem which is proportional simply to $\sqrt{1/z}$.

C. WAVE FRONTS IN THE MODAL EXPANSION

The solution given in equations 35 as integrals over the modes of propagation is an exact solution and must therefore contain information on the wave fronts. However, great difficulties are met when wave front information is sought in the modal solution. To investigate the wave fronts in a plate, rather than using equations 35 directly, a similar expansion for the plate will be found in terms of the Rayleigh-Lamb symmetric modes of propagation for the infinite plate in plane strain. The following discussion reveals no

new information about wave fronts but does give additional meaning to the high frequency part of the Rayleigh-Lamb spectrum. Only the head waves and the step will be found here from the modes. Analogous information can be found about the Pochhammer frequency spectrum of the rod.

We will use the double transforms given in equations 99i for the impact problem. The inversion theorem for the sine and cosine transforms given in equation 16b is applied by multiplying equations 99i by $\frac{1}{\pi} e^{i\kappa z} d\kappa$ and integrating over κ . To write a solution in terms of modes, residue theory is used to carry out the integration in a manner similar to Skalak's (5). It is easily seen that the integrand has no branch points; the only possibilities are $\kappa_d^2 = 0$ and $\kappa_s^2 = 0$ and expansion at those points quickly shows that they are not branch points. Since the integrand vanishes sufficiently rapidly for κ large and in the first two quadrants of the κ plane*, the integration can be expressed as a sum of the residues of all of the poles in the first two quadrants. It can easily be shown that the total residue of the pole at $\kappa_d^2 = 0$ in $\bar{\varphi}$ is zero and that the only other simple poles are the zeroes of F_g . The Rayleigh-Lamb modes of propagation. Thus, for example, $\bar{\varphi}$ is expressed as a sum over all zeroes of F_g , where $\kappa = \kappa_n(p)$, in the first two quadrants as

*The integrand vanishes at least as fast as $\frac{1}{\kappa} e^{i\kappa z}$ for large κ .

$$\bar{\phi} = \sum_n \frac{2iZ\lambda \frac{c_s^2}{\mu c_d \kappa_d^2} \left(\frac{p^2}{2} + 2\kappa^2\right)}{\frac{\partial F}{\partial \kappa}(p, \kappa)} \sin \kappa_s a \cosh \kappa_d y e^{i\kappa z} \Big|_{\kappa = \kappa_n(p)} \quad (181)$$

Next, we wish to integrate along the Bromwich contour in accordance with the Mellin inversion theorem, equation 15b. Now, equation 181 holds everywhere in the p plane including on the Bromwich contour, which must be located to the right of all singularities. In the present case, it is known that the Bromwich contour need only be located infinitesimally to the right of the imaginary p axis because the solution is expected to be stable with time. Then, we select in equation 181 the modes for which the $\kappa_n(p)$ have a positive imaginary part when p is located on the Bromwich contour Br_1 , located slightly to the right of the imaginary axis. The answer is found by writing for the Bromwich contour $p = i\omega + \epsilon$ with ω and ϵ real and ϵ small and positive. It is known that the Rayleigh-Lamb spectrum for ω real, which is consistent with the location of Br_1 , includes some modes for which κ has a positive imaginary part and other modes for which κ is real. (See Mindlin and Onoe (35). Use here of ω real is consistent with the lack of dissipation.) Among the modes for which κ is real, equation 181 admits only the modes for which $\frac{d\kappa_n}{d\omega} \cong i \frac{d\kappa_n}{dp}$ is negative* because then

* This is the same as requiring that the group velocity, $-\frac{d\omega}{d\kappa}$, be positive.

$$\kappa_n(p) = \kappa_n(i\omega + \epsilon) \approx \kappa_n(i\omega) + \epsilon \frac{d\kappa_n}{dp} = \kappa_n(i\omega) - i\epsilon \frac{d\kappa_n}{d\omega}$$

has a positive imaginary part. Then, from equations 181 and 15b the potentials are written as integrals over ω of sums over all modes for which $\text{Im } \kappa_n > 0$ or $\text{Im } \kappa_n = 0$ and $\frac{d\kappa_n}{d\omega} < 0$ in the form

$$\phi = \sum_n \int_{-\infty}^{\infty} \frac{iZ\lambda}{\pi \mu c_d \kappa_d} \frac{\left(\frac{p^2}{c_s^2} + 2\kappa^2 \right)}{\frac{\partial F}{\partial \kappa} g(p, \kappa)}$$

$$\sinh \kappa_s \quad a \cosh \kappa_d y e^{i\kappa z + i\omega t} \quad \left| \quad d\omega, \quad (182) \right. \\ \left. \kappa = \kappa_n(p) \right.$$

where $p^2 = -\omega^2$. In equation 182 ϵ has been taken as zero. Certain indentations of the Bromwich contour may be necessary where the integrand in equation 182 is not finite**.

It is convenient now to look at the right hand side of equation 182 as integrals to be taken over all parts of all modes in any desirable order. To study wave fronts it is necessary to integrate in a useful order over the terraced part of the spectrum, which was investigated by Mindlin (36). The Rayleigh-Lamb equation for symmetric waves is

** $\partial F / \partial \kappa$ may have zeroes, which are branch points of the integrand (see reference 18). These do not occur in the high frequency part of the spectrum, which is of interest here.

$$F_g = \left(\frac{P^2}{c_s^2} + 2k^2 \right)^2 \cosh \kappa_d a \sinh \kappa_s a - 4\kappa^2 \kappa_d \kappa_s \sinh \kappa_d a \cosh \kappa_s a$$

$$= 0 \tag{183}$$

In equation 183 κ_d and κ_s are imaginary in the terraced parts of the spectrum ($\omega > c_d |k|$). As mentioned before, the branches of κ_d and κ_s are not branches of the double transforms and make no difference in the solution, and so they will be chosen arbitrarily to be positive imaginary in the following. We will let

$$\kappa_d = ik_d \quad \text{and} \quad \kappa_s = ik_s,$$

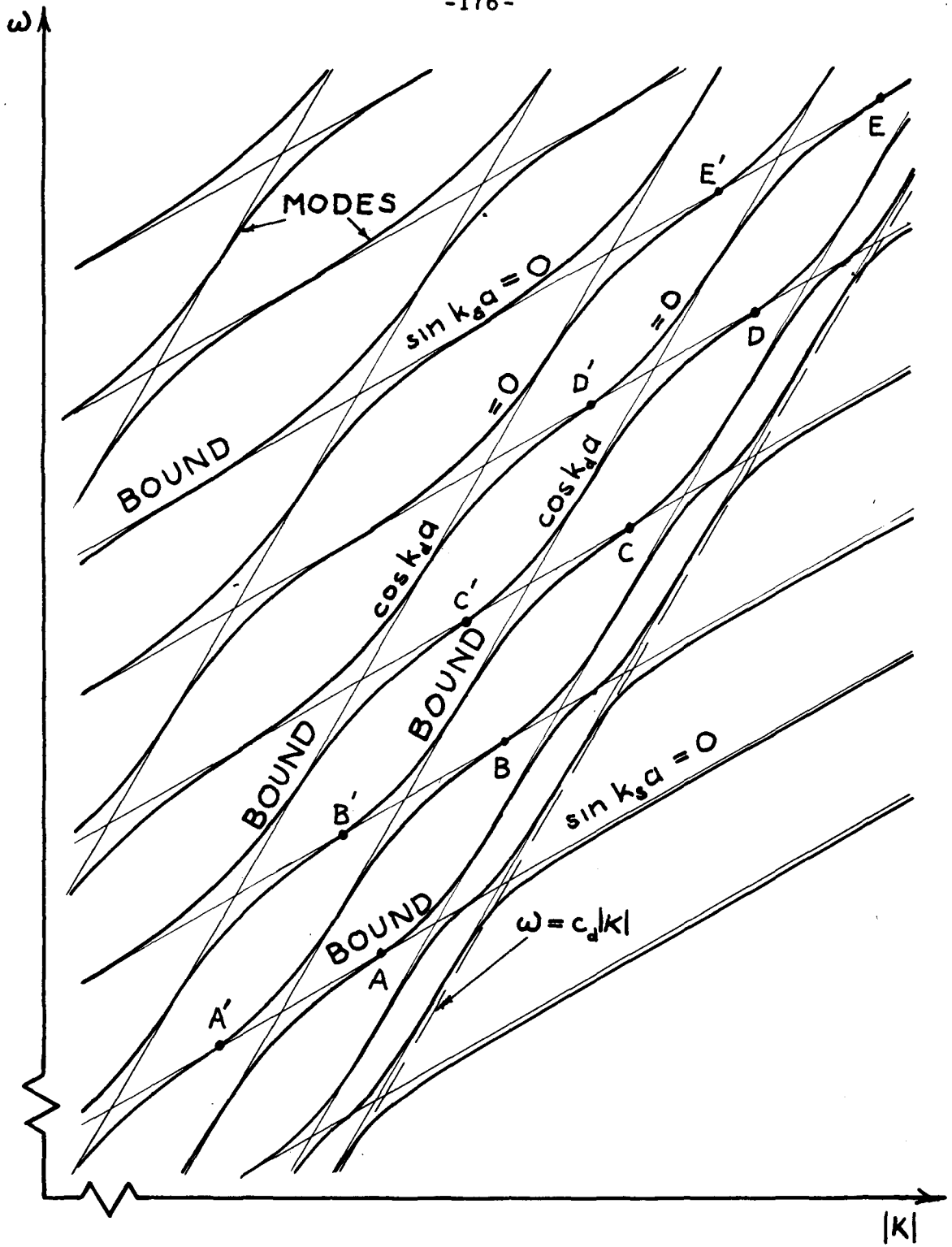
where k_d and k_s are positive real. Then, the Rayleigh-Lamb equation is

$$F_g = i \left\{ \left(2\kappa^2 - \frac{\omega^2}{c_s^2} \right)^2 \cos k_d a \sin k_s a + 4\kappa^2 k_d k_s \sin k_d a \cos k_s a \right\}$$

$$= 0. \tag{184}$$

In the terraced region ω , κ , and k_s are large with $\omega \approx -c_d$. The wave number k_d is small causing the second term of the Rayleigh-Lamb equation to be small compared to the first unless either $\cos k_d a$ or $\sin k_s a$ is small also. Each mode is shown in figure 23 to approach alternately the curves $\cos k_d a = 0$ and $\sin k_s a = 0$.

Those curves were called bounds by Mindlin. Our present interest is in the parts of the modes near $\cos k_d a = 0$ along which



TERRACED SPECTRUM

Figure 23

$k_d a = (m + 1/2)\pi$ with $m = 0, 1, 2, \dots$. The integration and sum in equation 182 will be rearranged by integrating over parts of successive modes in a certain convenient order. The idea will be to integrate along the bounds $\cos k_d a = 0$ rather than along the modes. This will be indicated by replacing the sum over the modes in equation 182 by a sum over the bounds, that is, over m . Then, for instance, in figure 23 the integral along the bound for which $m = 2$ would include an integration from A' to B plus an integration from B' to C , an integration from C' to D , an integration from D' to E , etc.

For large frequency various approximations can be made along the bounds. Because the approximations are good only for large ω , the results will only be good for the wave fronts. The largest term in the derivative $\partial F_g / \partial \kappa$ in the denominator of equation 182 comes from differentiating $\cos k_d a$ in the first term of equation 184. Then,

$$\frac{\partial F_g}{\partial \kappa} \approx i \frac{\kappa a}{k_d} \left(2\kappa^2 - \frac{\omega^2}{c_s^2} \right)^2 \sin k_d a \sin k_s a.$$

Substituting the several approximations appropriate to the terraced region into equation 182, we have

$$\Phi \approx \sum_m \int_{-\infty}^{\infty} \frac{Z \lambda \cos k_d y e^{i(\kappa z + \omega t)}}{i \omega \mu a c_d k_d K (2k^2 - \frac{\omega^2}{c_s^2}) \sin k_d a} d\omega, \quad (185a)$$

or, since $\kappa \approx -\omega/c_d$ and $k_d a \approx (m + 1/2)\pi$,

$$\Phi \approx \sum_m \int_{-\infty}^{\infty} \frac{Z c_d^2 \cos [(m + 1/2)\pi y/a]}{i \pi^2 \omega^3 (m + 1/2) (-1)^m} e^{i\omega(t - z/c_d)} d\omega. \quad (185b)$$

The strain in the z direction due only to Φ is then found by differentiating equation 185b twice with respect to z;

$$\epsilon_z \approx \frac{-Z}{i\pi^2} \sum_m \frac{(-1)^m \cos [(m + 1/2)\pi y/a]}{(m + 1/2)} \int_{-\infty}^{\infty} e^{i\omega(t - z/c_d)} \frac{d\omega}{\omega}. \quad (186)$$

The integral over ω is quite similar* to the Mellin inversion integral, equation 15b, of the Laplace transform of the Heaviside step, $1/p$.

*The integrals are similar in the large ω region, which determines the wave fronts. Actually, because of the poor approximations near ω equal to zero, the integral in equation 186 does not converge.

That Mellin inversion integral to be compared to equation 186 is

$$H(t) = \frac{1}{2\pi i} \int_{Br_1} \frac{e^{pt}}{p} dp .$$

We then deduce that the discontinuity in strain must be of the form

$$\epsilon_z \approx -Z \left\{ \sum_m \frac{2(-1)^m \cos [(m + 1/2)\pi y/a]}{\pi(m + 1/2)} \right\} H(t - z/c_d).$$

The sum over m ranges from zero to an unspecified number which may be quite large if the solution ranges over very high frequencies. Summing from zero to infinity, the expression in braces is a Fourier series for a function which vanishes for $2 > |y/a| > 1$ and which is unity for the range of interest, $1 > |y/a|$. Then,

$$\epsilon_z \approx -Z H(t - z/c_d)$$

is the strain at the wave front found by approximating the modal solution at high frequencies. This is the same as the step given in equation 113.

Further refinement of the calculations for large ω can be accomplished by considering the error introduced near $\text{sinc } a = 0$ where the above integration has the greatest error. Then, the next step is to write for ϕ sums along lines $\cos k_d a = 0$ over the integers n with $k_d a = n\pi$ so that $\text{sinc } a$ is zero. Each term of the sum represents a correction to the simple result which was found above. The condition is

$$\left(\frac{n\pi}{a}\right)^2 \approx k_s^2 = \frac{\omega^2}{c_s^2} - k^2 \approx \frac{\omega^2}{c_s^2} - \frac{\omega^2}{c_d^2}.$$

And so ω takes on the values

$$\omega \approx \left(\frac{n\pi}{a}\right) \frac{1}{\sqrt{\frac{1}{c_s^2} - \frac{1}{c_d^2}}} = \frac{c_d n\pi}{a \sqrt{k^2 - 1}}.$$

Then, one must sum over terms with phase

$$t + z \frac{c_d}{2a \sqrt{k^2 - 1}} (t - z/c_d) 2n\pi.$$

A Fourier series of that form is periodic in $t - z/c_d$ with frequency

$$\frac{c_d}{2a \sqrt{k^2 - 1}},$$

which is precisely the frequency of the reflection of

the head waves back and forth across the plate. The sum then represents the dilatational potential caused by the reflecting head waves at the points A, G, etc. in figures 11 and 12.

For the shear potential one is led by the same arguments to a sum of integrals along bounds similar to equation 185a. The important differences are the appearance of $\sin k_s a$ in the denominator

and $\sin k_g y$ in the numerator. To the approximation of equation 185a, the integrand goes to infinity when $\sin k_g a$ equals zero. Thus, the first approximation is a sum over those points where the integrand becomes very large. The phase, $\omega t + \kappa z$, may be augmented by $n\pi y/a \approx k_g y$ from $\sin k_g y$, which is contained in the integrand. Then, the total phase is

$$\frac{c_d}{2a \sqrt{k^2 - 1}} \left(t - \frac{z}{c_d} - \frac{\sqrt{k^2 - 1}}{c_d} y \right) 2n\pi$$

and one can deduce the form of the head waves by the argument used above.

It is apparent that the leading wave fronts come out of the terraced region of the frequency spectrum. The parts of the modes in the terraced region are made up of a plane harmonic dilatational wave moving almost parallel to the free surfaces plus a shear wave moving at the angle of the head wave. The limiting phase and group velocities are c_d , the same as the speed of the leading wave fronts. The periodic structure of the frequency spectrum is related to the periodic arrival of the head waves. It is also reasonable to expect that the first mode, which approaches a phase and group velocity of c_r at high frequency, accounts for the Rayleigh wave in the plate. The arrival of the circular shear front at time z/c_s at the surface is probably related to the fact that all modes but the first go off to a limiting speed c_s .

D. EXACT SOLUTIONS FOR LIMITED TIME INTERVALS

The solution by Cagniard's method is useful for more than just finding the wave fronts. For plane strain Cagniard's method gives an exact solution, equation 120. This exact solution is valid for all z and all t . Cagniard's method is far more powerful than either the method of stationary phase, which is limited to large t , or other wave front methods, which are limited to the vicinity of the wave fronts. The solution by Cagniard's method is built up by adding terms, one term for the disturbance following each wave front. The only limitation is that for times long after the first arrival too many wave fronts have passed and the numerical work becomes very involved.

Cagniard's method has been used here to calculate the strain and displacement at the surface of a plate for times before the arrival of the first reflected head wave. For those early times equation 114 for the Cagniard contour can be solved by the quadratic formula since either α or β is zero for every wave. Calculations for times after the arrival of the first reflected head wave would require numerical solution of equation 114. The results are compared to the experiments of Miklowitz and Nisewanger (19) and Meitzler (33). Their experiments covered a much larger time scale than the theory and so only gross features can be compared. Besides the limit on the time interval covered by the theoretical calculations, there are two fundamental differences between the theory and experiment. First, the experiments were done on a circular rod and the theory is valid for plane strain. Second, to a very good approximation the experiments involved

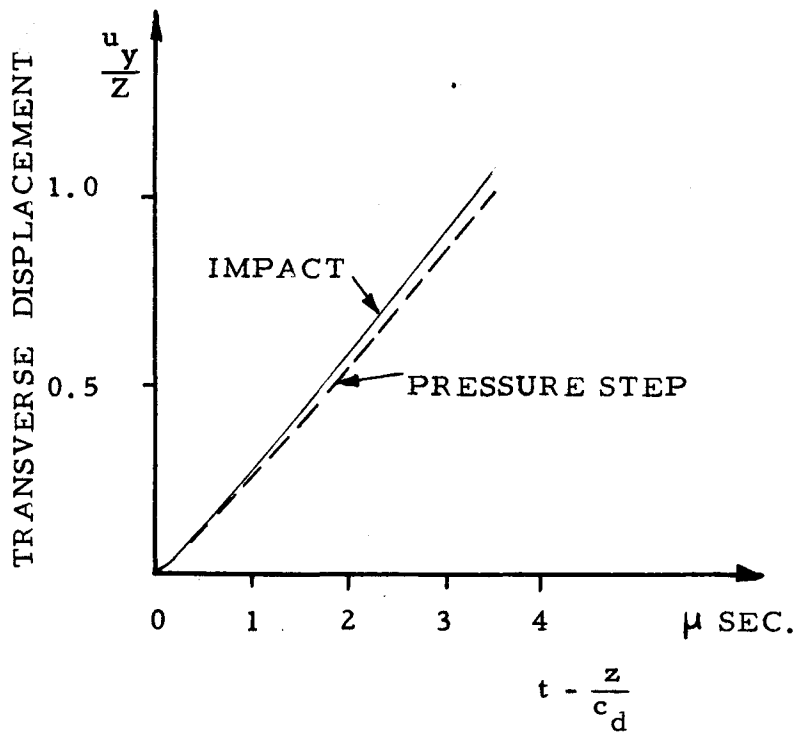
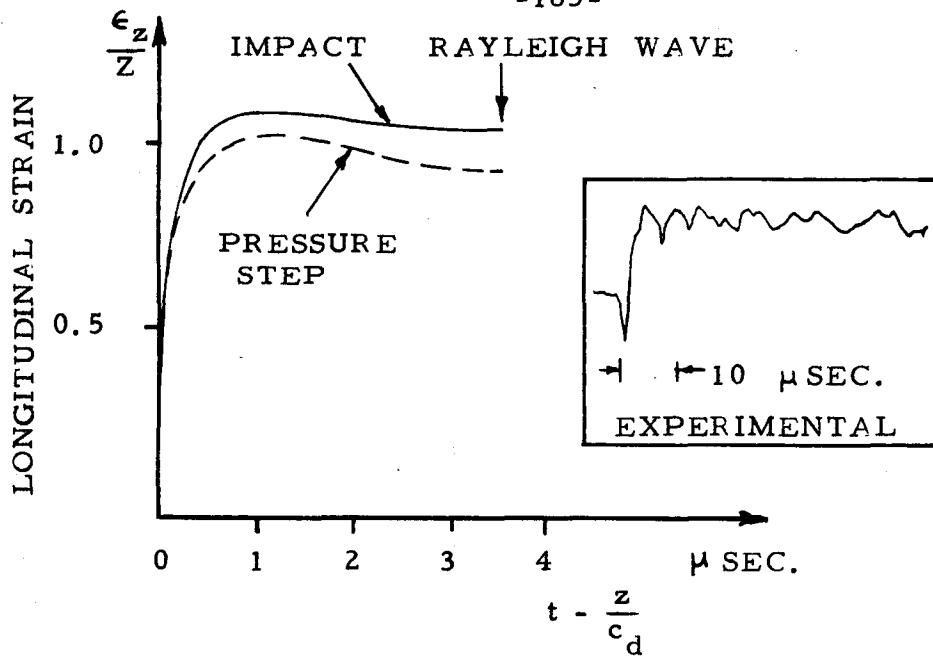
the nonmixed end conditions of the pressure shock problem, whereas the theory was done for mixed boundary conditions on the end of the plate. To assess the importance of the second difference between theory and experiment, the calculations were carried out for two different problems, the impact problem and the pressure step problem. On the basis of approximate theory work Miklowitz (7) anticipated a similarity between the responses to different boundary conditions. Folk, Fox, Shook, and Curtis (6, 37) expected similarities in the responses at large z and therefore applied an exact theory solution for mixed boundary conditions to experiments with nonmixed boundary conditions. The present calculations are for relatively small z .

The solution by Cagniard's method was used in a straightforward manner. Rather than using the potentials, the double transforms for the longitudinal strain $\epsilon_z = \frac{\partial u}{\partial z}$ and the displacement u_y at the surface were derived from the double transforms of the potentials. The double transforms were then expanded to form integrals like equation 108. Since the work was specialized to $y = a$, the results took on a form different from equations 112. At the surface one sees not the individual wave fronts shown in figures 11 and 12, but rather the junctions of three or four incident and reflected wave fronts. That is why the derivations were done over again with the double transforms evaluated at $y = a$. It would have been possible to use equations 112 and add together the displacements and strains of the many wave fronts at the

surface. In order to eliminate waves which are delayed by a traversal of the plate as an S wave, $S = e^{-2K_s a}$ was set equal to zero. The remaining terms represented waves which traverse the bar only as P waves. The integral like equation 108 with $n = 0$ and the integral for the step were combined; the result has no pole at $s = i$. Then, equation 120 was taken as the inversion of the double transform. N in equation 120 is 1 for the strain and 2 for the displacement. Therefore, a single integration was necessary for the strain and a double integration for the displacement. Equation 120 was applied directly with one exception. At the wave fronts the function being integrated had a singularity in the form $1/\sqrt{t}$. In order to integrate accurately, this singularity was subtracted out. After integrating numerically, the integral of the singularity ($2\sqrt{t}$) was added back in.

The resulting plots of strain and displacement versus time are shown in figures 24, 25, and 26 and compared to the experiments. The first figure corresponds to one of Meitzler's records for strain and the other two figures correspond to records given by Miklowitz and Nisewanger for strain and displacement. The values for the constants used are the values given for the rods tested in the experimental work. The calculations were done with source magnitudes, Z , such that the long time strain or displacement in the plate would be unity. Wave front arrivals are indicated by arrows.

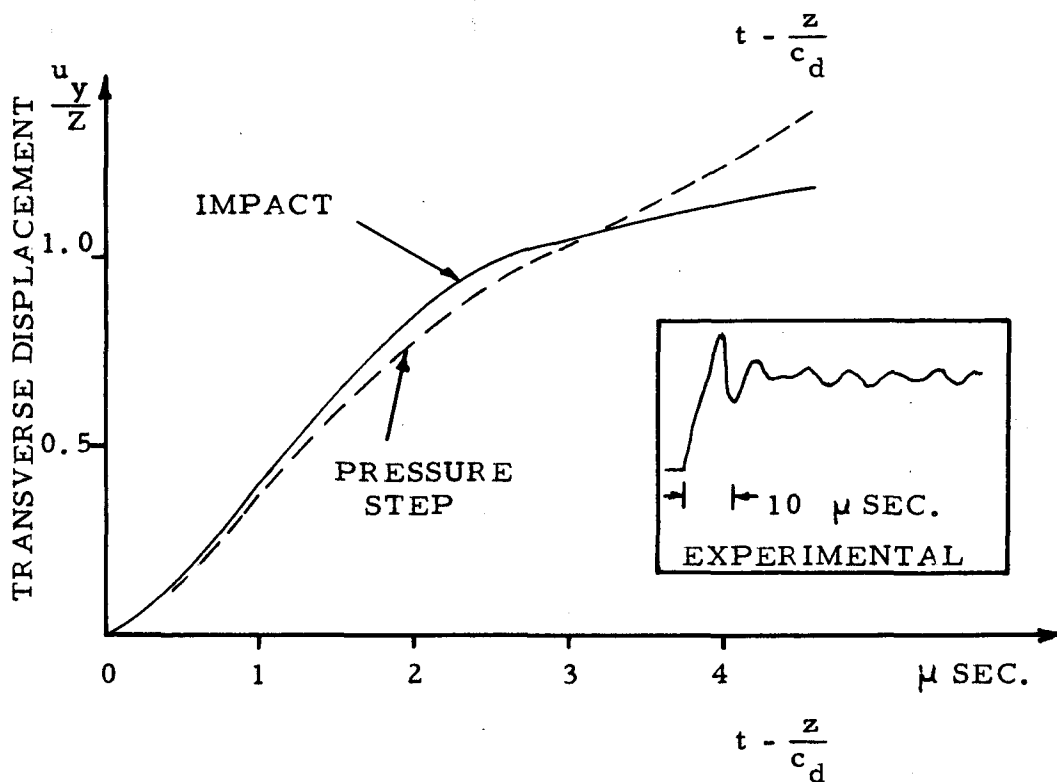
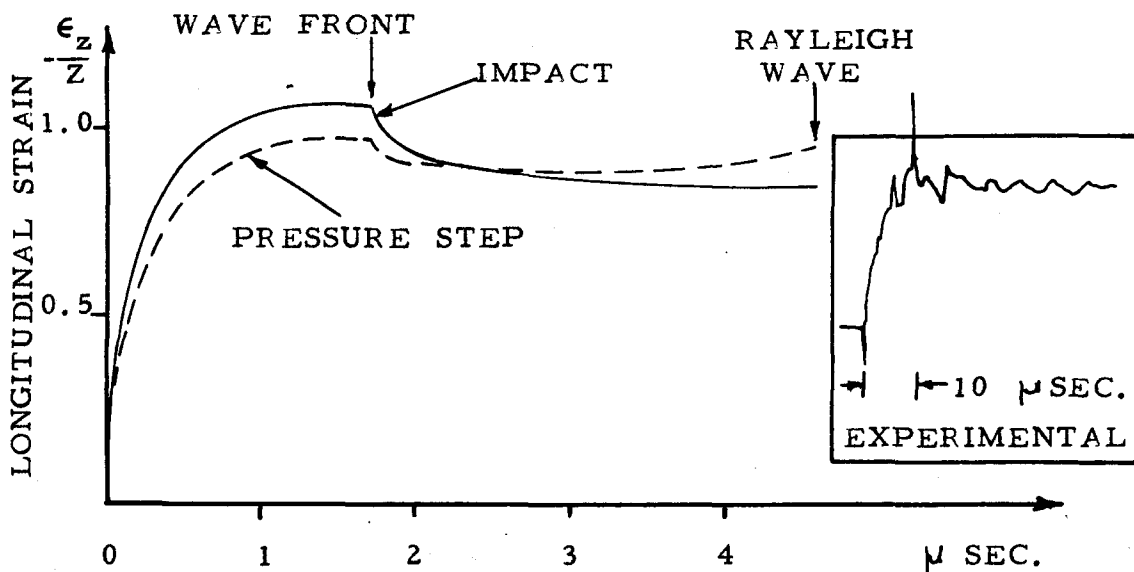
In figure 24 the calculations were stopped at the Rayleigh wave for simplicity. Only the first wave front is seen because the station is so close to the end of the plate. Notice that the



$z/2a=0.525$ $a/c_d=3.27 \mu$ sec. $k^2=3.495$

STRAIN AND DISPLACEMENT RESPONSE

Figure 24



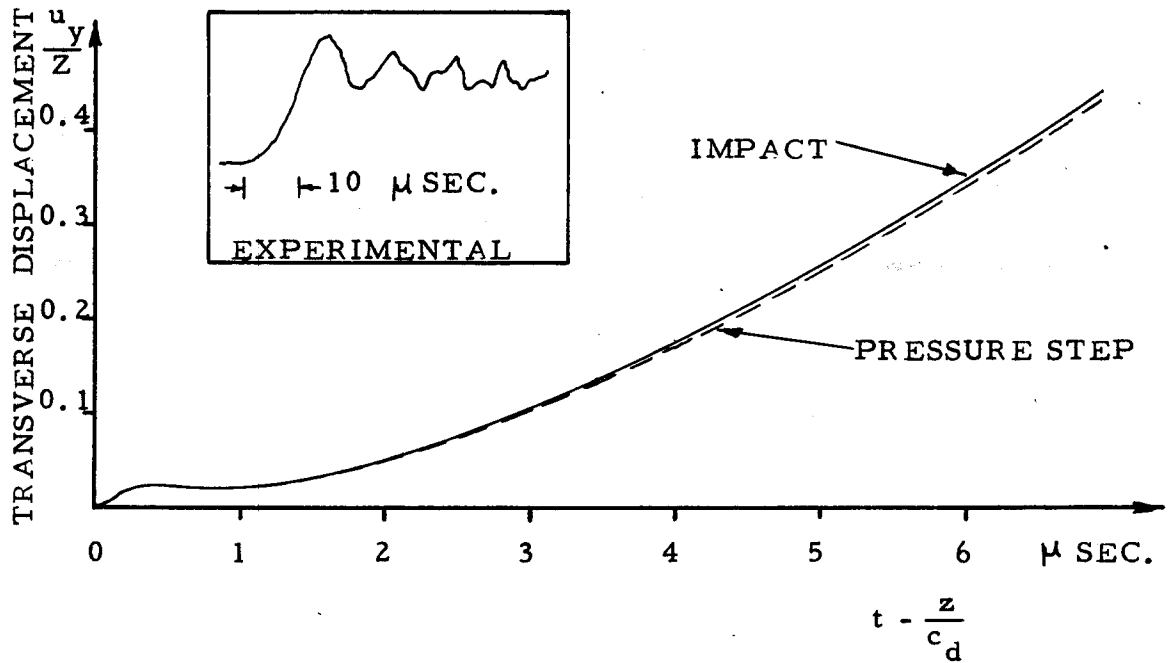
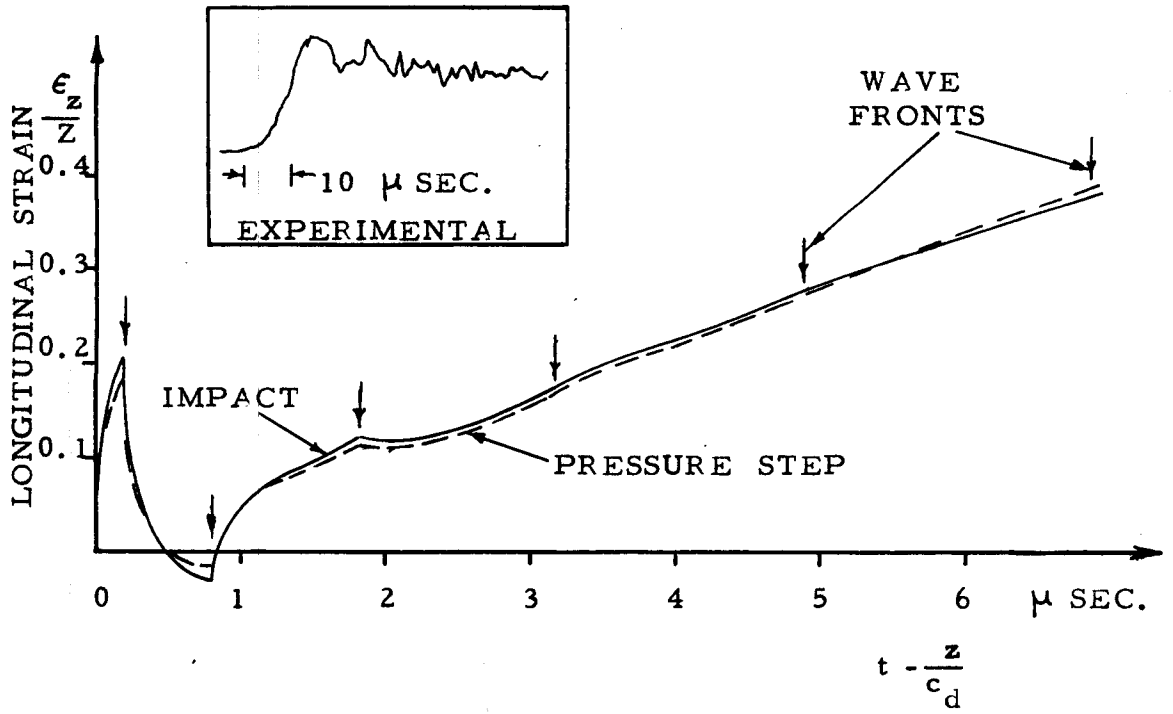
$z/2a=1.0$

$a/c_d=2.05 \mu\text{sec.}$

$k^2=3.8571$

STRAIN AND DISPLACEMENT RESPONSE

Figure 25



$z/2a=10.0$

$a/c_d=2.05 \mu$ sec.

$k^2=3.8571$

STRAIN AND DISPLACEMENT RESPONSE

Figure 26

strain rises very rapidly as the square root of t exactly as the wave front theory predicts, but after one-half microsecond the strain stays essentially constant. The displacement behaves according to the wave front theory only for a fraction of a microsecond and then rises nearly linearly.

The strain shown in figure 25 rises in the same manner as the strain in figure 24 and then levels out at a nearly constant value. After a little more than one and one-half microseconds a far weaker wave front arrives as shown and the strain again continues at an approximately constant value until the Rayleigh wave arrives. The weaker wave front corresponds to the point B on figures 11 and 12. The resulting wave front behavior shown in figure 25 is due to an incident wave and two reflected waves all acting together. Figure 26 for the strain at a station farther from the end of the rod shows that during the first microsecond three wave fronts arrive. The first is compressional and the second tends to destroy the effect of the first. Then, with the arrival of the third wave front the theoretical strain starts to build up the same as shown on the experimental records, the later wave fronts being much weaker.

The experimental records can be compared with the theoretical calculations by looking at the figures. It is immediately apparent that the experiments are not able to follow the rapidly changing strains. A negative rate of change of strain response is indicated by the small negative spikes on the experimental records in figures 24 and 25. Neitzler noted the rate of change of strain response in his

work. In figure 26 it is seen that the experiments do not pick up the small pulse arriving with the dilatational speed in nearly the correct magnitude, if at all. The strain record of Miklowitz and Nisewanger for the station where $z/2a = 5$ (not shown here) does show the arrival at the dilatational velocity, but at a magnitude greatly reduced from that of the theoretical curve. It can be seen by comparing the curves in figures 24 and 25 that the strain rises faster in the theory than in the experiment. All of the above conclusions are independent of the differences between rod and plate and the differences in the end conditions as prescribed in theory and as created by the shock tube for the experiments. The experiment and theory can also be compared by looking at the displacements. In figures 25 and 26 it can be seen that by the last time on the theoretical curves the displacement has risen approximately the same amount in the theory as in experiment. The small difference between the two is possibly due to the differences between the plane strain and the circular rod. The difference in boundary conditions is evidently not important because both boundary conditions used in the theoretical calculations give similar results.

REFERENCES

1. Miklowitz, J., Traveling Compressional Waves in an Elastic Rod According to the More Exact One-dimensional Theory, Proceedings of the Second U. S. National Congress of Applied Mechanics, A. S. M. E., (New York, 1955), 179-186.
2. Miklowitz, J., The Propagation of Compressional Waves in a Dispersive Elastic Rod, Part I -- Results from the Theory, J. Appl. Mech., 24, (1957), 231-239.
3. Mindlin, R. D., and Herrmann, G., A One-dimensional Theory of Compressional Waves in an Elastic Rod, Proceedings of the First U. S. National Congress of Applied Mechanics, A. S. M. E., (New York, 1952), 187-191.
4. Herrmann, G., Application of Green's Method in Deriving Approximate Theories of Elasticity, O. N. R. Project NR-064-388, Contract Nonr-266(09), Technical Report No. 13, (February, 1954).
5. Skalak, R., Longitudinal Impact of a Semi-infinite Circular Elastic Bar, J. Appl. Mech., 24, (1957), 59-64.
6. Folk, R., Fox, G., Shook, C. A., and Curtis, C. W., Elastic Strain Produced by Sudden Application of Pressure to One End of a Cylindrical Bar, I. Theory, J. Acoust. Soc. Amer., 30, (1958), 552-558.
7. Miklowitz, J., On the Use of Approximate Theories of an Elastic Rod in Problems of Longitudinal Impact, Proceedings of the Third U. S. National Congress of Applied Mechanics, A. S. M. E., (New York, 1958), 215-224.
8. Love, A. E. H., A Treatise on the Mathematical Theory of Elasticity, (New York, Dover, 1944).

9. Mencher, A. G., Epicentral Displacement Caused by Elastic Waves in an Infinite Slab, J. Appl. Phys., 24, (1953), 1240-1246, 1529.
10. Broberg, K. B., A Problem on Stress Waves in an Infinite Elastic Plate, Trans. Roy. Inst. Tech., Stockholm, Rep. No. 139, (1959).
11. Davids, N., Transient Analysis of Stress-Wave Penetration in Plates, J. Appl. Mech., 26, (1959), 651-660.
12. Knopoff, L., Surface Motions of a Thick Plate, J. Appl. Phys., 29, (1958), 661-670.
13. Knopoff, L., and Gilbert, F., First Motion Methods in Theoretical Seismology, J. Acoust. Soc. Amer., 31, (1959), 1161-1168.
14. Karal, F. C., Jr., and Keller, J. B., Elastic Wave Propagation in Homogeneous and Inhomogeneous Media, J. Acoust. Soc. Amer., 31, (1959), 694-705.
15. Babich, V. M., and Alekseev, A. S., On the Ray Method of Calculation of the Intensity of Wave Fronts, Izv. Akad. Nauk S.S.S.R., Ser. Geofiz., (1958), 17-31.
16. Courant, R., and Hilbert, D., Methods of Mathematical Physics, Vol. I. (New York, Interscience, 1953).
17. Miklowitz, J., Transient Compressional Waves in an Infinite Elastic Plate or Elastic Layer Overlying a Rigid Half-Space, J. Appl. Mech., 29, (1962), 53-60, footnote 6.
18. Lloyd, J. R., Wave Propagation in an Elastic Plate Resting on an Elastic Foundation, Thesis, California Institute of Technology, (1962).

19. Miklowitz, J., and Nisewanger, C. R., The Propagation of Compressional Waves in a Dispersive Elastic Rod, Part II -- Experimental Results and Comparison with Theory, J. Appl. Mech., 24, (1957), 240-244.
20. Mindlin, R. D., and McNiven, H. D., Axially Symmetric Waves in Elastic Rods, J. Appl. Mech., 27, (1960), 145-151.
21. Chree, C., The Longitudinal Vibrations of Aeolotropic Bars with an Axis of Material Symmetry, Quart. J. of Pure and Appl. Math., 24, (1890), 340-358.
22. Gazis, D. C., and Mindlin, R. D., Influence of Width on Velocities of Long Waves in Plates, J. Appl. Mech., 24, (1957), 541-546.
23. Volterra, E., Dispersion of Longitudinal Waves, Proc. of Amer. Soc. of Civil Eng., 83, (1957), Paper 1322.
24. Mindlin, R. D., and Fox, E. A., Vibrations and Waves in Elastic Bars of Rectangular Cross Section, J. Appl. Mech., 27, (1960), 152-158.
25. Kane, T. R., and Mindlin, R. D., High-Frequency Extensional Vibrations of Plates, J. Appl. Mech., 23, (1956), 277-283.
26. Erdélyi, A., Asymptotic Expansions, (New York, Dover, 1956).
27. Curtis, C. W., Propagation of Elastic and Plastic Deformations in Solids, O. O. R. Report, Lehigh Univ., Contract DA-36-034-Ord-1456 Sup. 2, Project TB 2-0001 (187), (Sept., 1956).

28. Borgnis, F. E., and Papas, C. H., Electromagnetic Waveguides and Resonators, Encyclopedia of Physics, (Berlin, Springer-Verlag, 1958), Vol. XVI, 285-422.
29. Ewing, W. M., Jardetzky, W. S., and Press, F., Elastic Waves in Layered Media, (New York, McGraw-Hill, 1957).
30. Copson, E. T., Theory of Functions of a Complex Variable, (London, Oxford Univ. Press, 1935).
31. Widder, D. V., The Laplace Transform, (Princeton, Princeton Univ. Press, 1941), 59-63.
32. Hughes, D. S., Pondrom, W. L., and Mims, R. L., Transmission of Elastic Pulses in Metal Rods, Physical Review, 75, (1949), 1552-1560.
33. Meitzler, A. H., Propagation of Elastic Pulses Near the Stressed End of a Cylindrical Bar, Thesis, Lehigh Univ., (1955).
34. Goodier, J. N., and Bishop, R. E. D., A Note on Critical Reflections of Elastic Waves at Free Surfaces, J. Appl. Physics, 23, (1952), 124-126.
35. Mindlin, R. D., and Onoe, M., Mathematical Theory of Vibrations of Elastic Plates, Proceedings 11th Annual Symposium on Frequency Control, U. S. Army Signal Corps Engr. Labs., Ft. Monmouth, N. J., (1957), 17-40.
36. Mindlin, R. D., An Introduction to the Mathematical Theory of Vibrations of Elastic Plates, Monograph, U. S. Army Signal Corps Engr. Labs., Ft. Monmouth, N. J., Signal Corps Contract DA-36-039, Sc-56772, (1955).

37. Fox, G., and Curtis, C. W., Elastic Strain Produced by a Sudden Application of Pressure to One End of a Cylindrical Bar, II. Experimental Observations, J. Acoust. Soc. Amer., 30, (1958), 559-563.